

REPORT DOCUMENTATION PAGE			Form Approved OMB No. 0704-0188	
Public reporting burden for this collection of information is estimated to average 1 hour per response, including the time for reviewing instructions, searching existing data sources, gathering and maintaining the data needed, and completing and reviewing the collection of information. Send comments regarding this burden estimate or any other aspect of this collection of information, including suggestions for reducing this burden, to Washington Headquarters Services, Directorate for Information Operations and Reports, 1215 Jefferson Davis Highway, Suite 1204, Arlington, VA 22202-4302, and to the Office of Management and Budget, Paperwork Reduction Project (0704-0188), Washington, DC 20503.				
1. AGENCY USE ONLY (Leave blank)		2. REPORT DATE 17 Jul 00		3. REPORT TYPE AND DATES COVERED THESIS
4. TITLE AND SUBTITLE ANALYSIS OF A GREAT BASIN CYCLONE AND ATTENDANT MESOSCALE FEATURES			5. FUNDING NUMBERS	
6. AUTHOR(S) CAPT BLAZEK THOMAS R				
7. PERFORMING ORGANIZATION NAME(S) AND ADDRESS(ES) UNIVERSITY OF UTAH			8. PERFORMING ORGANIZATION REPORT NUMBER	
9. SPONSORING/MONITORING AGENCY NAME(S) AND ADDRESS(ES) THE DEPARTMENT OF THE AIR FORCE AFIT/CIA, BLDG 125 2950 P STREET WPAFB OH 45433			10. SPONSORING/MONITORING AGENCY REPORT NUMBER FY00-246	
11. SUPPLEMENTARY NOTES				
12a. DISTRIBUTION AVAILABILITY STATEMENT Unlimited distribution In Accordance With AFI 35-205/AFIT Sup 1			12b. DISTRIBUTION CODE	
13. ABSTRACT (Maximum 200 words)				
<div style="display: flex; justify-content: space-between; align-items: center;"> <div style="text-align: center;"> DISTRIBUTION STATEMENT A Approved for Public Release Distribution Unlimited </div> <div style="font-size: 2em; font-weight: bold;">20000727 170</div> </div>				
14. SUBJECT TERMS			15. NUMBER OF PAGES 122	
			16. PRICE CODE	
17. SECURITY CLASSIFICATION OF REPORT	18. SECURITY CLASSIFICATION OF THIS PAGE	19. SECURITY CLASSIFICATION OF ABSTRACT	20. LIMITATION OF ABSTRACT	

ANALYSIS OF A GREAT BASIN CYCLONE AND
ATTENDANT MESOSCALE FEATURES

by

Thomas R. Blazek

A thesis submitted to the faculty of
The University of Utah
in partial fulfillment of the requirements for the degree of

Master of Science

Department of Meteorology

The University of Utah

August 2000

Copyright © Thomas R. Blazek 2000

All Rights Reserved

THE UNIVERSITY OF UTAH GRADUATE SCHOOL

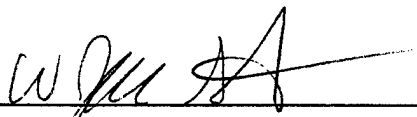
SUPERVISORY COMMITTEE APPROVAL

of a thesis submitted by

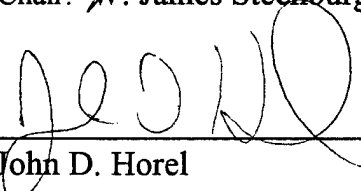
Thomas R. Blazek

This thesis has been read by each member of the following supervisory committee and by majority vote has been found to be satisfactory.

May 3, 2000


Chair: W. James Steenburgh

May 3, 2000


John D. Horel

May 3, 2000


Lawrence Dunn


THE UNIVERSITY OF UTAH GRADUATE SCHOOL

FINAL READING APPROVAL

To the Graduate Council of the University of Utah:

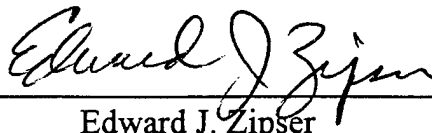
I have read the thesis of Thomas R. Blazek in its final form and have found that (1) its format, citations, and bibliographic style are consistent and acceptable; (2) its illustrative materials including figures, tables, and charts are in place; and (3) the final manuscript is satisfactory to the supervisory committee and is ready for submission to The Graduate School.

May 22, 2000



W. James Steenburgh
Chair, Supervisory Committee

Approved for the Major Department



Edward J. Zipser
Chair

Approved for the Graduate Council

David S. Chapman
Dean of The Graduate School

ABSTRACT

The synoptic and mesoscale evolution of a Great Basin cyclone and its attendant mesoscale features are described using high resolution surface observations provided by MesoWest, a collection of observing networks located over the western United States. Specific aspects of the event that are examined in detail include: (1) the distortion of the cold front over the Sierra Nevada, (2) the evolution of the cold front and several mesoscale circulation centers over northern Utah, (3) the evolution and distortion of the cold front over southern and central Idaho, and (4) the development of persistent troughing and a Snake River Plain convergence zone over southern Idaho. Possible dynamical mechanisms for the evolution of the observed mesoscale features are discussed, as well as issues related to surface analysis in regions of complex terrain.

TABLE OF CONTENTS

ABSTRACT	iv
ACKNOWLEDGMENTS	vi
1 INTRODUCTION	1
2 DATA AND METHODS	6
Data Resources	6
Surface Analysis Methods	8
3 SYNOPTIC-SCALE EVOLUTION.....	20
4 MESOSCALE CHARACTERISTICS OF CYCLONE AND FRONTAL INTERACTION WITH TOPOGRAPHY.....	48
Frontal Distortion over the Sierra Nevada	48
Frontal Interaction with the Complex Terrain of Northern Utah	69
Southern Idaho Orographic Effects and Development of Snake River Convergence Zone	89
5 SUMMARY AND CONCLUSIONS	114
REFERENCES	118

ACKNOWLEDGMENTS

I would like to thank my advisor, Dr. W. James Steenburgh, for his guidance, patience, and scientific insight throughout the research and writing of this thesis, and Drs. John Horel and Larry Dunn for their valuable comments on this manuscript. Additionally, I would like to thank the United States Air Force for granting an Air Force Institute of Technology (AFIT) scholarship and the faculty of the University of Utah Meteorology Department for acceptance into this outstanding program.

My appreciation is also heartily expressed to my fellow classmates, in particular, Linda Cheng and Craig Clements, with whom I underwent the rigors of classwork and qualifying examinations. Without their assistance, I would likely have not made it to this point. I am very grateful to Daryl Onton for his support with GEMPAK scripts and the intricacies of Framemaker, and to Bryan White for the answers to many MesoWest queries.

Last but certainly not least, my wife, Nancy, and my daughter, Katie, have been essential in providing support toward accomplishing this goal as well as an ulterior motive to do so. I will remember their daily sacrifices forever.

This research was supported in part by National Science Foundation Grant ATM-9634191 and NOAA Grants NA67WA0465 and NA77WA0572 to the NOAA Cooperative Institute for Regional Prediction at the University of Utah.

CHAPTER 1

INTRODUCTION

Cyclones that develop over the Great Basin have a dramatic impact on the meteorology of the western United States. Studies by Petterssen (1956), Klien (1957), Zishka and Smith (1980), and Whittaker and Horn (1982) show that the Great Basin is a region of frequent cyclogenesis, particularly in the late winter and early spring. Great Basin cyclones can produce high winds and heavy snowfall, creating major public safety and socio-economic impacts. For example, in the state of Utah, weather associated with Great Basin cyclones caused nearly \$100 million dollars in damage in just a 4-year period (1993-1997)¹. Over half this total (\$50M) was due to a single Great Basin cyclone that produced heavy snowfall and resulted in the collapse of several hundred roofs in the Salt Lake City metropolitan area. Other impacts include vehicle accidents and avalanches, with the latter a concern along several major highways and in the winter recreation areas.

Prior studies examining cyclone interaction with complex terrain have examined aspects of cyclogenesis to the lee of major mountain chains such as the Rocky Mountains (e.g., Newton 1956; McClain 1960; Palmen and Newton 1969; Hobbs et al. 1996; Davis 1997; Davis and Stoelinga 1999) and European Alps (e.g., Egger 1972; Buzzi and Tibaldi 1978; McGinley 1982; Mattocks and Bleck 1986; Tibaldi et al. 1990). Present theory

1. Storm damage information was obtained from *Storm Data*, published by the National Oceanic and Atmospheric Administration.

views such lee cyclogenesis as a secondary cyclone development associated with the interaction of a large-scale trough or cyclone with orography (e.g., Palmen and Newton 1969; Tibaldi et al. 1990; Bannon 1992; Davis 1997; Davis and Stoelinga 1999). Although cyclone development would occur even in the absence of topography, the location and strength of the cyclone are vastly altered by the terrain. Other studies have explored the influence of topography on frontal structure including the distortion of low-level cold fronts by topographic features such as the European Alps (e.g., Godske et al. 1957; Steinacker 1981; Smith 1986), and the influence of the terrain-induced flow field on windward frontolysis and leeward frontogenesis (e.g., Bannon 1983, 1984; Zehnder and Bannon 1988; Williams et al. 1992). Work over the central and southern plains of the western United States has highlighted the significant decoupling of low-level and upper-level frontal zones that can be found to the lee of the Rocky Mountains (e.g., Hobbs et al. 1996; Neiman et al. 1998).

Relatively few studies have, however, specifically examined the structural and dynamical evolution of cyclones developing over the Great Basin. This vast region, located between the Sierra Nevada and Continental Divide, contains “basin and range” topography, which is characterized by narrow, steeply sloped mountain ranges that are separated by broad lowland valleys (Fig. 1.1). Significant topographic features of the region include the meridionally-oriented mountain ranges of central and northern Nevada, Wasatch Mountains of Utah, and Great Salt Lake Desert of northern Utah. Adjoining topographic features include the Colorado Rockies, mountain ranges of northwest Wyoming, Snake River Plain, and Central Idaho Mountains.

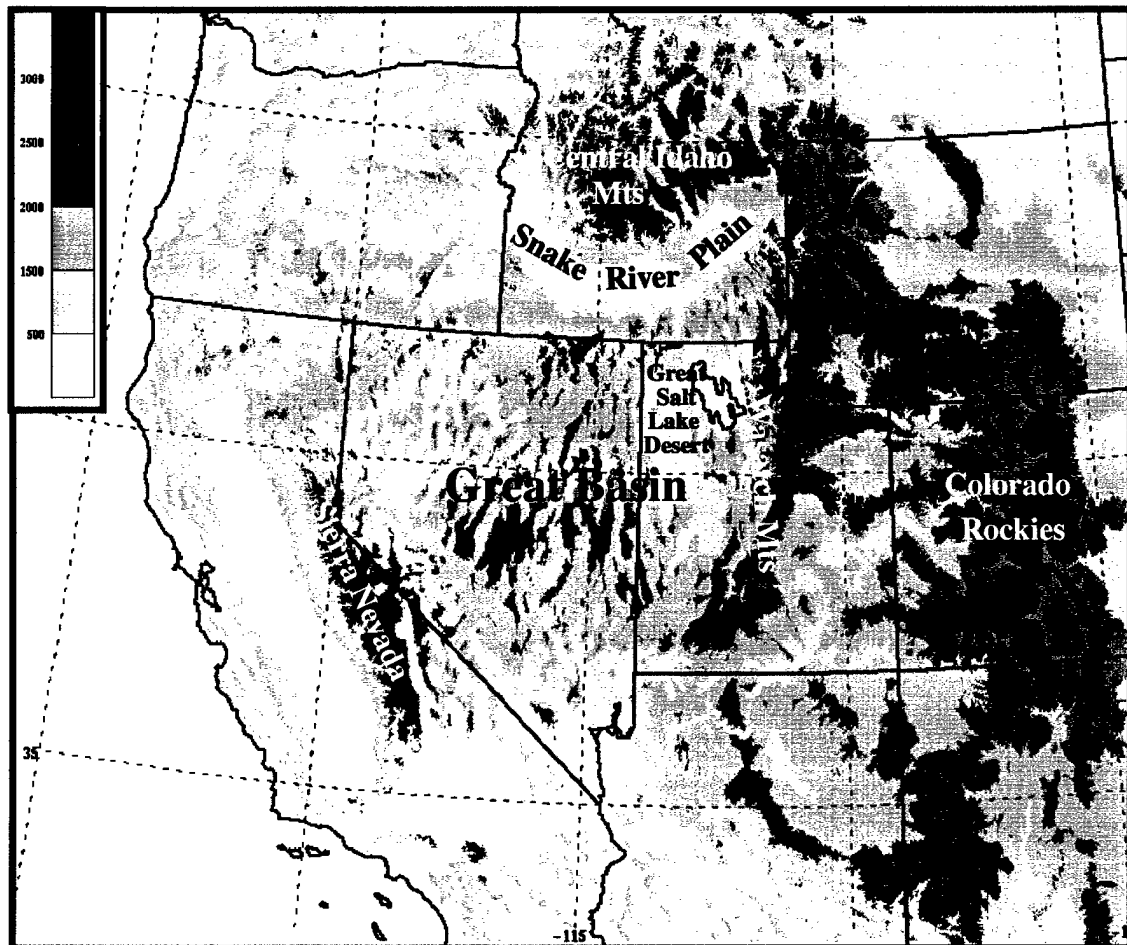


Figure 1.1. Major terrain and geographic features of the Great Basin and adjoining region. Elevation (m) based on scale at upper left.

Studies examining cyclone evolution over the Great Basin include that by Bell and Bosart (1994), who used composite 500 hPa height fields decomposed into three wave groups, planetary (zonal waves 1-3), large synoptic scale (zonal waves 4-9), and small synoptic-scale (zonal waves 10-25), to discern the important contributors to closed cyclone formation. They found that a closed cyclonic circulation developed when the large and small synoptic-scale waves became superposed. While lower tropospheric forcing and flow interaction with topography provided some trough amplification, it was not the predominant dynamical trigger. Williams (1962) developed a diagnostic tool for forecasting the development of closed 500 hPa circulation centers over the Great Basin, based on upper-air wind profiles from upstream stations. Other researchers have used objective analyses of specific parameters, such as vertical velocity and vorticity, to monitor the evolution and track of mature cyclones. Roark (1978) found a decrease in the vertical velocity derived from vorticity advection when a cyclone traversed mountains with an average height of 2000-2500 m, and Eisenson (1984) concluded that the tilting term and low-level convergence were both significant contributors to the development of low-level positive vorticity during the initial and the intensification stages of cyclogenesis. More recently, case studies have been used to test the accuracy of new mesoscale models (Horel and Gibson 1993) and to assess the performance of pre-existing ones (Conger 1994).

Because of the limited amount of research conducted over the region, a number of questions remain concerning the evolution of Great Basin cyclones. These questions include:

- What is the mesoscale structure of a Great Basin cyclone? How is the structure modified as it interacts with regional and local terrain features?
- How is the low-level structure of fronts distorted by regional and local topographic features? Do fronts tend to deform around major topographic barriers as is commonly observed over the European Alps (e.g., Godske et al. 1957; Steinacker 1981; Smith 1986)?
- What mesoscale circulation and precipitation features develop due to the interaction of a cyclone with the topography of the Great Basin?

To answer these questions, this thesis examines the structural evolution of a Great Basin cyclone using conventional data, operational gridded analyses, and high resolution surface observations provided by MesoWest, a collection of cooperating mesonets in the western United States. The selected case occurred from 3–5 December 1998 and was chosen because of its common location and track of the cyclone (Zishka and Smith 1980; Whittaker and Horn 1982). Large-scale and mesoscale subjective analyses are used to describe the cyclogenesis event and illustrate three major mesoscale aspects of the event: (1) distortion of the attendant cold front over the Sierra Nevada, (2) interaction of the cyclone and attendant fronts with the topography of northern Utah, and (3) frontal distortion and the development of persistent surface troughing and a Snake River Plain Convergence Zone (e.g., Andretta and Hazen 1998) over central and southern Idaho.

CHAPTER 2

DATA AND METHODS

Data Resources

To examine the mesoscale structure of the 3–5 December 1998 cyclone, manual surface analyses were generated using data from MesoWest. During the event period, 25 observing networks provided data to MesoWest from 1300 surface stations that are operated and maintained by several government and commercial agencies (Fig. 2.1). Collection of these data was managed jointly by the University of Utah Department of Meteorology and the Salt Lake City National Weather Service Forecast Office (NWSFO). Since each network was designed to meet the specific needs of each operating agency, there was considerable variance in the temporal resolution, spatial density, sensor characteristics, and level of quality control of the observations. As a result, the University of Utah performed internal quality control of all incoming observations (except ASOS) by comparing the observed station value to an objective analysis produced using multivariate linear regression (Splitt and Horel 1998). Observations deemed questionable using this objective analysis or by subjective examination were not considered in the analyses. Data were archived in GEneral Meteorological PAcKage (GEMPAK) format and plotted with topographic backgrounds over a variety of geographic regions for subjective analysis.

The synoptic structure of the event was also examined using three-dimensional gridded analyses produced by the National Center for Environmental Prediction (NCEP)

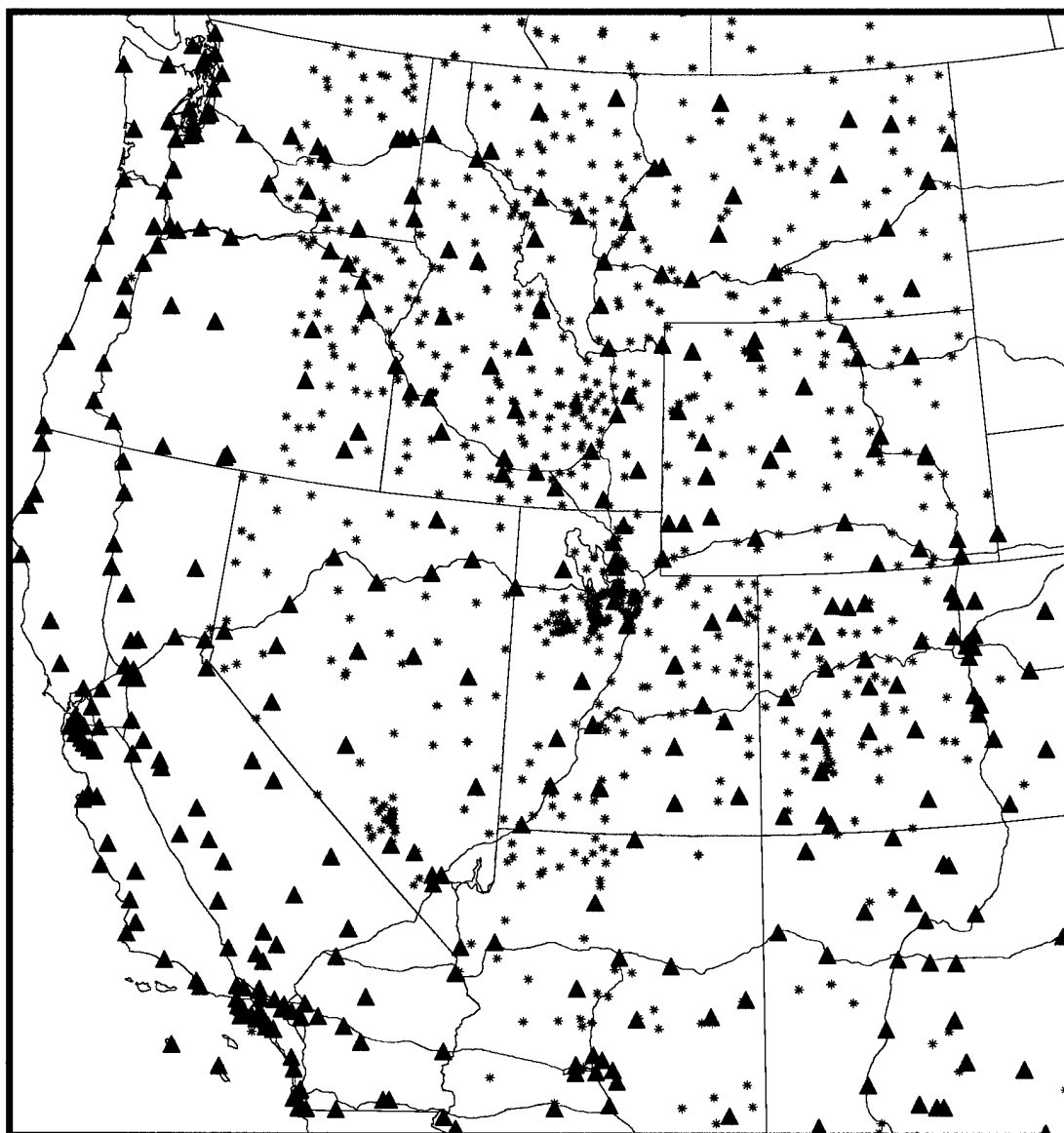


Figure 2.1. Location of MesoWest surface observation sites available December 1998. Green triangles denote locations of National Weather Service/ Federal Aviation Administration sites. Asterisks denote additional MesoWest sites.

Rapid Update Cycle (RUC2; Benjamin et al. 1991,1994) and conventional rawinsonde observations from the western United States. Originally featuring a horizontal resolution of 40 km, RUC2 analyses were downloaded and archived at the University of Utah on a grid featuring 60-km horizontal, 25-hPa vertical, and 1-h temporal resolution. Radar images used for analysis were generated using GEMPAK from data that were received and archived at the University of Utah in NEXRAD Information Dissemination Service (NIDS) format (Baer 1991). Composite radar images for the western United States were generally available every 10 min and featured a spatial resolution of 2 km. The NIDS product suite provided information on 16 categories of reflectivity values (Baer 1991; Crum et al. 1993), resulting in an approximate data resolution of 5 dBZ. Visible and infrared satellite images were displayed using GEMPAK from digital data archived at the University of Utah that was originally obtained from the Space Science and Engineering Center (SSEC) at the University of Wisconsin-Madison and the Scientific Services Division of the National Weather Service Western Region.

Surface Analysis Methods

The methods used to perform manual surface analyses were selected to minimize the problems created by the complex topography of the western United States. It has been shown that numerous problems are created when station pressure is reduced to sea level (e.g., Sangster 1960; Benjamin and Miller 1990; Mass et al. 1991). To mitigate these problems, surface analyses feature contours of pressure at 1500 m, a level roughly corresponding to the mean elevation of lowland stations in the Great Basin. Such an approach was recommended by Pauley (1998) to minimize pressure reduction errors. The

1500 m pressure was calculated by determining the station pressure from the altimeter setting and then using the U. S. Standard Atmosphere to reduce or extrapolate this value to 1500 m.

Additional complications arise from the definition and identification of surface based fronts in an area of complex terrain. We have adopted the traditional definition of a front as an elongated zone of strong horizontal temperature gradient (e.g., Bluestein 1986; Keyser 1986), but note that there are many apparent problems when applying this definition to the analysis of observational data (e.g., Petterssen 1940; Mass 1991; Uccellini et al. 1992; Sanders and Doswell 1995; Sanders 1999). The first concern is what constitutes a strong horizontal temperature gradient. Sanders (1999) arbitrarily chose a value of $8\text{ }^{\circ}\text{C (110 km)}^{-1}$ and applied this threshold to several cases using conventional data. One problem with this approach, however, is that conventional data often does not possess sufficient spatial resolution to determine the magnitude of the horizontal temperature gradient associated with the front. This is illustrated by Figs. 2.2 and 2.3, which compare horizontal analyses over southern Idaho at 0600 UTC 3 December 1998 derived using standard National Weather Service/Federal Aviation Administration (NWS/FAA) network (Fig. 2.2) to high-density MesoWest observations (Fig. 2.3). The analysis in Fig. 2.2 places the cold front coincident with the largest temperature gradient evident in the observations. A pressure trough is analyzed corresponding to the wind shift that is accompanied by little change in temperature. The addition of MesoWest data, however, reveals that the wind shift evident in the western Snake River Plain in Figs. 2.2 and 2.3 is coincident with a horizontal temperature gradient, as shown by the $13\text{ }^{\circ}\text{C}$ observations just south of the frontal placement (Fig. 2.3). Although this well-defined front would not meet

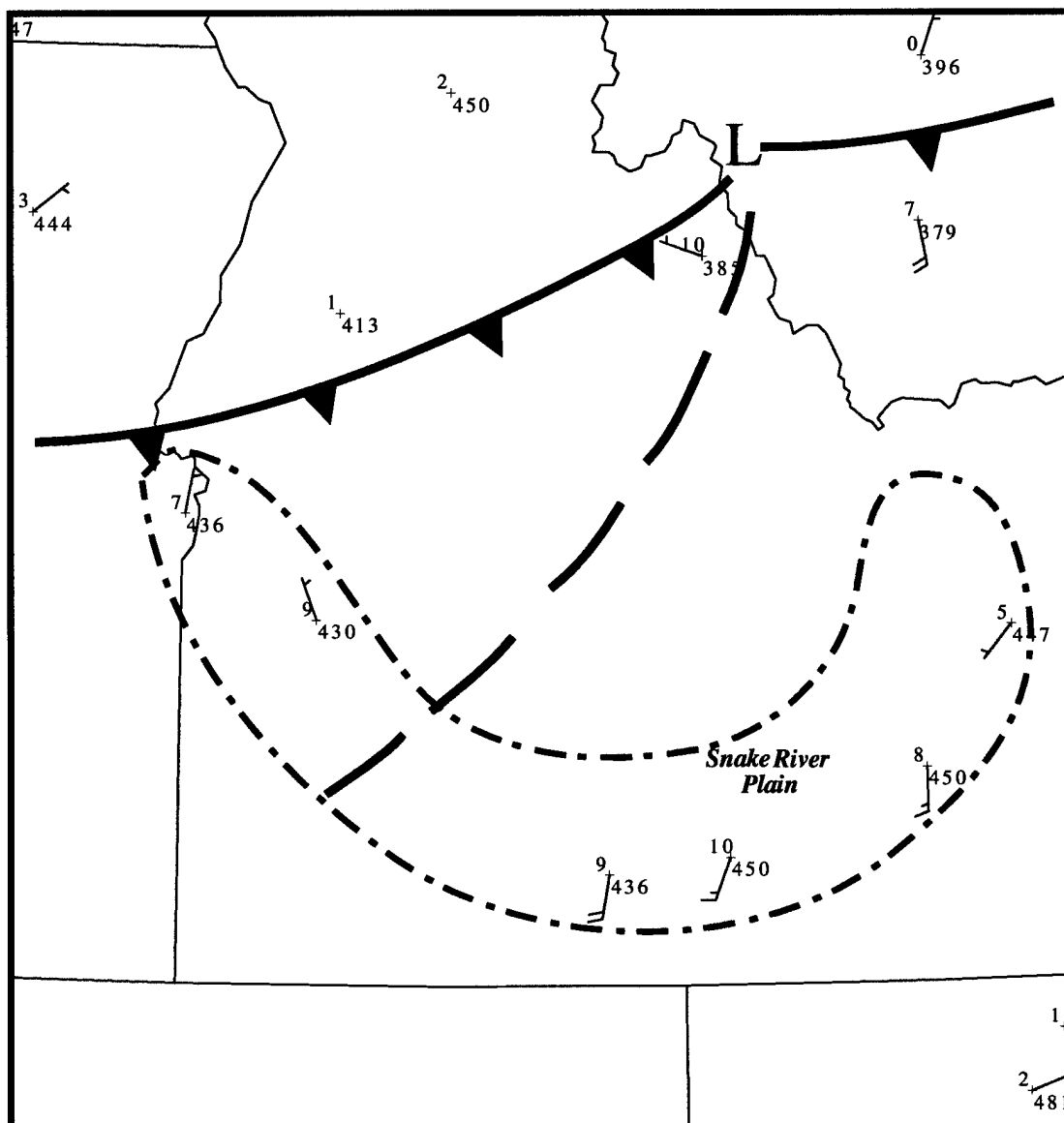


Figure 2.2. Subjective surface analysis for 0600 UTC 3 December, over southern Idaho using only NWS/FAA observations. Dot-dashed line marks boundary of lower elevation Snake River Plain.

the Sanders (1999) frontal definition when only conventional data were available, high density data reveal a temperature difference of 4 °C across the front, which is very near Sanders' (1999) specified 8 °C (110 km)⁻¹. Time series using coarse temporal resolution data (e.g., 1 h resolution) can also obscure significant frontal passages. For example, Fig. 2.4 compares meteograms from the University of Utah (WBB; see Fig. 2.5 for location) that were generated using 5-min resolution and 1-h resolution data. The 5-min resolution meteogram shows a period of cooling around 1300 UTC, which was produced by evaporative cooling due to the onset of precipitation, and the passage of the leading edge of the cold front at 1420 UTC (Fig. 2.4a). In contrast, the meteogram based on 1-h data shows only a gradual fall in temperature from 1300–1600 UTC, greatly reducing the ability to determine strength of the front and its time of passage (Fig. 2.4b).

A second concern is the utility of using surface observations to identify frontal temperature gradients. As noted by Petterssen (1940) and Sanders (1999), diabatic effects and local boundary layer processes can often obscure airmass changes associated with frontal passages. This is particularly problematic in regions of complex terrain where wind fields may be terrain induced and strong temperature inversions are common in lowland regions at night or during the winter months. If an inversion is present at a lowland station, temperatures may rise with cold frontal passage when warmer air from aloft mixes to the surface. Nearby stations may, however, be more representative of large-scale airmass changes either because of their altitude or because local conditions prevented the development of the surface inversion. For example, Fig. 2.6 compares meteograms from two lowland stations in the Snake River Valley that are approximately 60 km apart. The prefrontal environment at Richfield (RHF; see Fig. 2.5 for location) is characterized by

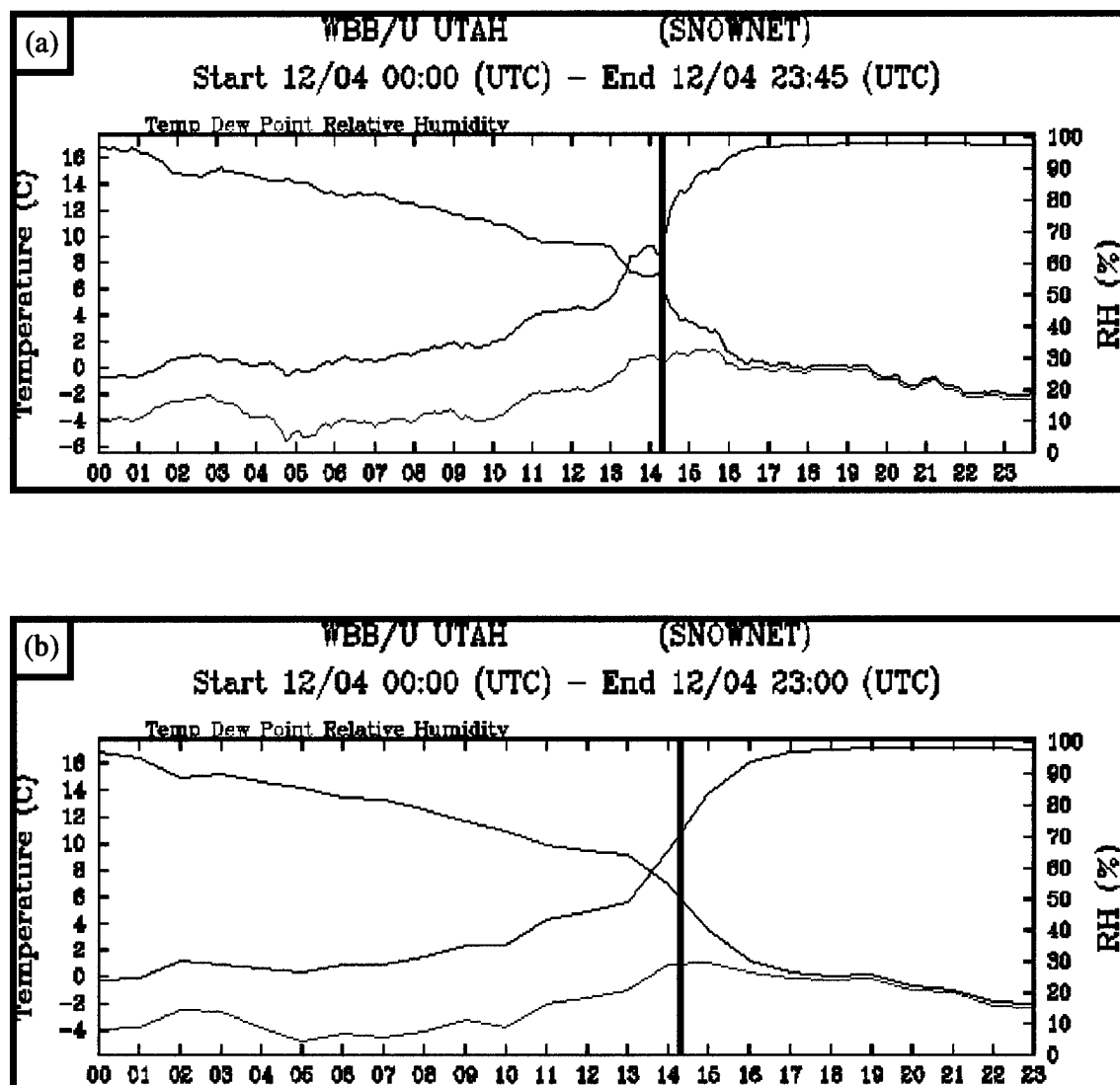


Figure 2.4. Meteograms of temperature (red), dew point (green), and relative humidity (blue), at the University of Utah (WBB; see Fig. 2.5 for location) from 0000-2345 UTC 4 December 1998 based on (a) 5-min observations and (b) 1-h observations. Solid lines denote frontal passage.

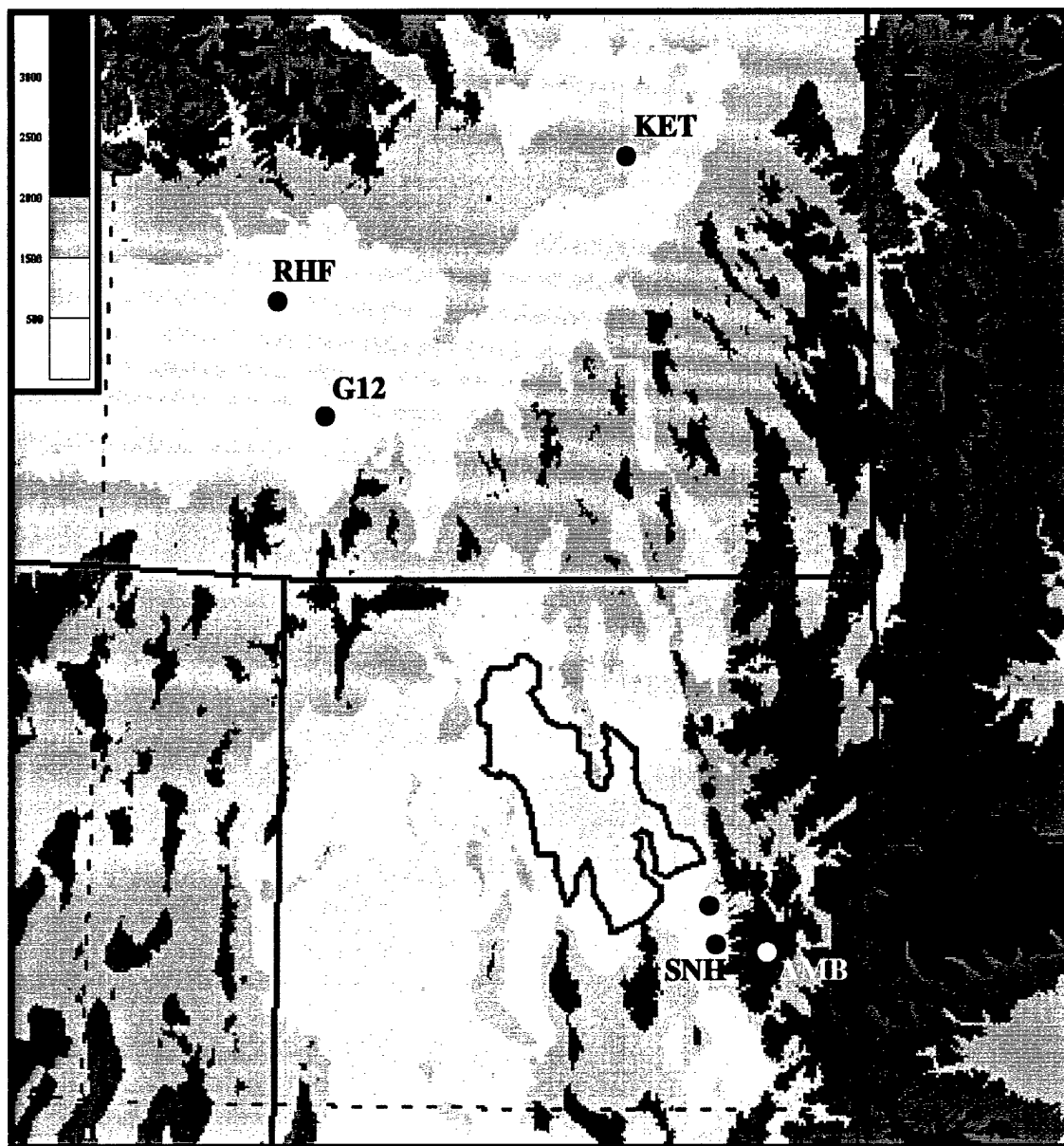


Figure 2.5. Location of MesoWest stations discussed in Chapter 2 including Mt. Baldy, UT (AMB), Sandy, UT (SNH), University of Utah, UT (WBB), Richfield, ID (RHF), Rupert, ID (G12), and Kettle Butte, ID (KET). Elevation (m) shaded according to scale at upper left.

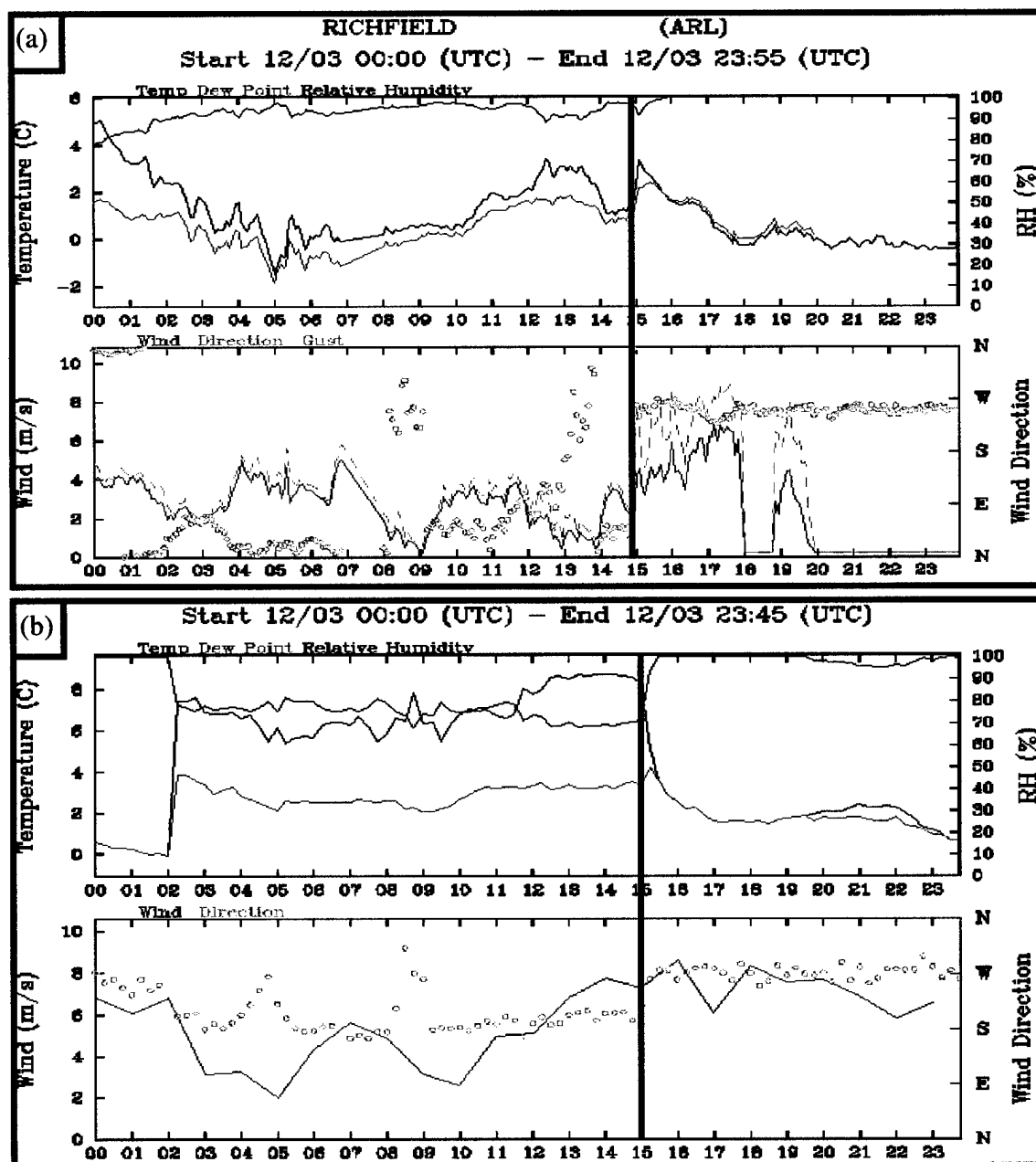


Figure 2.6. Meteograms of temperature (red), dew point (green), relative humidity (blue), wind speed (solid), wind gust (dashed), and wind direction (open circles) at (a) Richfield, ID (RHF) and (b) Rupert, ID (G12; see Fig. 2.5 for locations) from 0000-2355 UTC 4 December 1998. Solid lines denote frontal passage.

light, generally northeasterly winds, temperatures near 2-4 °C, and dew point depressions of less than 2 °C (Fig. 2.6a). Because of the presence of a nocturnal inversion, temperatures at RHF rose 3 °C with frontal passage as warmer air from aloft was mixed to the surface. Conversely, Rupert (G12; see Fig. 2.5 for location) experienced pronounced prefrontal southerly winds, temperatures from 5-7 °C, and dew-point depressions of greater than 3 °C (Fig. 2.6b). A nocturnal inversion did not develop at this location and, as a result, the meteogram was more representative of the large-scale airmass change.

Additional complications arise in some cases where high elevation observations experience a weaker and delayed frontal passage compared to valley locations. This is shown in Fig. 2.7, which compares meteograms from Sandy (SNH) and Mt. Baldy (AMB; see Fig. 2.5 for locations). These two stations are only 15 km apart but vary in altitude by almost 2000 m. The sharp frontal passage shortly before 1600 UTC at SNH is not evident at AMB, where instead a gradual veering from southerly to westerly flow is observed. Finally, terrain-induced circulations, which can be thermally-driven (e.g., Whiteman 1990) or produced by the dynamic interaction of the topography with the large-scale flow (e.g., Carruthers and Hunt 1990; Durran 1990), can make the identification of horizontal wind shear associated with a front difficult. As shown in Fig. 2.8, southerly winds can dominate the post-frontal flow at Kettle Butte, ID (KET; see Fig. 2.5 for location) as a direct result of terrain channeling into the upper Snake River Plain.

For these reasons, the frontal analyses presented in this study are based on the subjective inspection and integration of all available MesoWest observations using the definition of a front presented above and the constraint of producing an analysis of low-level frontal evolution that is temporally, horizontally, and vertically continuous.

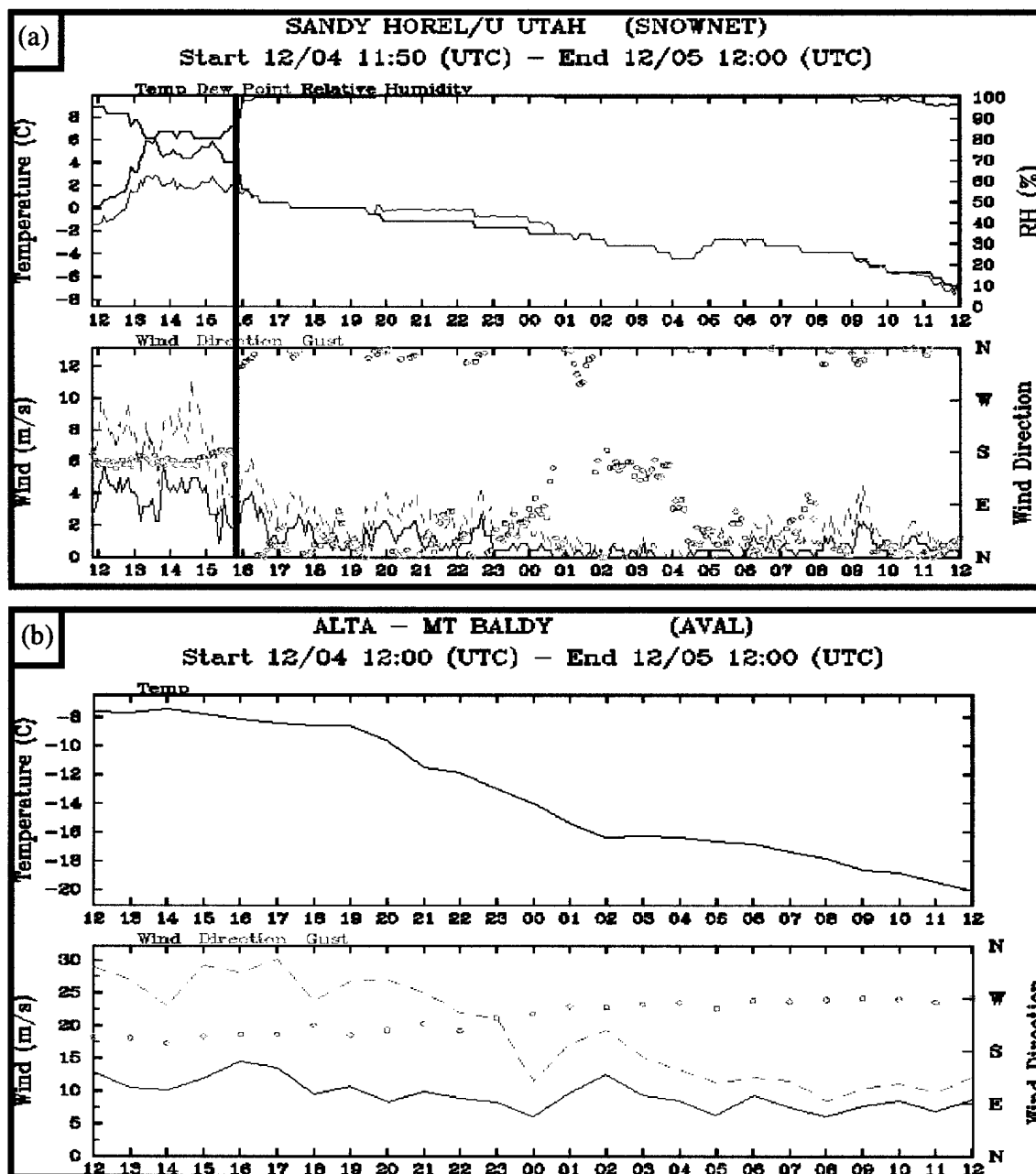


Figure 2.7. Meteograms of temperature (red), dew point (green), relative humidity (blue), wind speed (solid), wind gust (dashed), and wind direction (open circles) at (a) Sandy, UT (SNH) and (b) Mt. Baldy, UT (AMB; see Fig. 2.5 for locations) from 1150 UTC 4 December - 1200 UTC 5 December 1998. Solid line denotes frontal passage.

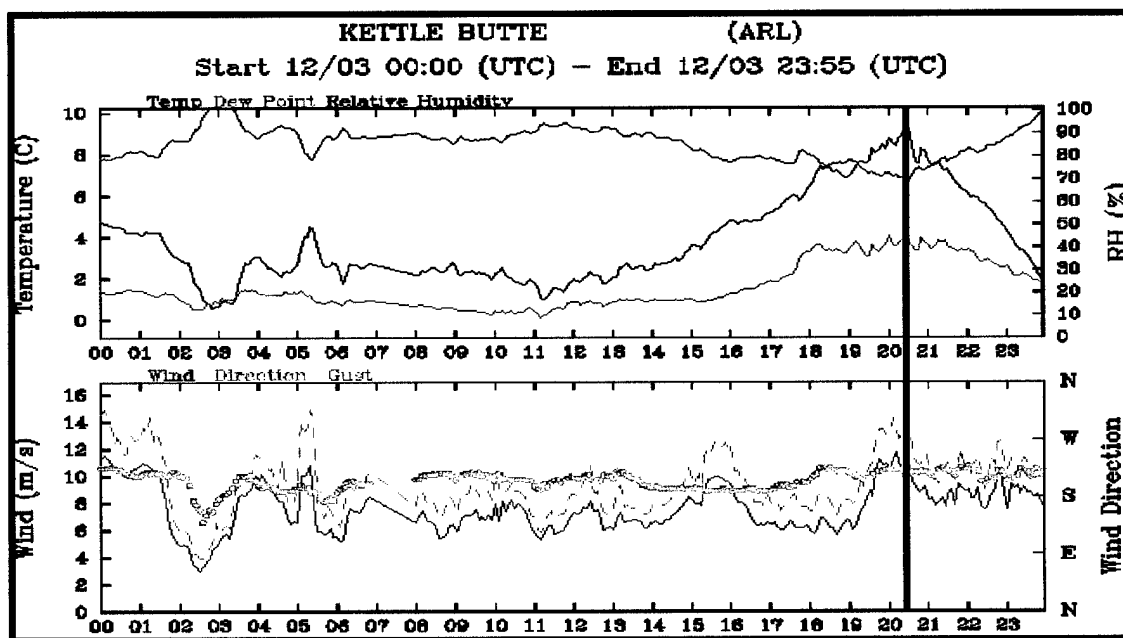


Figure 2.8. Meteograms of temperature (red), dew point (green), relative humidity (blue), wind speed (solid), wind gust (dashed), and wind direction (open circles) at Kettle Butte, ID (KET; see Fig. 2.5 for location) from 0000-2355 UTC 3 December 1998. Solid line denotes frontal passage.

Meteograms of surface observations were used extensively to help identify changes in temperature, humidity, wind direction, and wind speed accompanying frontal passage. Surrounding stations and temporal and spatial continuity were used in some instances to identify frontal positions near surface stations or over mesoscale regions where local surface effects obscured the frontal structure. Since the position of a front may vary with altitude, all analyses over the Great Basin reflect the position of the front at altitudes similar to that of valley or basin locations rather than mountain crest level.

CHAPTER 3

SYNOPTIC-SCALE EVOLUTION

The synoptic pattern prior to the development of the 3–5 December 1998 cyclone featured a strong ($> 80 \text{ m s}^{-1}$) zonally-oriented upper-level jet that was located over the northwest United States, southwest Canada, and the eastern Pacific (not shown). Associated with this feature was a broad baroclinic zone that extended through much of the troposphere between 45° and 50° N. By 1200 UTC 2 December, the upper-level pattern was beginning to amplify (Fig. 3.1). A 500-hPa absolute vorticity maximum was centered over Washington (Fig. 3.1b), while a surface-based cold front stretched from a Gulf of Alaska cyclone (not explicitly shown) through British Columbia and the northwest United States (Fig. 3.2). A low-level high pressure ridge (based on 1500 m pressure) was elongated over the Great Basin, from central California to the southern Rockies. By 0000 UTC 3 December, the 500-hPa vorticity maximum and poleward portion of the cold front had pushed eastward across the northern Rockies, resulting in lee cyclogenesis over Alberta and Saskatchewan (Figs. 3.3b and 3.4; cyclogenesis not explicitly shown). Further to the south, the cold front was moving equatorward and eastward and now extended from northcentral Montana to the northwest coast of California (Fig. 3.4). Concurrently, the flow was amplifying across the eastern Pacific as an upper-level shortwave trough and associated cyclonic potential vorticity (PV) anomaly, located poleward of the strong baroclinic zone, moved east-southeastward toward the California coastline (Fig. 3.3a,b).

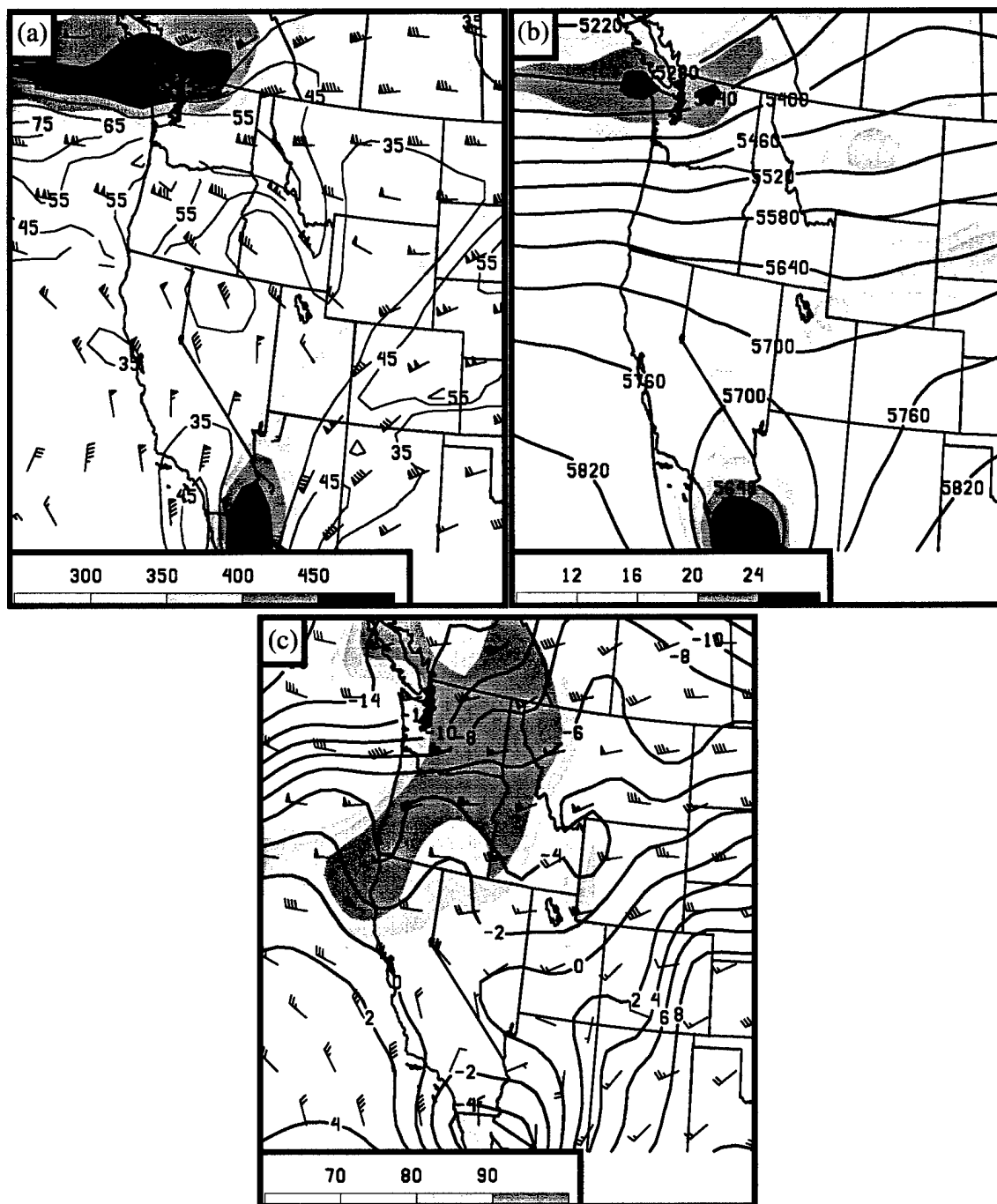


Figure 3.1. RUC2 analysis for 1200 UTC 2 December 1998. (a) Dynamic tropopause pressure (hPa, shaded according to scale at bottom), winds (pennant, full and half barbs denote 25, 5 and 2.5 m s⁻¹, respectively), and isotachs (contours every 10 m s⁻¹ from 35 m s⁻¹, breaks caused by data voids). (b) 500-hPa geopotential height (m) and absolute vorticity (s⁻¹, shaded according to scale at bottom). (c) 700-hPa temperature (°C), relative humidity (%), and wind [as in (a)].

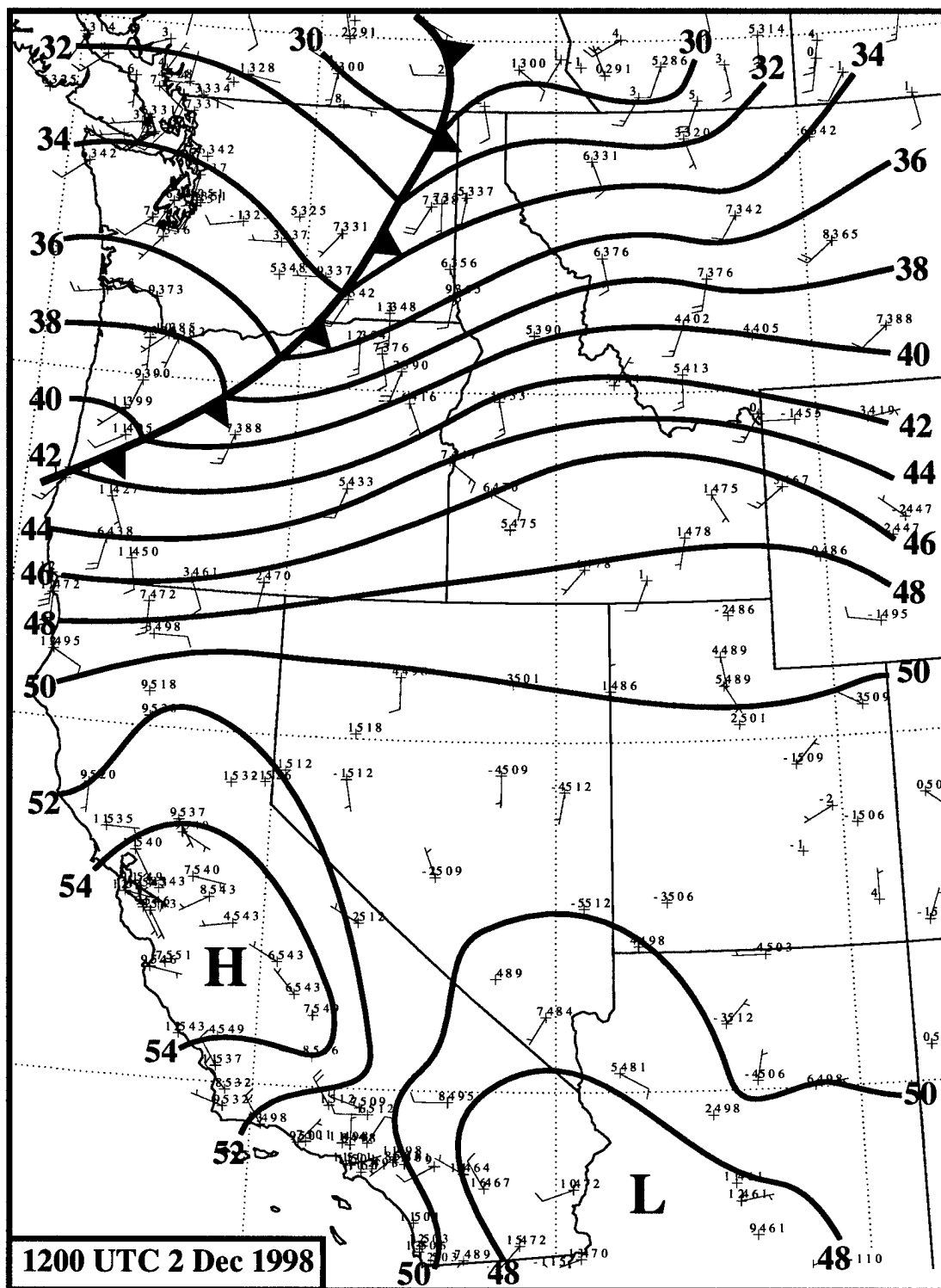


Figure 3.2. Manually analyzed surface map for 1200 UTC 2 December 1998. 1500-m pressure isobars every 2 hPa. Surface station reports include temperature ($^{\circ}\text{C}$, upper left), 1500-m pressure (tenths of hPa with leading 8 truncated), and winds [full (half) barbs denote 5 (2.5) m s^{-1}].

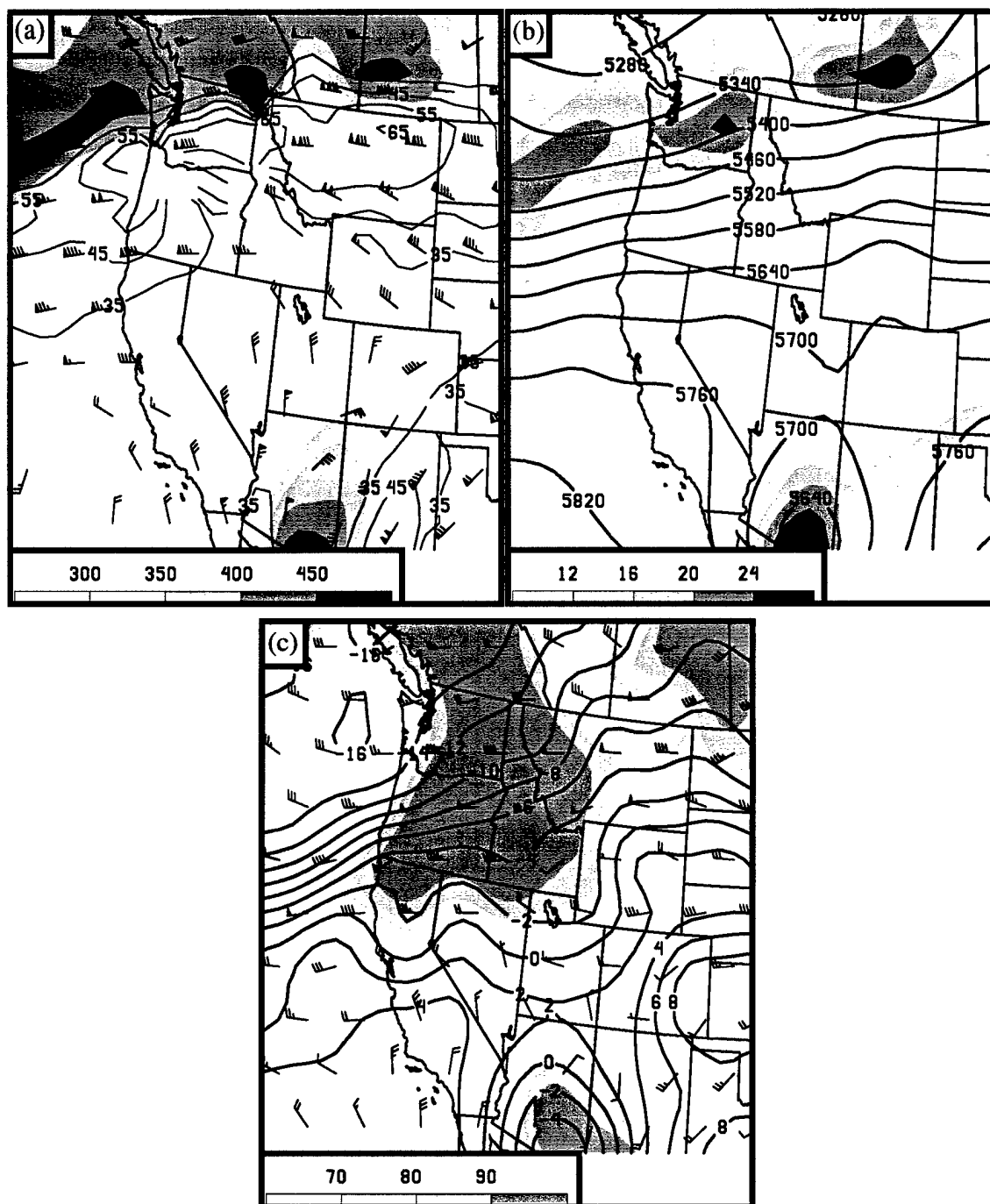


Figure 3.3. RUC2 analysis for 0000 UTC 3 December 1998. (a) Dynamic tropopause pressure (hPa, shaded according to scale at bottom), winds (pennant, full and half barbs denote 25, 5 and 2.5 m s⁻¹, respectively), and isotachs (contours every 10 m s⁻¹ from 35 m s⁻¹, breaks caused by data voids). (b) 500-hPa geopotential height (m) and absolute vorticity (s⁻¹, shaded according to scale at bottom). (c) 700-hPa temperature (°C), relative humidity (%), shaded according to scale at bottom), and wind [as in (a)].

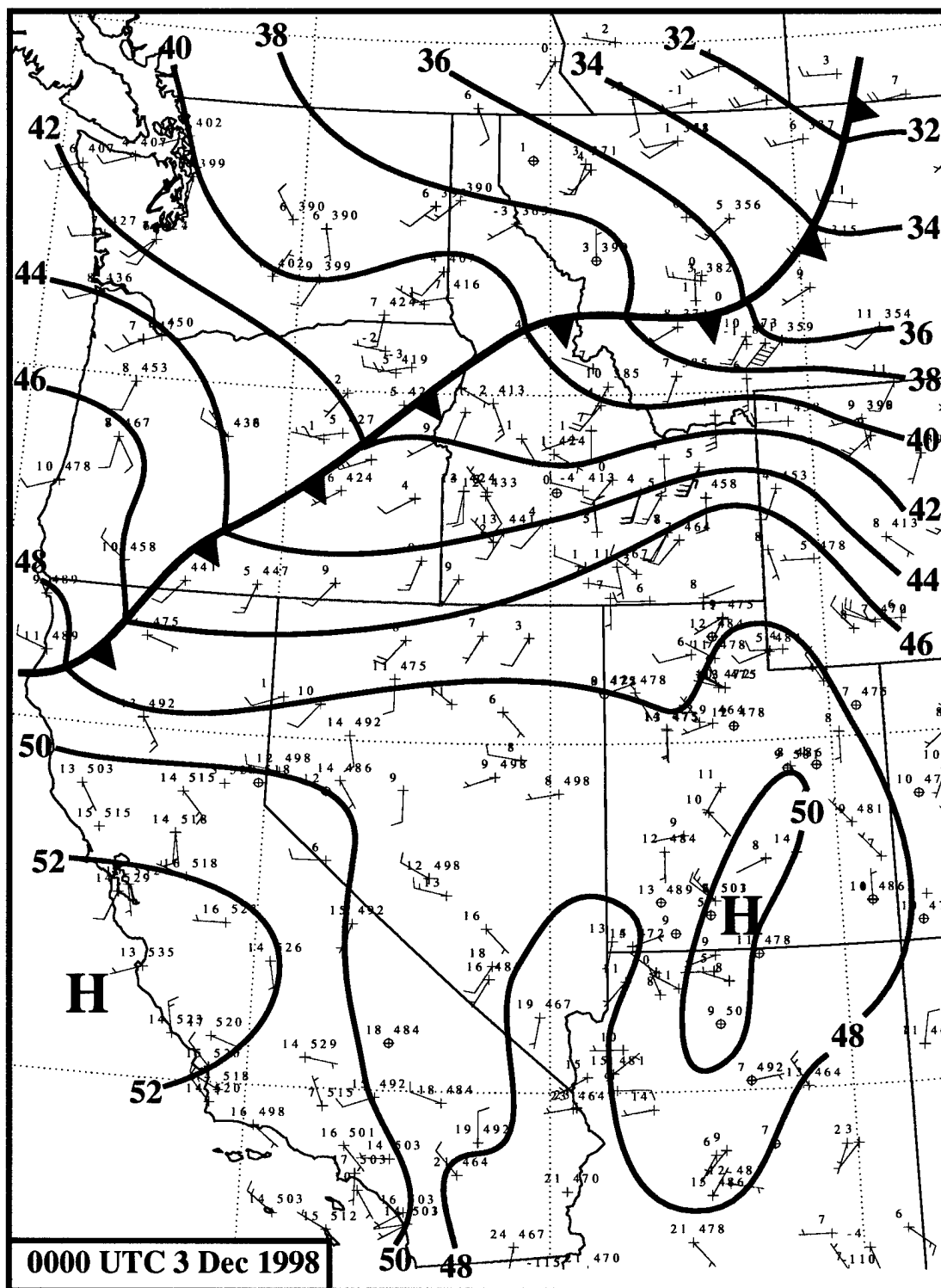


Figure 3.4. Manually analyzed surface map for 0000 UTC 3 December 1998. 1500-m pressure isobars every 2 hPa. Surface station reports include temperature ($^{\circ}\text{C}$, upper left), 1500-m pressure (tenths of hPa with leading 8 truncated), and winds [full (half) barbs denote 5 (2.5) m s^{-1}].

Satellite imagery indicated baroclinic leaf development to the southeast of the strengthening trough with widespread open-cellular convection to the north and east (Fig. 3.5). Radar composites over the western United States showed showery precipitation falling over western Oregon and Washington, while a broad shield of stratiform precipitation was falling over northwest California and southern Oregon, immediately north of the surface frontal boundary (Fig. 3.6).

By 1200 UTC 3 December, the upper-level trough and cyclonic PV anomaly axis were located over the Pacific northwest (Figs. 3.7a,b; PV anomaly labeled with an X and dashed line), and the cold front was developing considerable mesoscale structure over the western United States (Fig. 3.8). Over southern Idaho, the front was moving rapidly up the Snake River Plain, apparently due to topographic channeling, and displayed a distinct eastward bulge in this region. A 1500-m pressure minimum was also beginning to develop in this region along the Idaho-Montana border. Further to the west, the front was draped along the Nevada-Oregon border with another distortion of the front across northern California where the front was moving rapidly equatorward west of the Sierra Nevada and along the coast. Clouds across the western United States were coincident with or north of the cold front (Fig. 3.9). To the south of the cold front, very dry air was located over the Great Basin, as evidenced by the 1200 UTC sounding from Desert Rock (located in the southern part of Nevada) which featured an 18 °C dew point depression at 700 hPa (not shown). Precipitation was also confined to along or north of the front (Fig. 3.10), with a broad shield of precipitation extending from the San Francisco Bay area, north to Klamath Falls, OR (LMT) and then northeast toward Boise, ID (BOI). Although large gaps in the radar coverage existed over southcentral and southeastern Oregon, surface observations

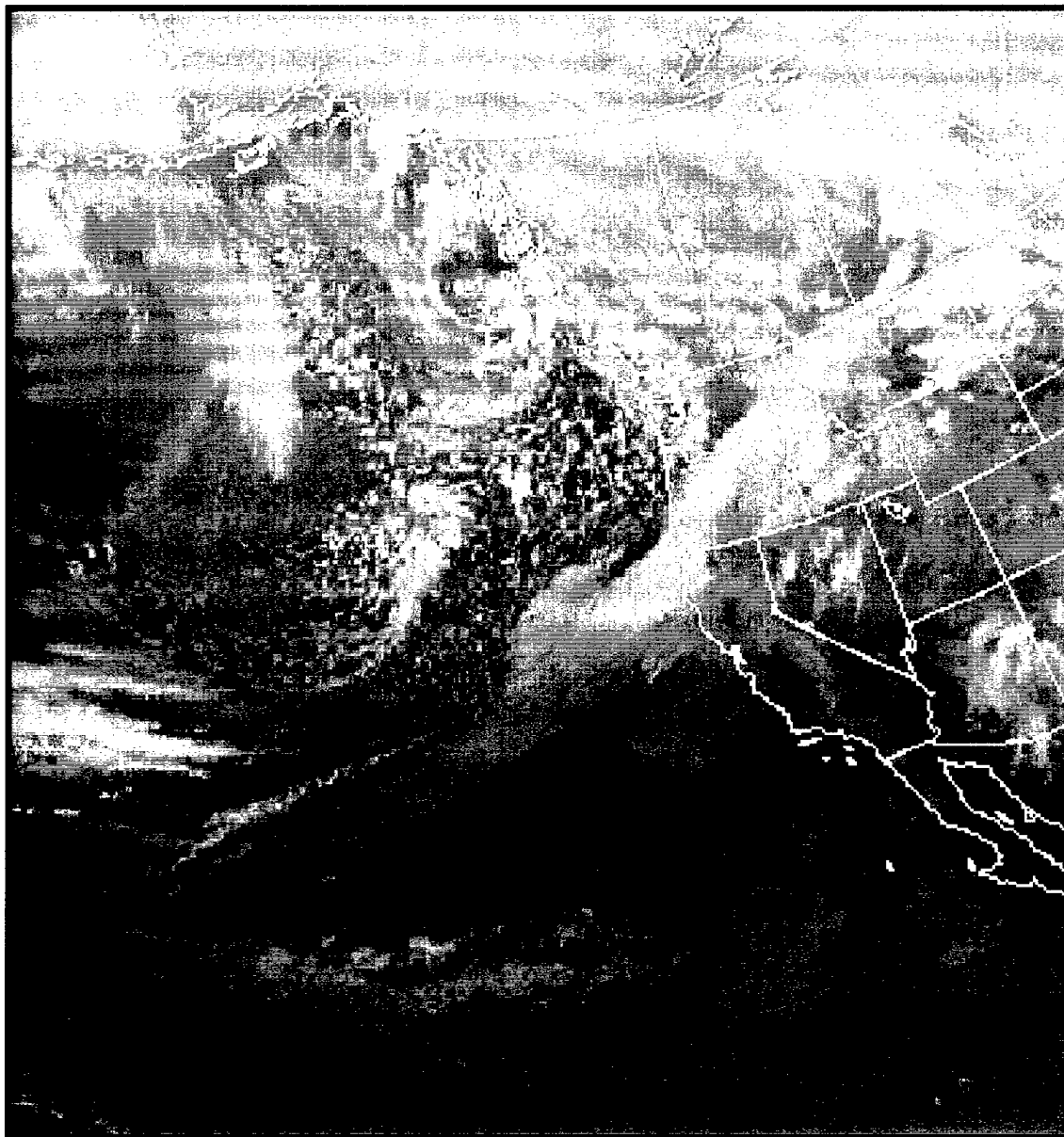


Figure 3.5. Infrared satellite imagery for 0000 UTC 3 December 1998.

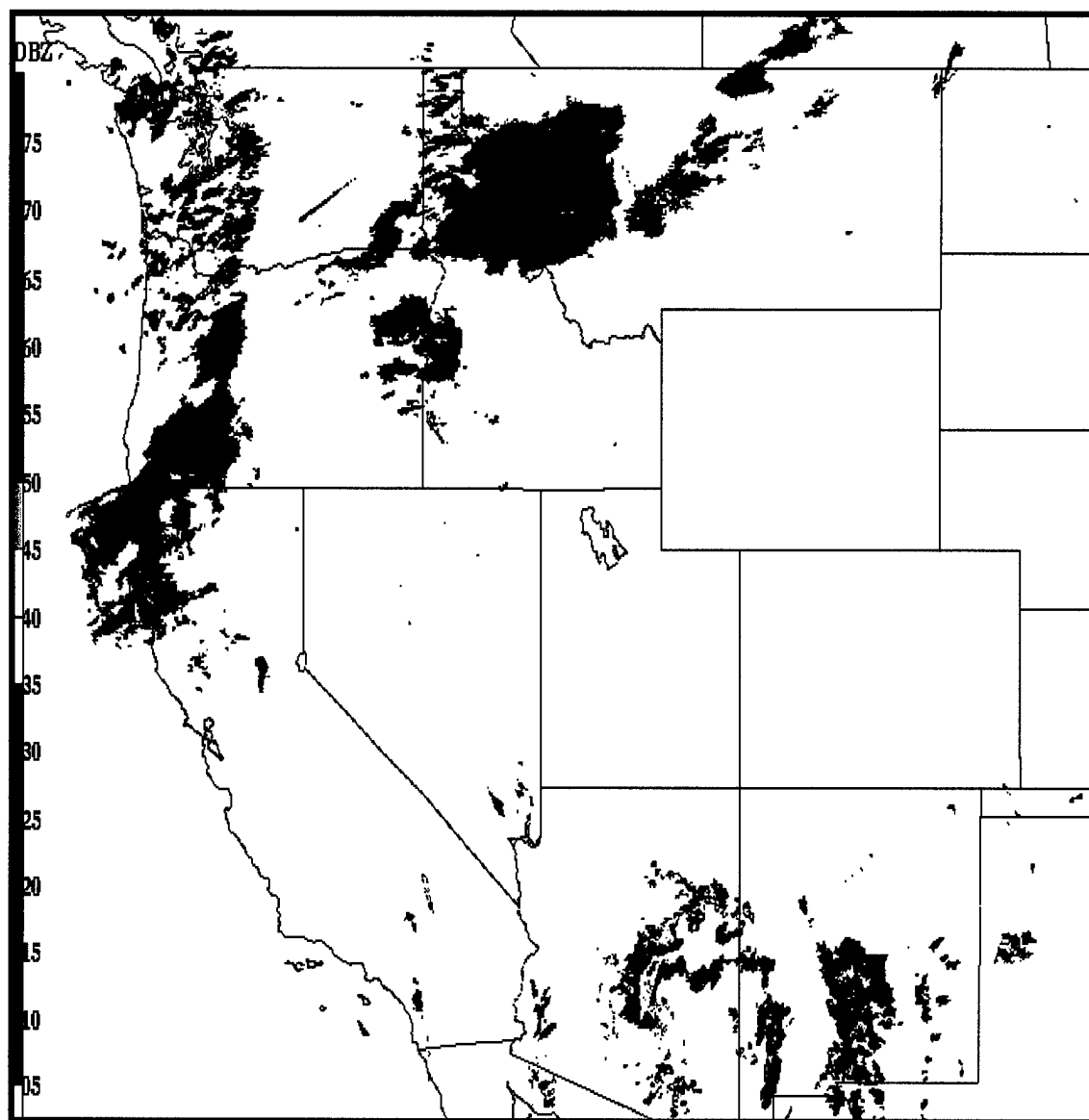


Figure 3.6. Composite NEXRAD imagery for 0000 UTC 3 December 1998.

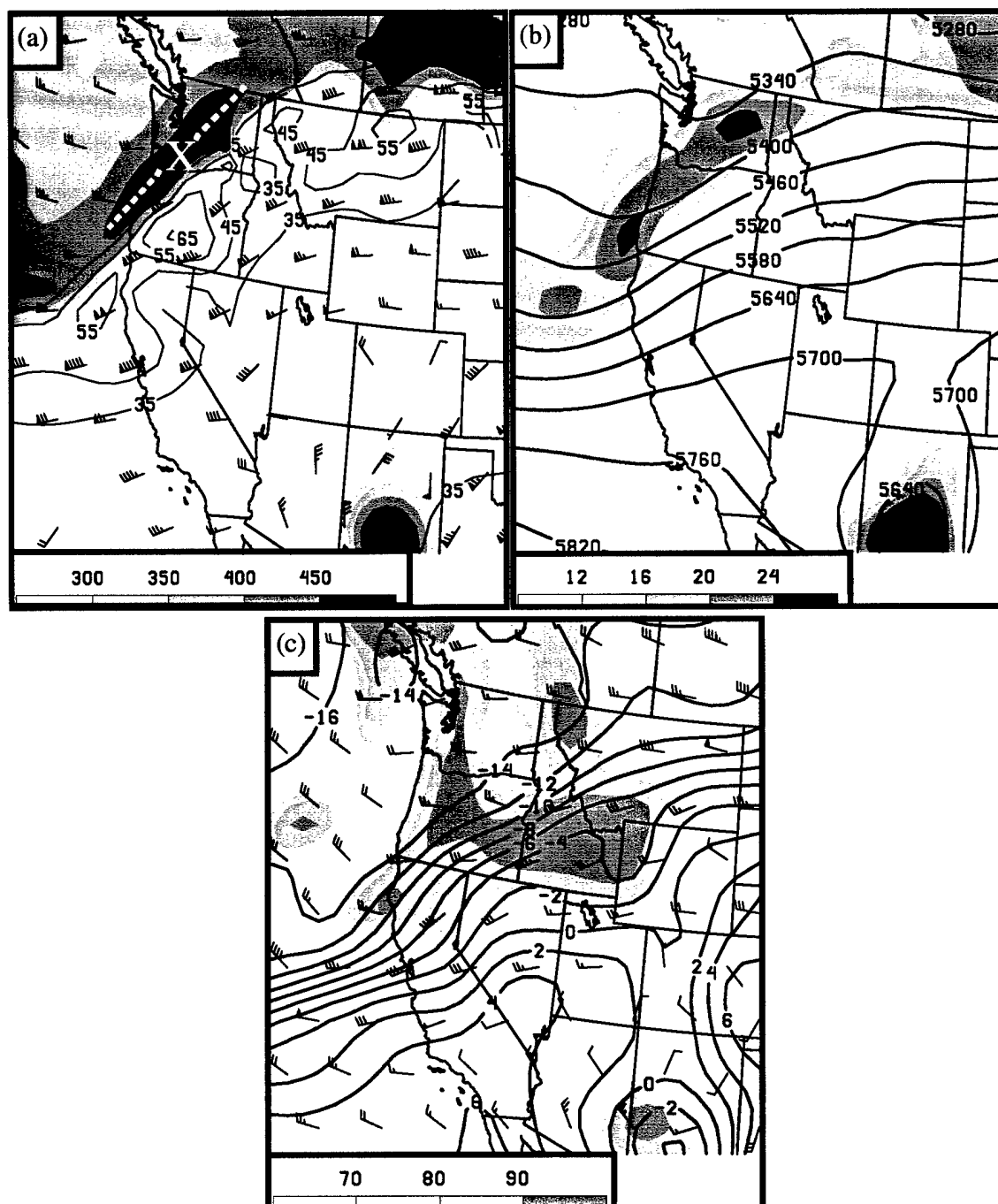


Figure 3.7. RUC2 analysis for 1200 UTC 3 December 1998. (a) Dynamic tropopause pressure (hPa, shaded according to scale at bottom), winds (pennant, full and half barbs denote 25, 5 and 2.5 m s⁻¹, respectively), and isotachs (contours every 10 m s⁻¹ from 35 m s⁻¹, breaks caused by data voids). (b) 500-hPa geopotential height (m) and absolute vorticity (s⁻¹, shaded according to scale at bottom). (c) 700-hPa temperature (°C), relative humidity (%), shaded according to scale at bottom, and wind [as in (a)].

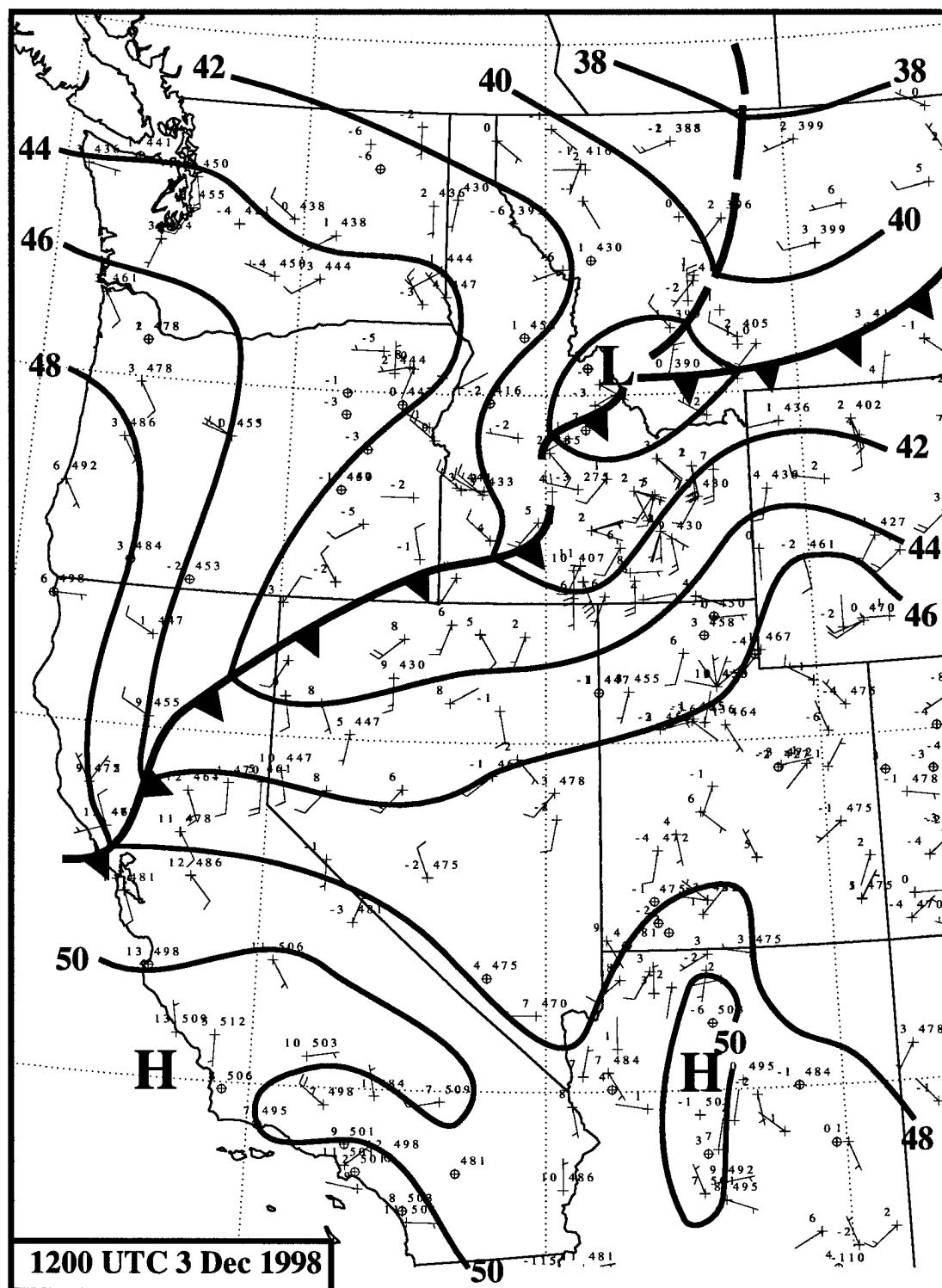


Figure 3.8. Manually analyzed surface map for 1200 UTC 3 December 1998. 1500-m pressure isobars every 2 hPa. Surface station reports include temperature ($^{\circ}\text{C}$, upper left), 1500-m pressure (tenths of hPa with leading 8 truncated), and winds [full (half) barbs denote 5 (2.5) m s^{-1}].

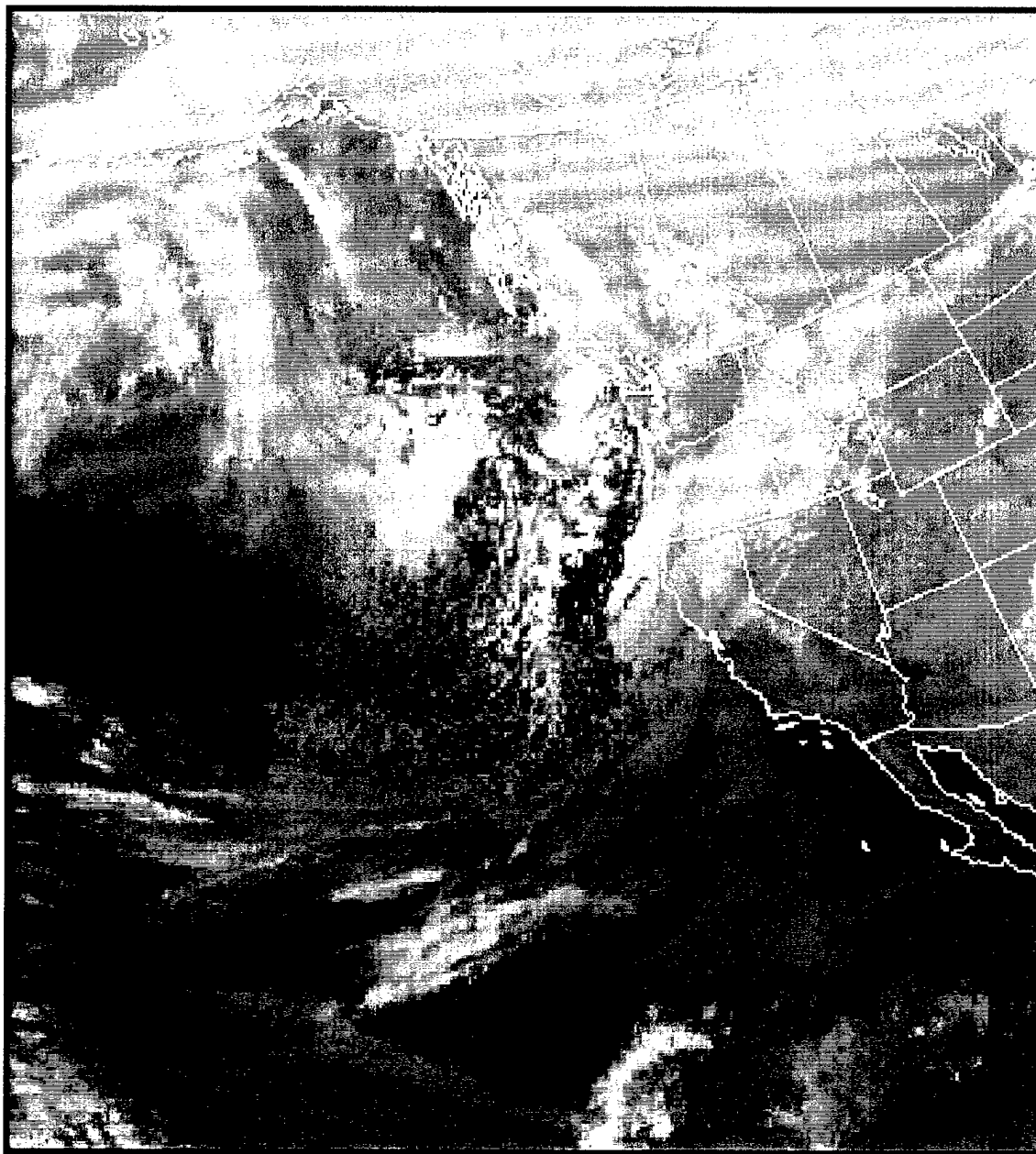


Figure 3.9. Infrared satellite imagery for 1200 UTC 3 December 1998.

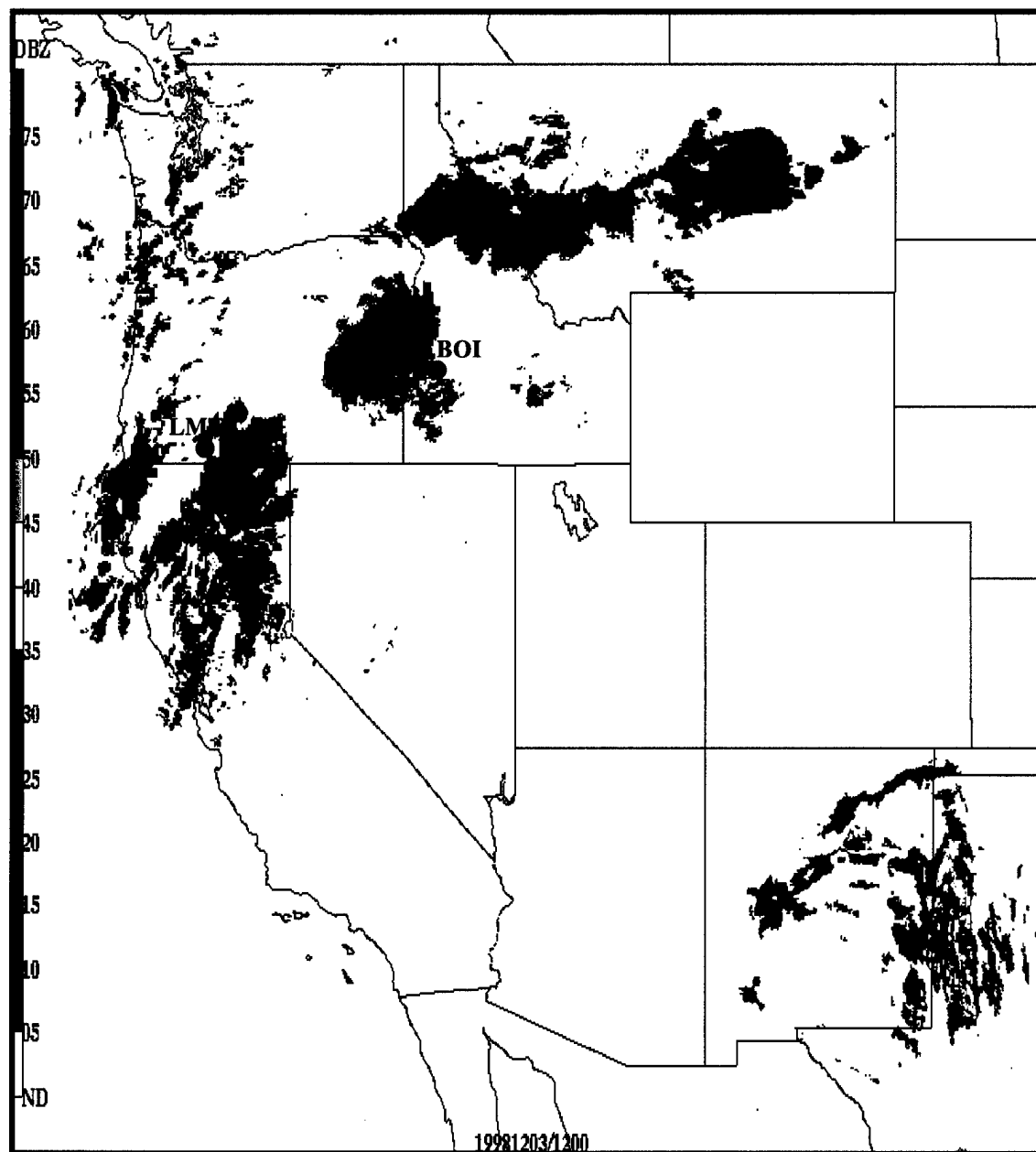


Figure 3.10. Composite NEXRAD imagery for 1200 UTC 3 December 1998.

confirmed the continuity of frontal precipitation across this region. Although difficult to discern in Fig. 3.10, a narrow cold frontal rainband was evident along the cold front over northern California.

As the 500-hPa trough moved southeastward along the west coast, southwesterly cross-barrier flow intensified over the Sierra Nevada. With the approach of the upper-level trough and associated cyclonic PV anomaly, and the development of downslope flow to the lee of the Sierra Nevada, cyclogenesis occurred along the surface cold front as many stations over the Great Basin recorded 1500 m pressure falls at rates of $\sim 1 \text{ mb h}^{-1}$. At 2100 UTC 3 December, a low-pressure center had developed along the cold front over northeastern Nevada, with troughing extending westward along the cold front and southward along the lee side of the Sierra Nevada (Fig. 3.11). During this period (i.e., from 1700-2300 UTC), Bishop, CA, experienced a 10 hPa fall in pressure. Low pressure centers were also evident along the eastern Idaho-Montana border and over north central Wyoming. A distinctive southward progression of the cold front was noted on the backside of the cyclone over central Nevada as cold advection increased in response to the developing cyclone. Likewise, warm advection to the east of the cyclone held the front in a quasi-stationary position over northeast Nevada and northwest Utah. Equatorward movement of the cold front appeared to be substantially faster along the cold front over the California coast than over the Sierra Nevada.

By 0000 UTC 4 December, an elongated cyclonic PV anomaly continued moving east-southeast and was located along the west coast with the associated 500-hPa absolute vorticity maximum located near San Francisco (Figs. 3.12a,b). A second cyclonic PV anomaly was moving southward in the flow on the backside of the trough near 135°W .

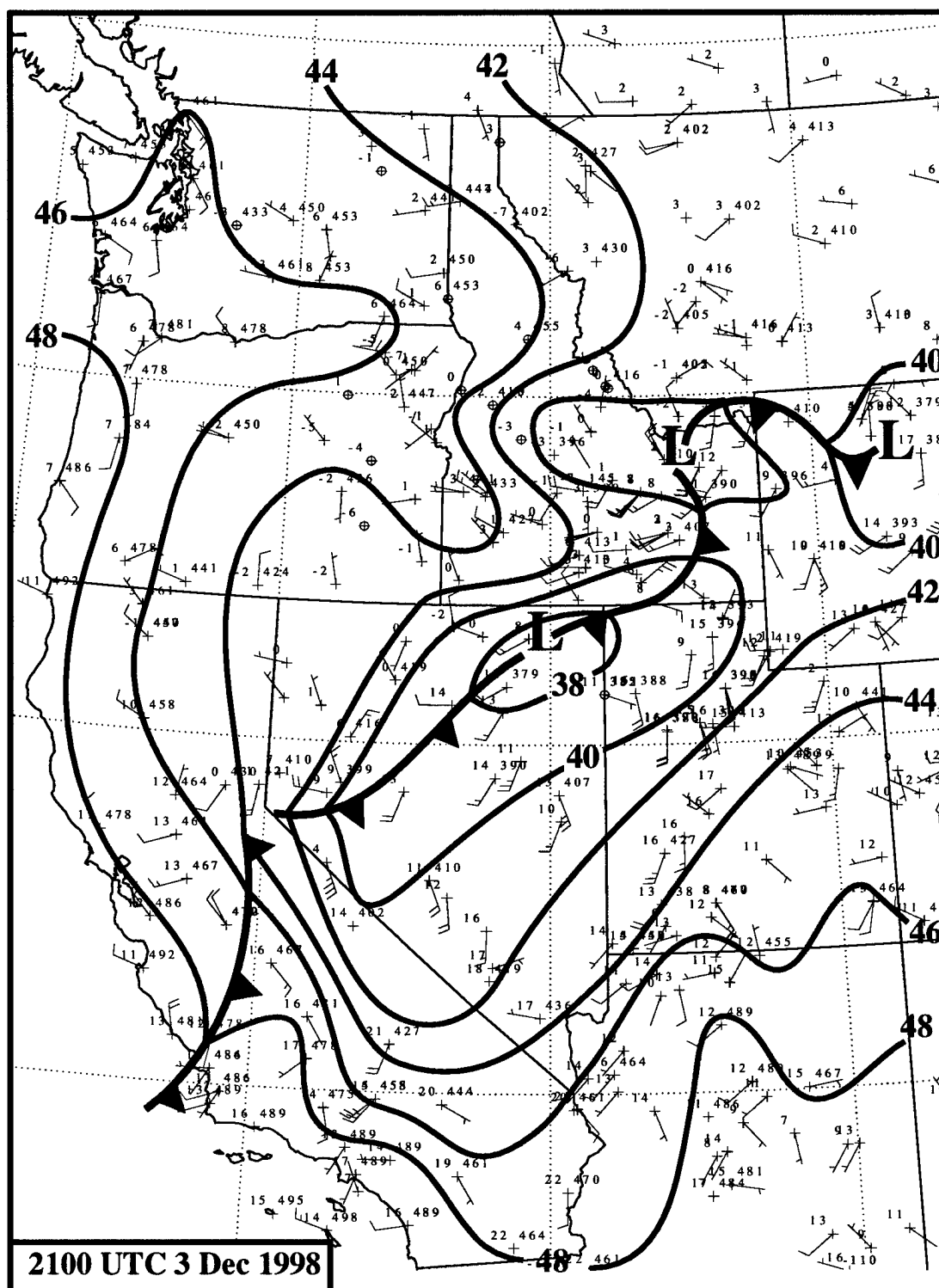


Figure 3.11. Manually analyzed surface map for 2100 UTC 3 December 1998. 1500-m pressure isobars every 2 hPa. Surface station reports include temperature ($^{\circ}\text{C}$, upper left), 1500-m pressure (tenths of hPa with leading 8 truncated), and winds [full (half) barbs denote 5 (2.5) m s^{-1}].

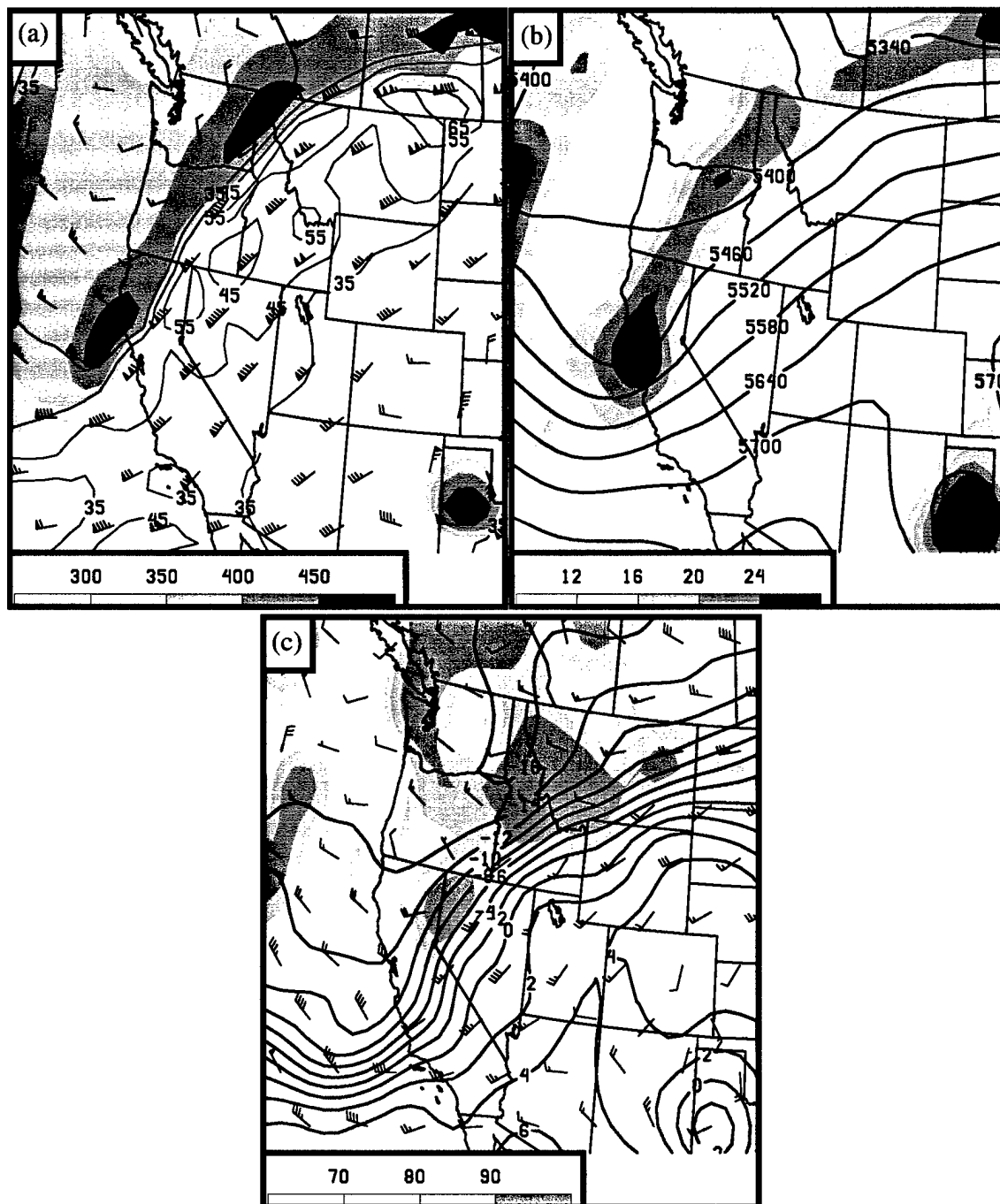


Figure 3.12. RUC2 analysis for 0000 UTC 4 December 1998. (a) Dynamic tropopause pressure (hPa, shaded according to scale at bottom), winds (pennant, full and half barbs denote 25, 5 and 2.5 m s⁻¹, respectively), and isotachs (contours every 10 m s⁻¹ from 35 m s⁻¹, breaks caused by data voids). (b) 500-hPa geopotential height (m) and absolute vorticity (s⁻¹, shaded according to scale at bottom). (c) 700-hPa temperature (°C), relative humidity (%), shaded according to scale at bottom), and wind [as in (a)].

The frontal structure was also becoming more complicated at this time with the northern extent of the front stretching across northern Wyoming into the Upper Snake River Plain of Idaho (Fig. 3.13). Broad troughing extended westward across the central Idaho mountains while the front dropped south and west toward the developing cyclone over northeast Nevada. From the cyclone, the front extended south and west to the Sierra Nevada, approximately 175 km south of Lake Tahoe. The front over interior California was nearly meridionally aligned at this time from the Sierra Nevada mountains to west of Los Angeles. A strengthening pressure gradient was evident south of the front over Utah with surface high pressure centered over northern Arizona. Southerly winds began gusting to 30 m s^{-1} over high elevation (above 2500 m) stations in the Wasatch mountains of northern Utah while most lower elevation stations in northern Nevada and Utah recorded gusts from $15\text{--}25 \text{ m s}^{-1}$. Cloudiness and precipitation continued to be confined near and to the north of the front from Lake Tahoe to northwest Wyoming (Figs. 3.14 and 3.15).

As the upper level pattern continued to evolve (1200 UTC 4 December), the second shortwave trough and associated PV anomaly rotated down the backside of the larger-scale trough off the California coast while the first shortwave trough moved northeast across Nevada (Fig. 3.16). The location and subsequent movement of the second shortwave trough possibly played a role in limiting the strength of the lead shortwave trough. As this second trough pushed further south, the lead trough continued to weaken significantly and moved rapidly east–northeast toward southern Idaho. The surface cyclone was located over northern Utah while surface high pressure began building in from the Pacific northwest, southward into the central valleys of California and eastward into the Snake River Plain (Fig. 3.17). Concurrently, pressures were increasing over

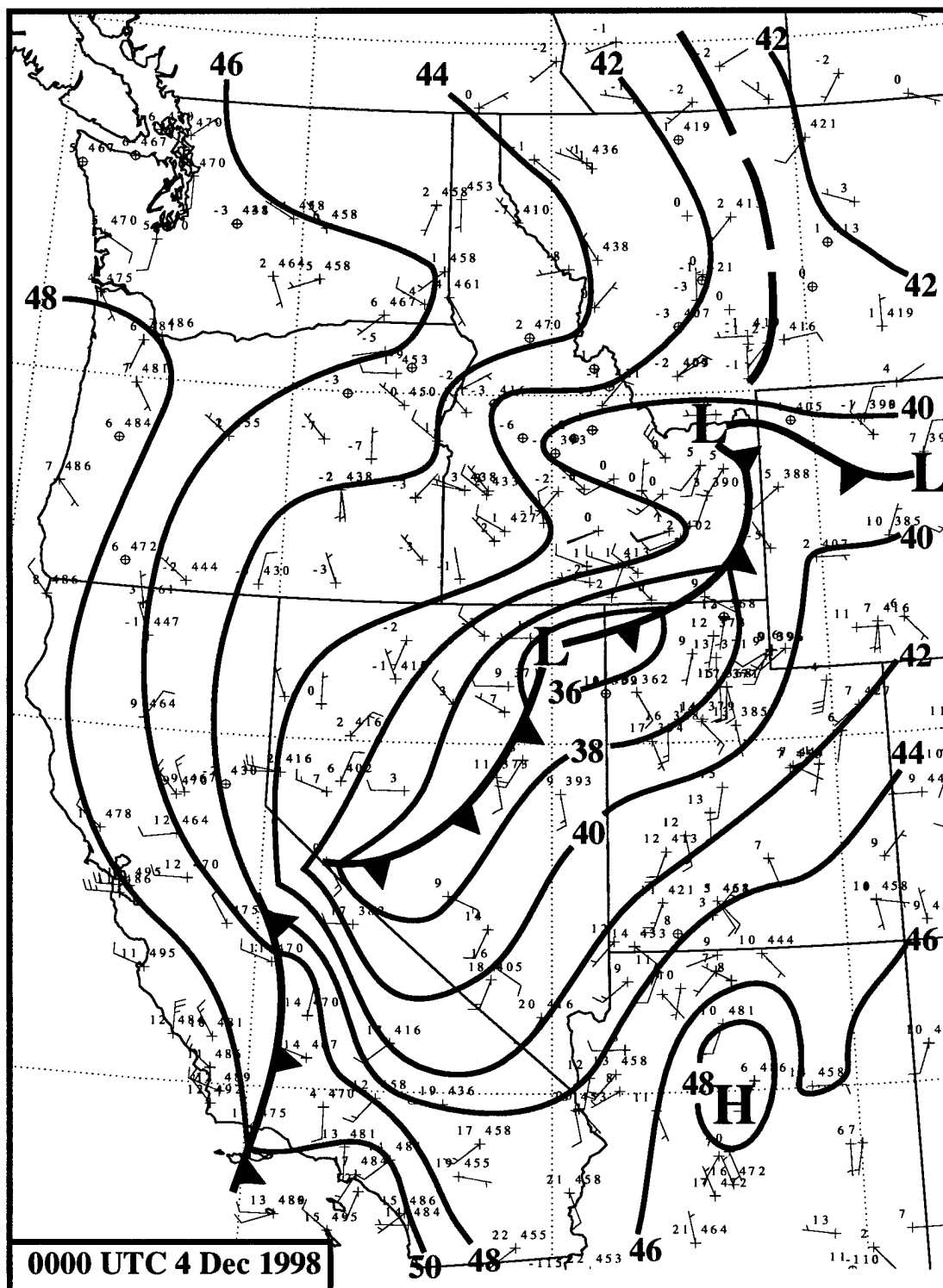


Figure 3.13. Manually analyzed surface map for 0000 UTC 4 December 1998. 1500-m pressure isobars every 2 hPa. Surface station reports include temperature ($^{\circ}\text{C}$, upper left), 1500-m pressure (tenths of hPa with leading 8 truncated), and winds [full (half) barbs denote 5 (2.5) m s^{-1}].

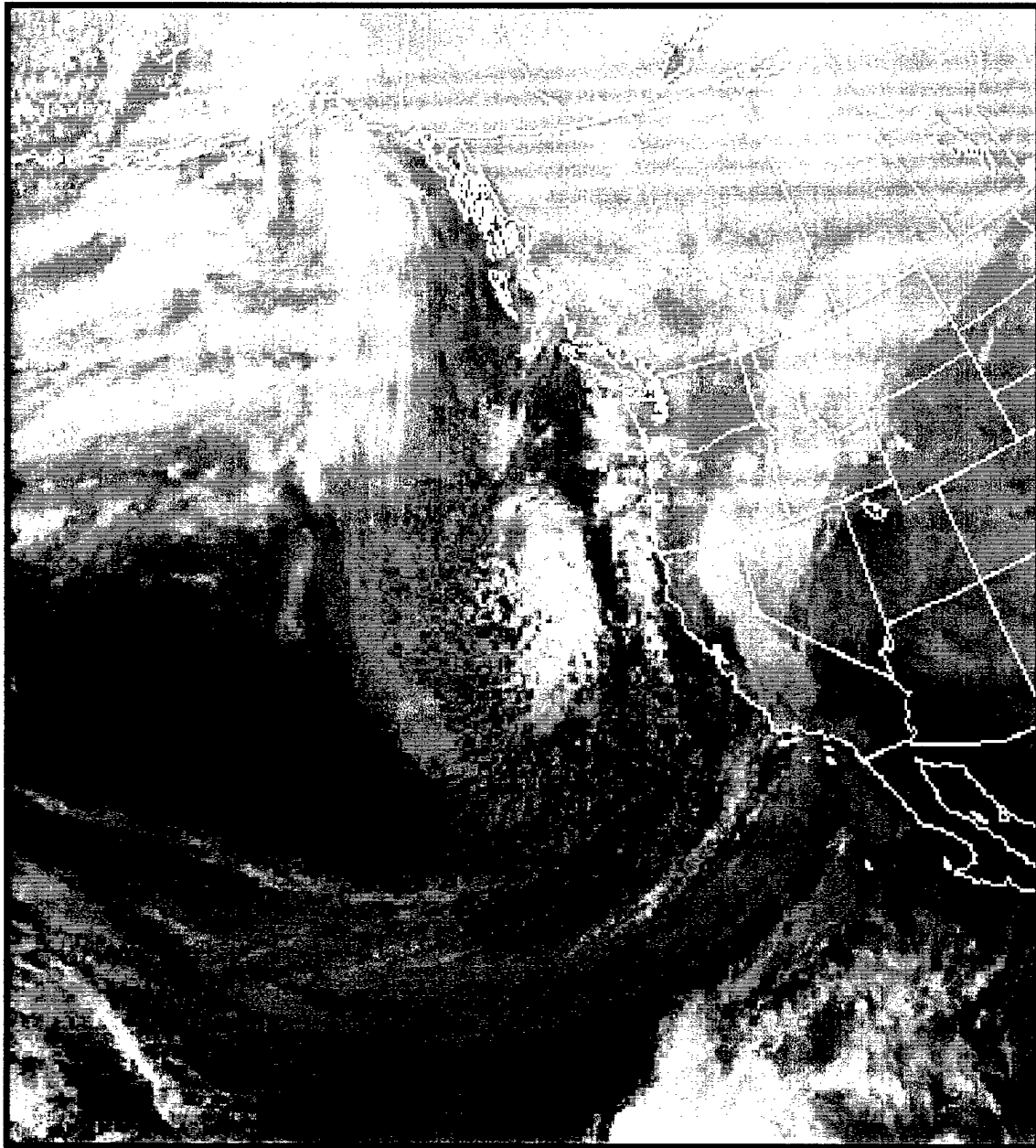


Figure 3.14. Infrared satellite imagery for 0000 UTC 4 December 1998.

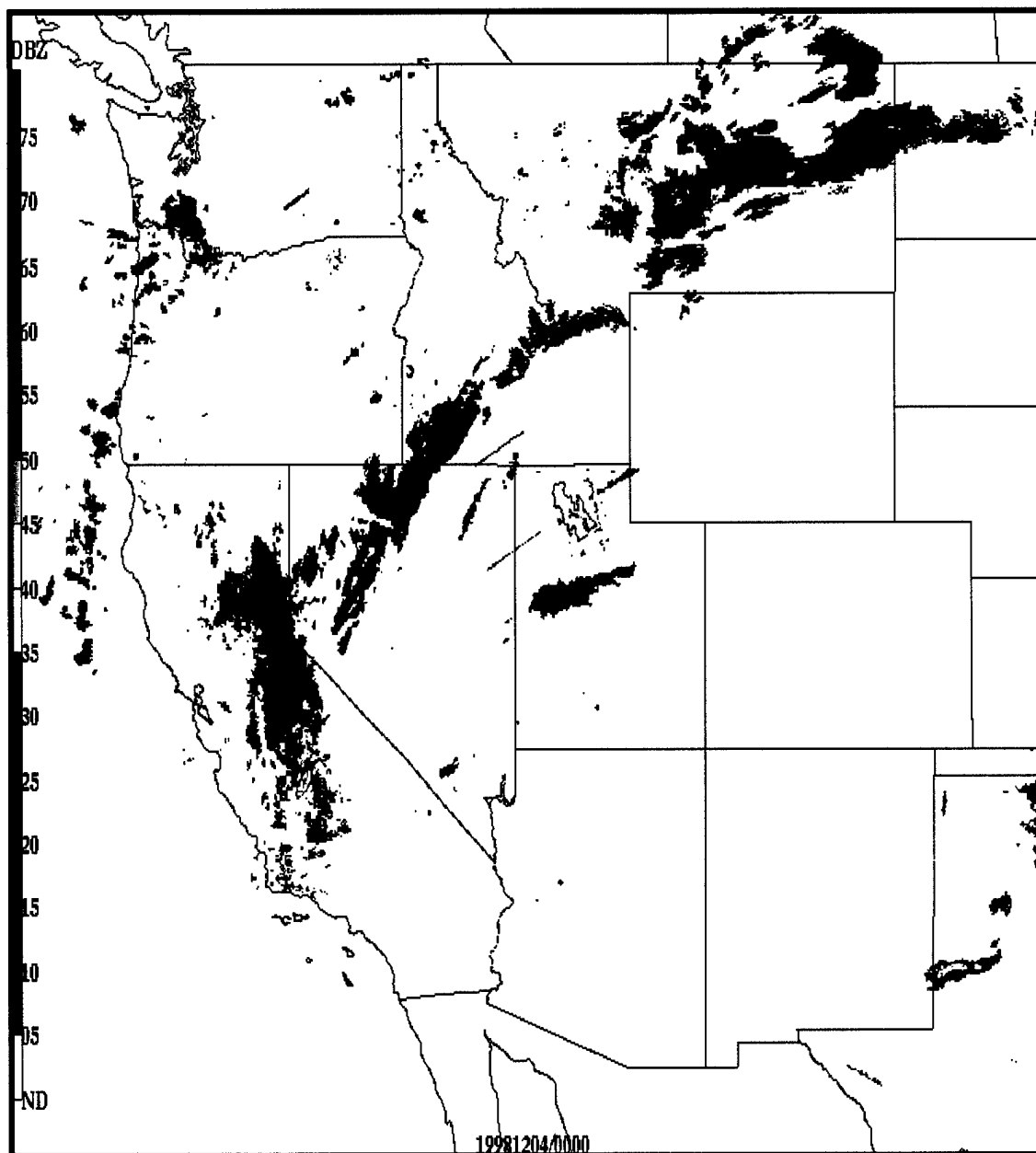


Figure 3.15. Composite NEXRAD imagery for 0000 UTC 4 December 1998.

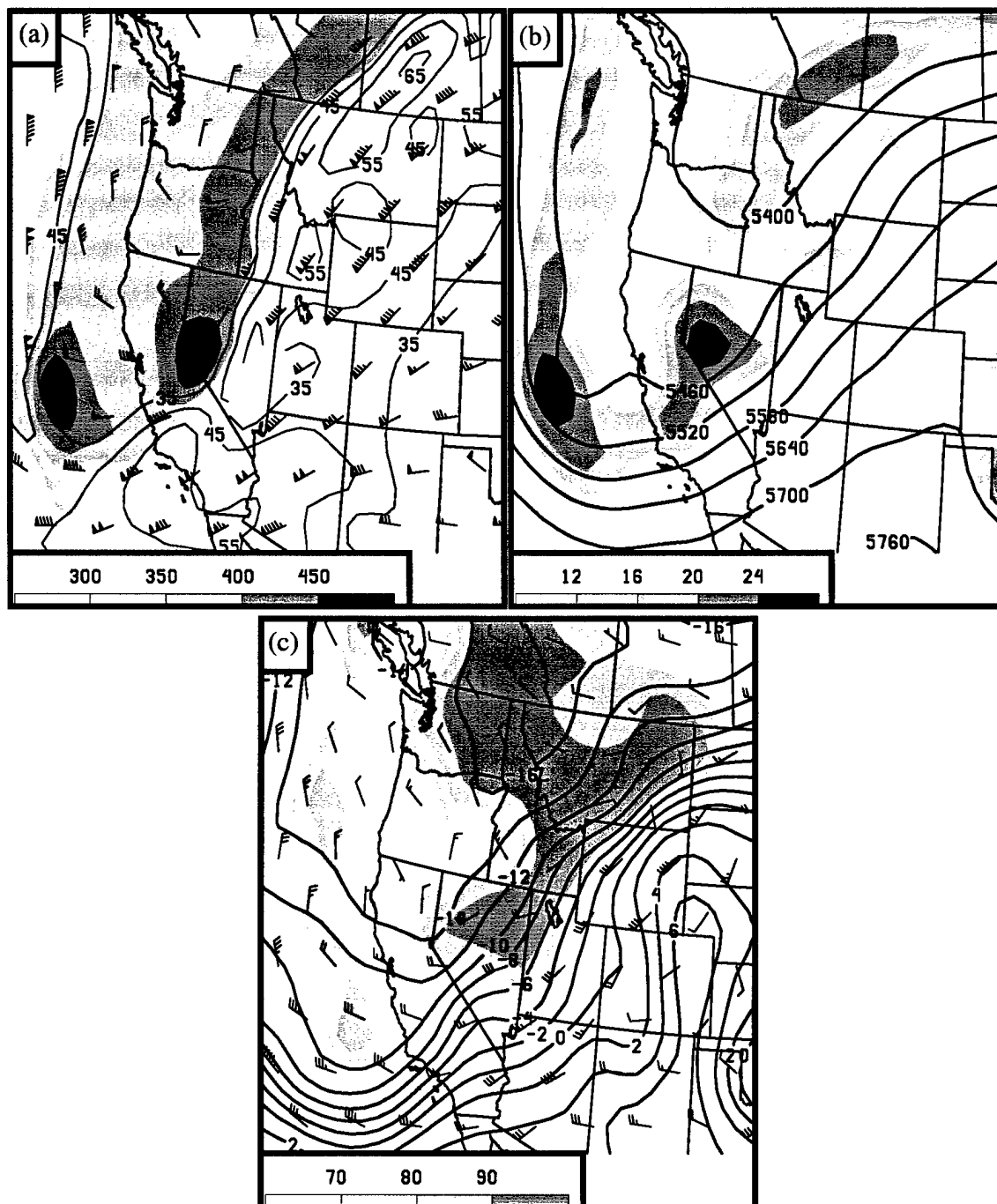


Figure 3.16. RUC2 analysis for 1200 UTC 4 December 1998. (a) Dynamic tropopause pressure (hPa, shaded according to scale at bottom), winds (pennant, full and half barbs denote 25, 5 and 2.5 m s⁻¹, respectively), and isotachs (contours every 10 m s⁻¹ from 35 m s⁻¹, breaks caused by data voids). (b) 500-hPa geopotential height (m) and absolute vorticity (s⁻¹, shaded according to scale at bottom). (c) 700-hPa temperature (°C), relative humidity (%), and wind [as in (a)].

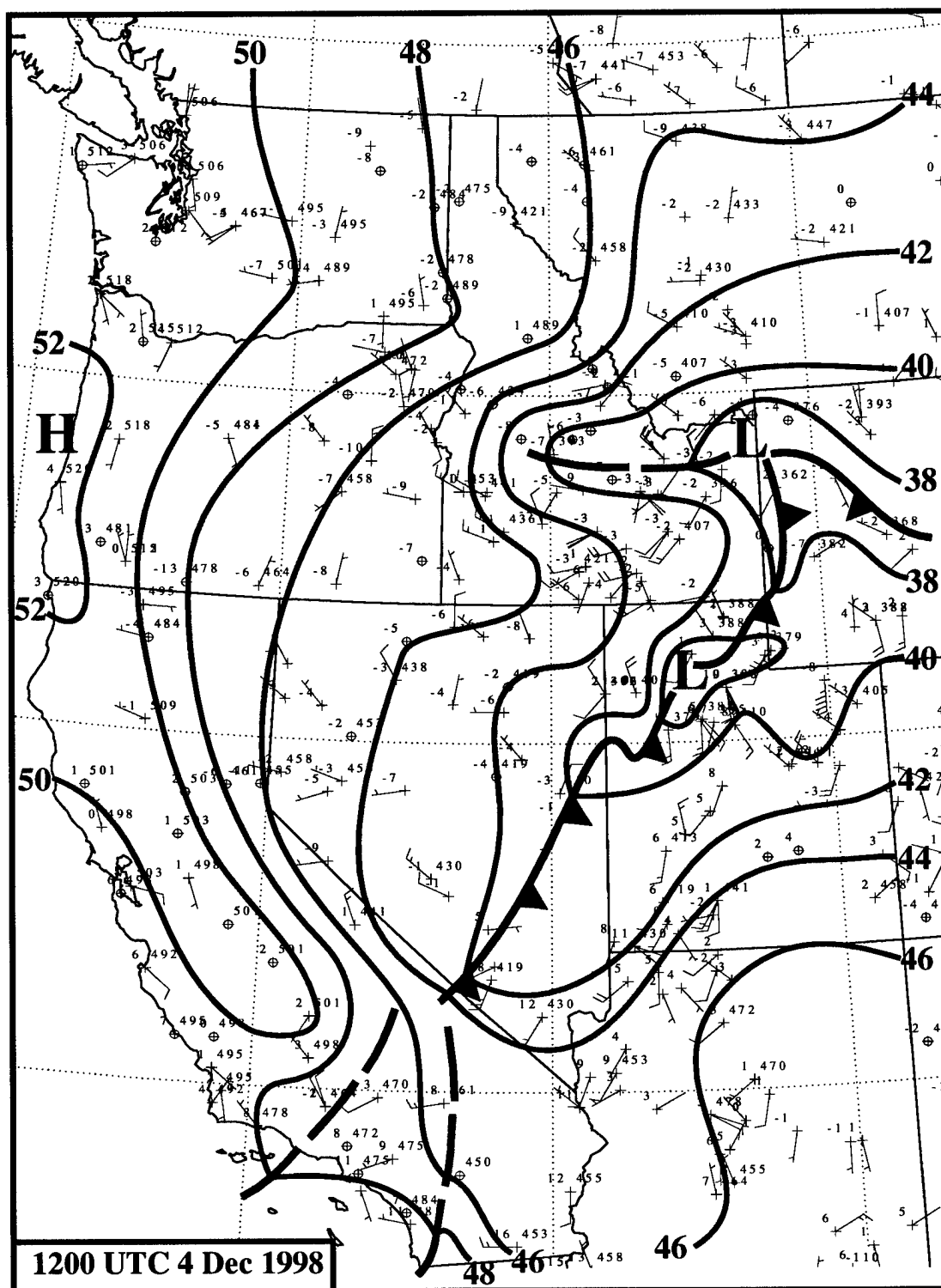


Figure 3.17. Manually analyzed surface map for 1200 UTC 4 December 1998. 1500-m pressure isobars every 2 hPa. Surface station reports include temperature ($^{\circ}\text{C}$, upper left), 1500-m pressure (tenths of hPa with leading 8 truncated), and winds [full (half) barbs denote 5 (2.5) m s^{-1}].

southern Montana while a pressure trough remained anchored over the central mountains of Idaho. Two separate cloud features with the surface cyclone in northern Utah (Fig 3.18, labeled with a C) and the shortwave trough over northern Nevada (Fig. 3.18, labeled with an X) were clearly evident on satellite imagery. Radar data continued to show the bulk of precipitation confined to the postfrontal environment (Figs. 3.19). Some light precipitation was generated ahead of the front in the Wasatch mountains of Utah, though snowfall amounts were generally light (< 5 cm). Heavy snow fell across much of northern Utah in the postfrontal environment (04/0800-2000 UTC) with 3 cm h^{-1} accumulation rates common at times in valley locales and up to 10 cm h^{-1} in the mountains.

During the ensuing 12 h period, the weakening shortwave trough axis moved into northern Utah while the cyclone moved northward into Wyoming and weakened significantly (Figs. 3.20 and 3.21). Satellite imagery showed the main cloud feature associated with the initial shortwave had moved into Idaho (Fig. 3.22). Precipitation was diminishing across most of the Great Basin by 0000 UTC 05 December (Fig. 3.23), with storm total snowfall ranging from 5–30 cm across the valleys and 20–50 cm in the mountains. The second cyclonic PV anomaly moved into southern California, deepening the larger-scale trough over the western US and shifting the strong southwesterly flow to the southern and central Rockies. By 1200 UTC 5 December (not shown), the larger-scale trough was still located over the western United States, though surface high pressure had developed over the Great Basin and the significant weather shifted east of the Continental Divide.



Figure 3.18. Infrared satellite imagery for 1200 UTC 4 December 1998. "X" denotes cloud feature associated with the upper level trough while "C" denotes location of surface cyclone center.

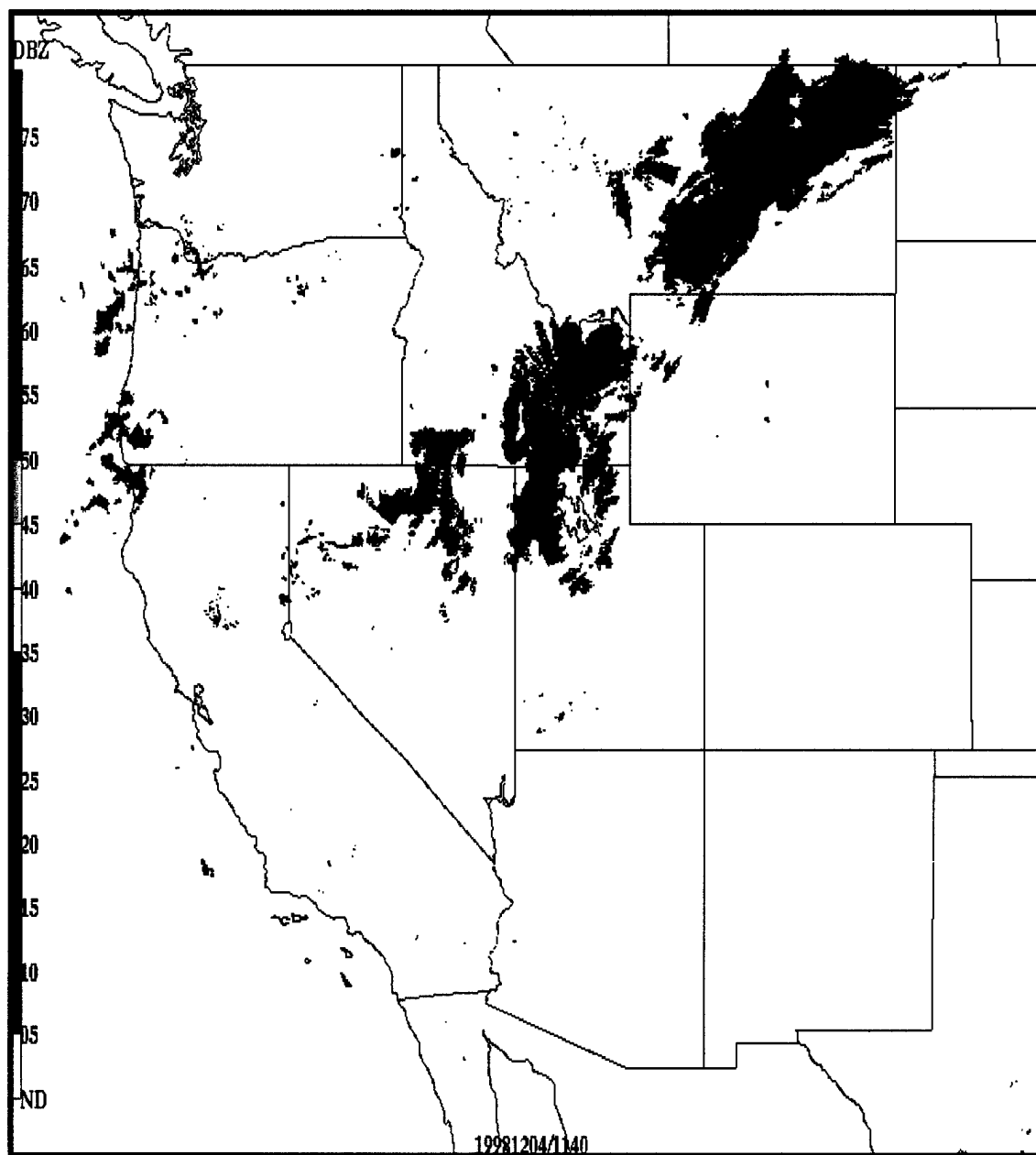


Figure 3.19. Composite NEXRAD imagery for 1140 UTC 4 December 1998. [Note: Composite data for 1200 UTC did not include the data from the Promontory Point site in northern Utah.]

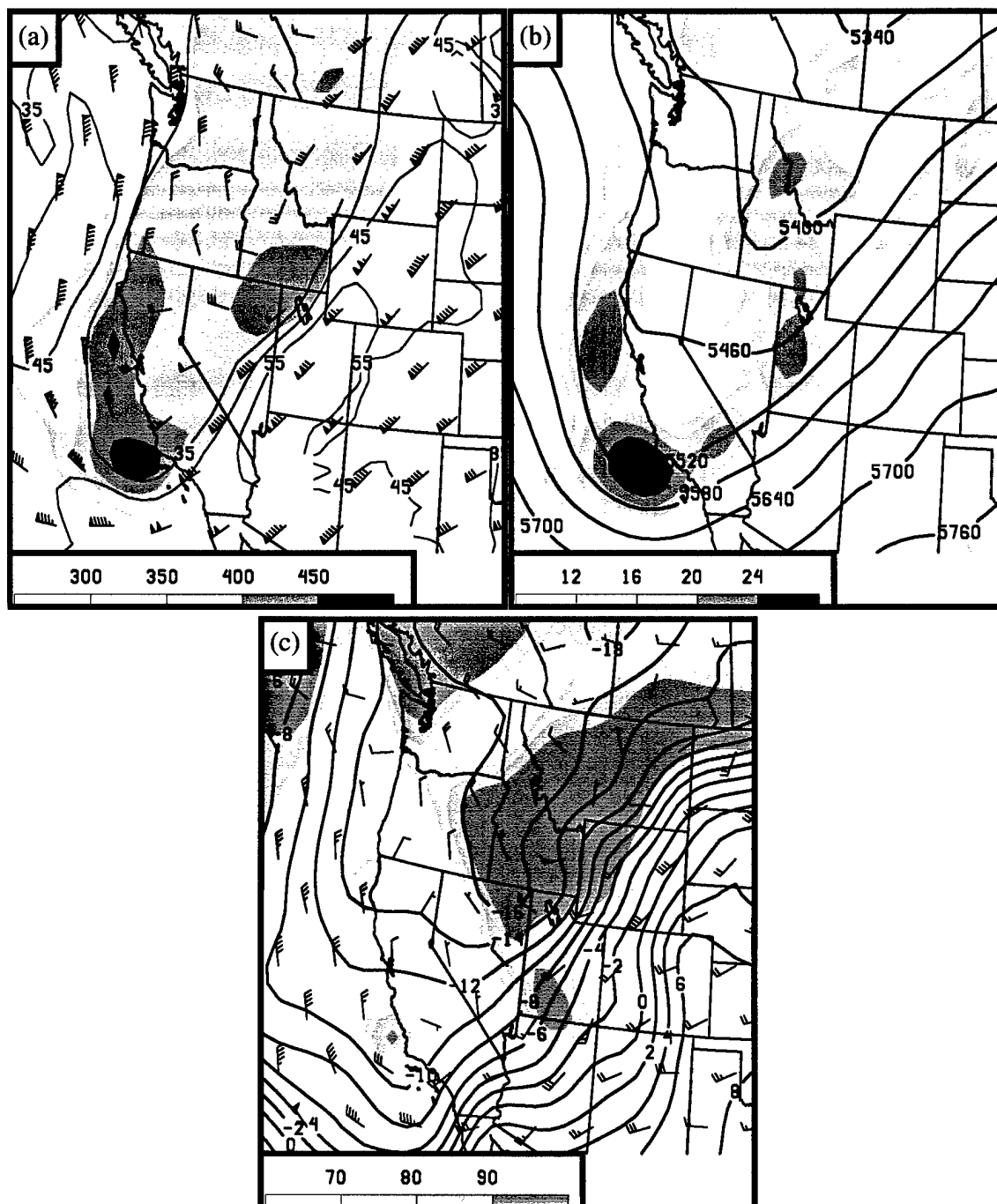


Figure 3.20. RUC2 analysis for 0000 UTC 5 December 1998. (a) Dynamic tropopause pressure (hPa, shaded according to scale at bottom), winds (pennant, full and half barbs denote 25, 5 and 2.5 m s⁻¹, respectively), and isotachs (contours every 10 m s⁻¹ from 35 m s⁻¹, breaks caused by data voids). (b) 500-hPa geopotential height (m) and absolute vorticity (s⁻¹, shaded according to scale at bottom). (c) 700-hPa temperature (°C), relative humidity (%), shaded according to scale at bottom), and wind [as in (a)].

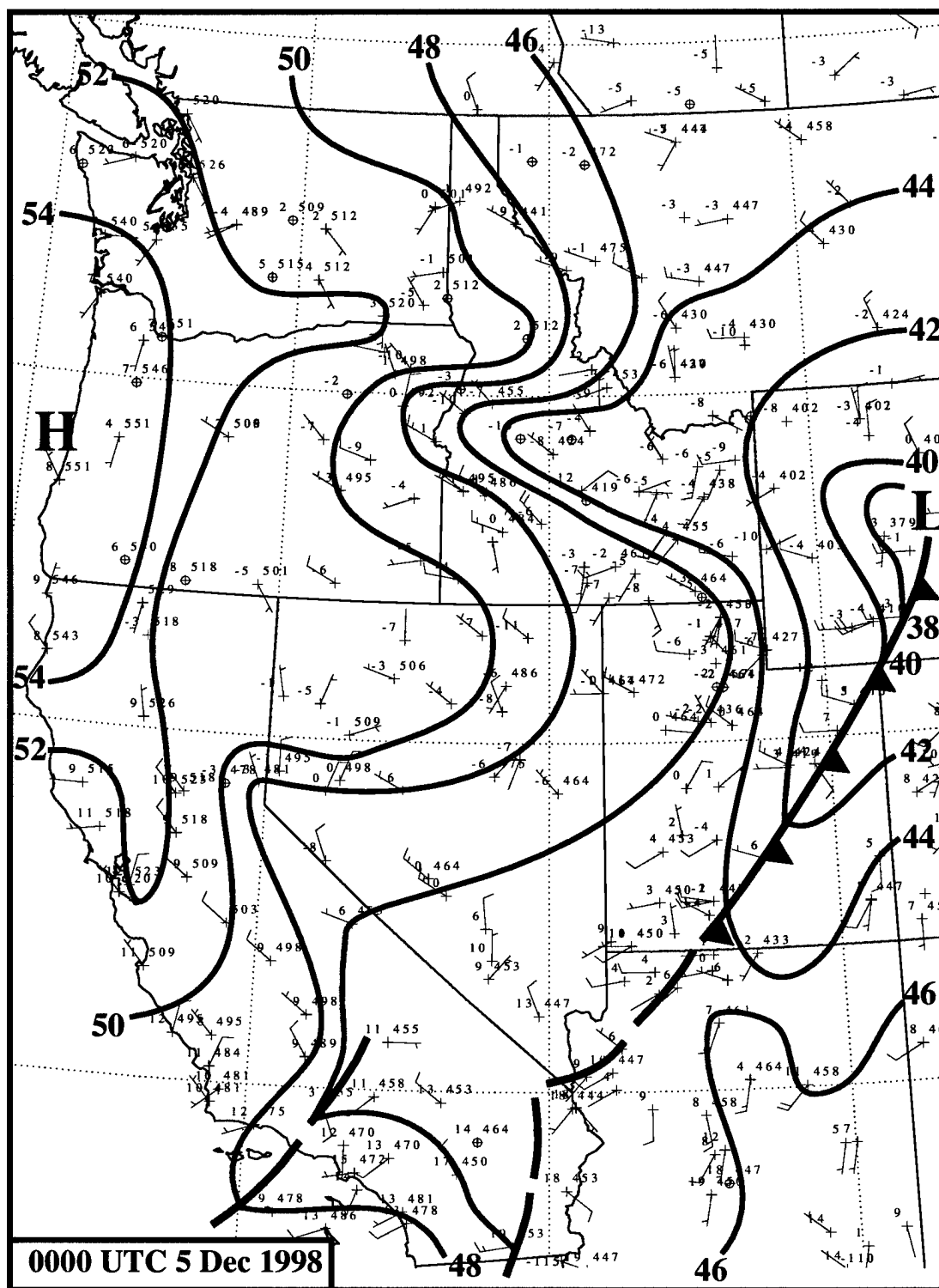


Figure 3.21. Manually analyzed surface map for 0000 UTC 5 December 1998. 1500-m pressure isobars every 2 hPa. Surface station reports include temperature ($^{\circ}\text{C}$, upper left), 1500-m pressure (tenths of hPa with leading 8 truncated), and winds [full (half) barbs denote 5 (2.5) m s^{-1}].

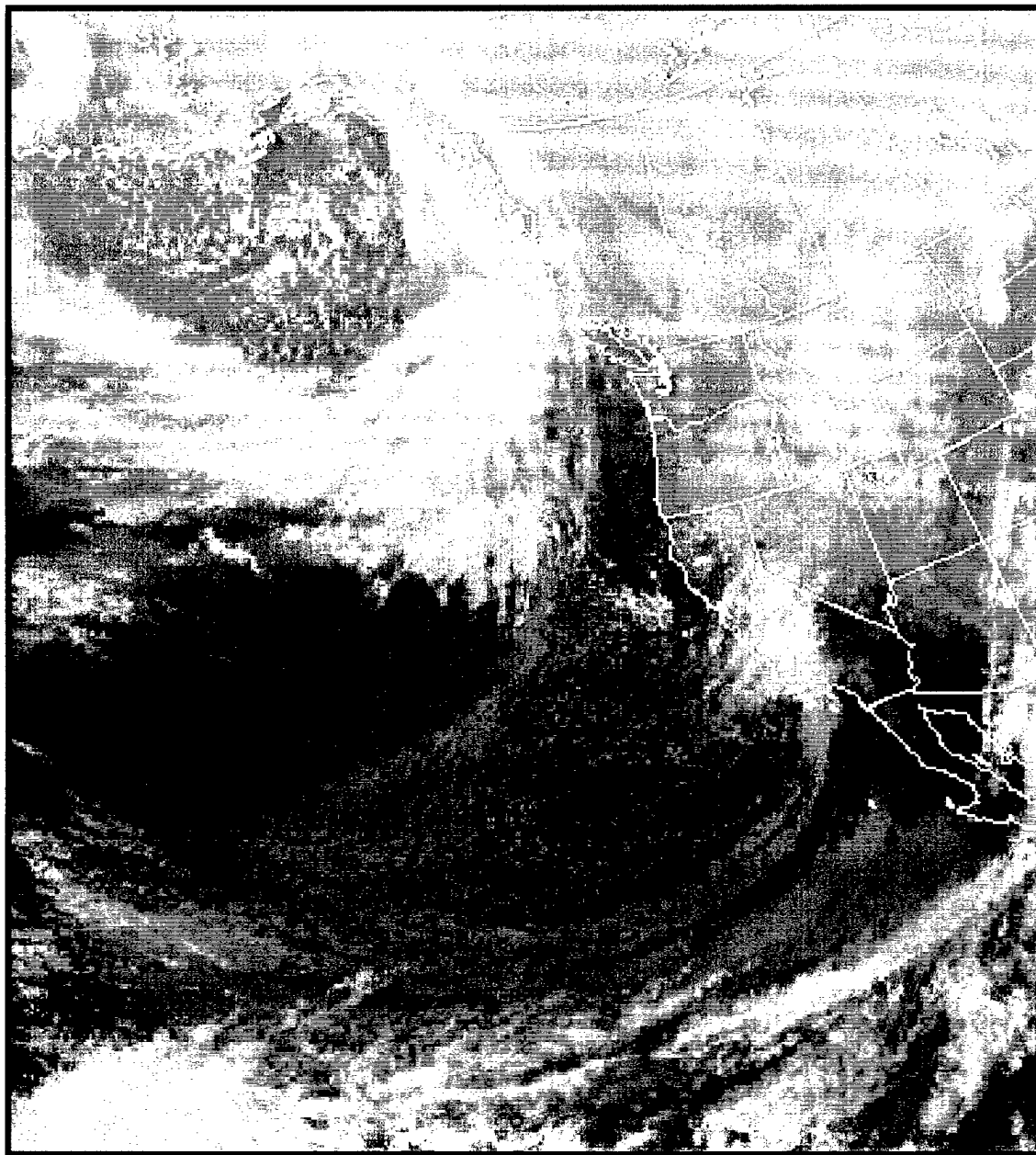


Figure 3.22. Infrared satellite imagery for 0000 UTC 5 December 1998.

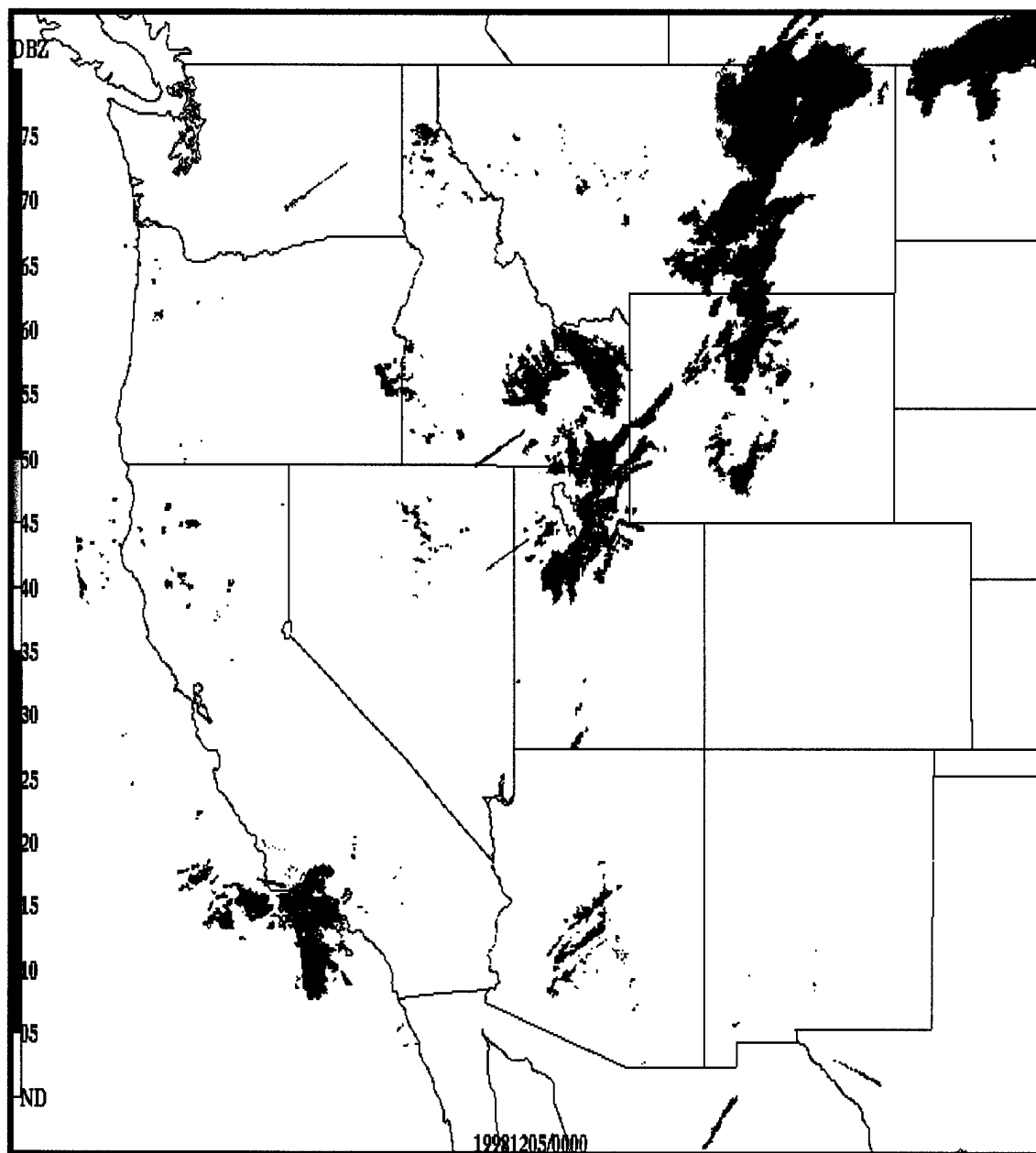


Figure 3.23. Composite NEXRAD imagery for 0000 UTC 5 December 1998.

CHAPTER 4

MESOSCALE CHARACTERISTICS OF CYCLONE AND FRONTAL INTERACTION WITH TOPOGRAPHY

Frontal Distortion over the Sierra Nevada

Although a number of studies have examined the influence of topography on frontal structure, including the distortion of low-level cold fronts by topographic features such as the Alps and other major mountain ranges (Bjerknes and Solberg, 1922; Godske, et al., 1957; Smith, 1985; Hoinka and Heimann, 1988; Tafferter and Egger, 1992), little work has been done to examine such interactions over the western United States. High resolution MesoWest surface observations allow detailed analysis of the evolution of the cold front associated with the 3–5 December 1998 cyclone, and its interaction with major topographic features such as California's Sierra Nevada (Fig. 4.1). This northwest-southeast oriented mountain range features crest levels of more than 3000 m, lies in close proximity to the Pacific Ocean, and regularly interacts with cold fronts moving towards the Great Basin during the cold season. This section describes the cold-frontal distortion that was observed over the Sierra Nevada during the 3–5 December 1998 event.

At 0000 UTC 3 December, the surface cold front stretched across northwest California into southcentral Oregon (Fig. 4.2a) and then northeastward into central Idaho (Fig. 3.4), with only minor perturbations evident in the southwest-northeast orientation of the front. Some evidence of frontal distortion began to appear by 0600 UTC 3 December

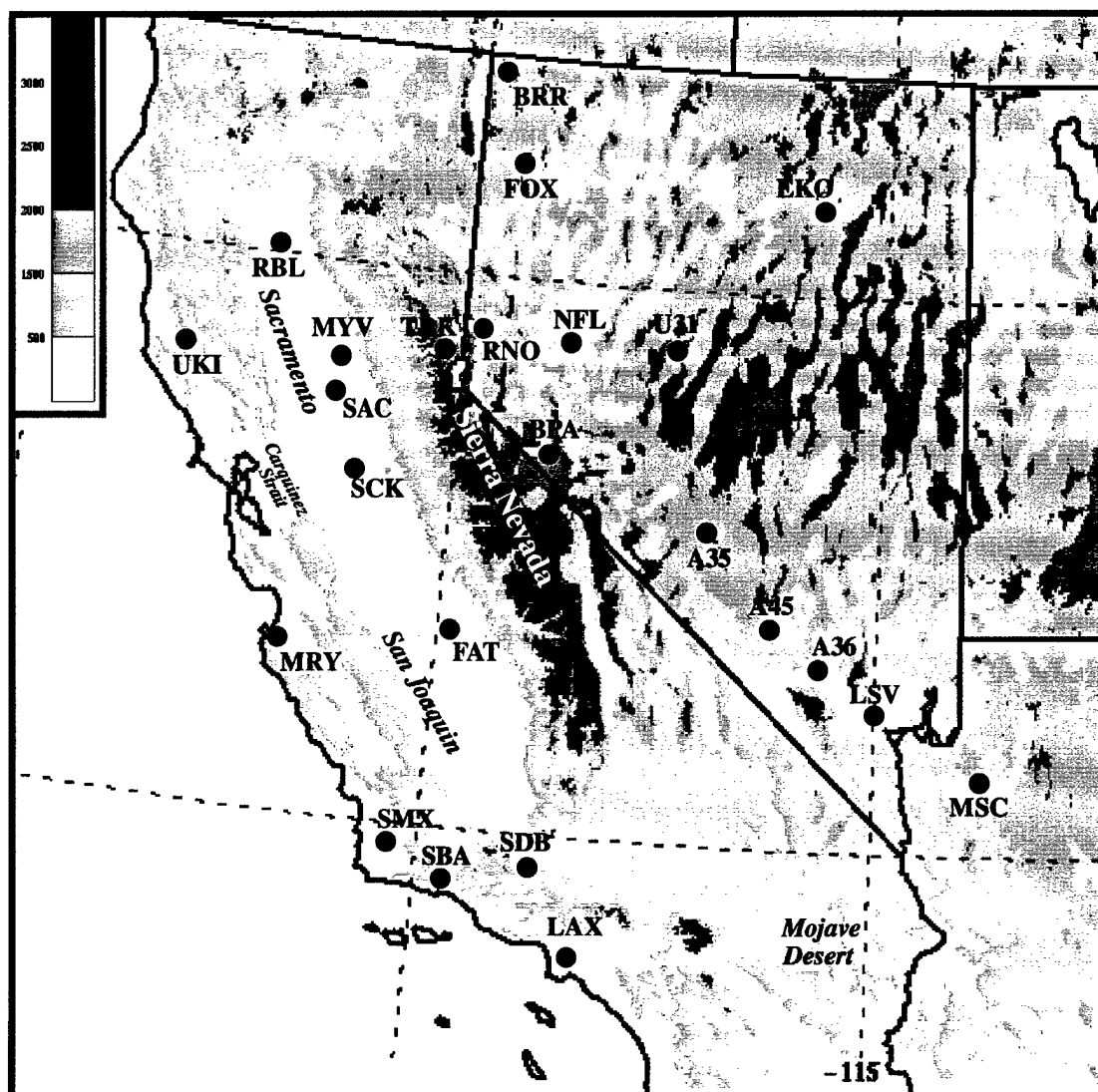


Figure 4.1. Topography and major geographic features of California, Nevada and adjacent region. MesoWest stations discussed in text include: Barrel Springs, NV (BRR), Fox Mountain, NV (FOX), Elko, NV (EKO), Red Bluff, CA (RBL), Ukiah, CA (UKI), Maryville, CA (MYV), Truckee, CA (TRK), Reno, NV (RNO), Fallon Naval Air Station, NV (NFL), Austin, NV (U31), Sacramento, CA (SAC), Stockton, CA (SCK), Brawley Peaks, NV (BPA), Monterey, CA (MRY), Fresno, CA (FAT), Tonopah Test Range sites, NV (A35, A45), Nellis Test Range site, NV (A36), Nellis Air Force Base, NV (LSV), Santa Maria, CA (SMX), Santa Barbara, CA (SBA), Sandberg, CA (SDB), Los Angeles, CA (LAX), and Music Mountain, AZ (MSC). Valley names and other specific geographic features are shown in italics. Elevation (m) shaded according to scale at upper left.

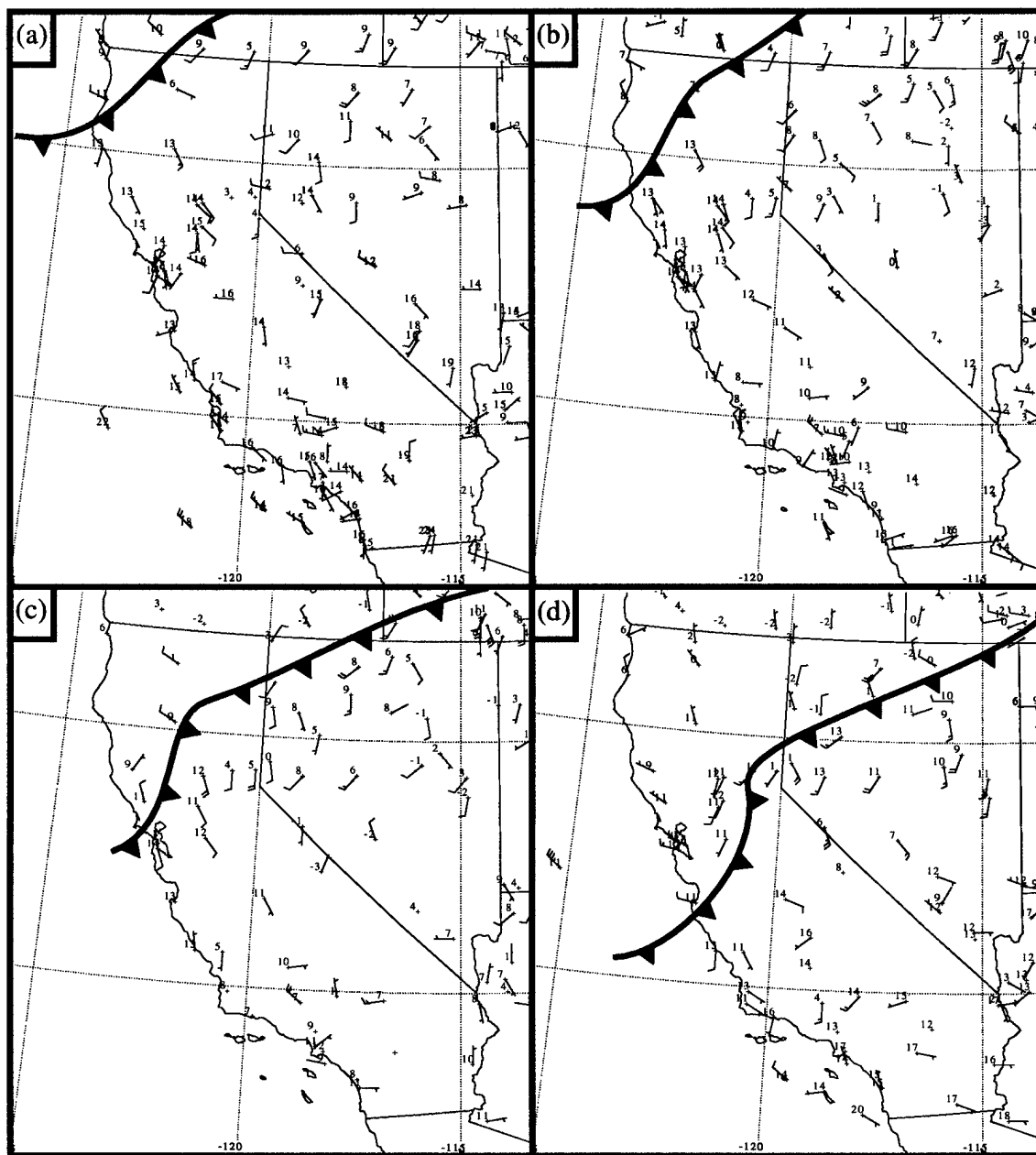


Figure 4.2. Subjective analyses of frontal progression over the western United States for 3 December at (a) 0000 UTC, (b) 0600 UTC, (c) 1200 UTC, and (d) 1800 UTC. Density of station plots reduced for clarity.

as the front moved across northern California (Fig. 4.2b). Frontal speed along the coast was $\sim 20 \text{ km h}^{-1}$, while over the interior the frontal speed was only $\sim 10 \text{ km h}^{-1}$. As the front continued its equatorward movement, meteograms showed a well-defined frontal passage at a near-coastal station, Ukiah (UKI), just before 0900 UTC, and an interior valley station, Red Bluff (RBL), around 1040 UTC (Fig. 4.3). Another 300 km farther northeast, the front passed through Barrel Springs, NV, (BRR) around 1000 UTC with a more impressive 8°C temperature drop in 1 h and a 180° windshift (not shown).

The front began to impinge on the northern portion of the Sierra Nevada by 1200 UTC 3 December, and from there extended to just north of the San Francisco Bay area (Fig. 4.2c). The front remained well defined as it continued to move equatorward along the California coast, as illustrated by the pronounced temperature fall and veering wind observed around 1700 UTC at Monterey (MRV; Fig. 4.4a), and as it moved more slowly equatorward over western Nevada, where an 8°C temperature fall was observed at Fox Mountain (FOX) in 1 h (not shown). Over the Sacramento Valley, however, the frontal signature was less pronounced due to the effects of daytime surface heating and local terrain-induced flows. At Stockton (SCK), the surface wind veered temporarily to westerly with frontal passage just after 1600 UTC and was accompanied by only a small decrease in temperature, presumably since the large-scale airmass change was partially obscured by diurnal surface heating (Fig. 4.4b). By 1800 UTC, the post-frontal winds at SCK, as well as other Sacramento Valley stations [i.e., Sacramento (SAC) and Maryville (MYV)], maintained a southerly component (Fig. 4.2d). Thus, with high pressure along the California Coast (e.g., Fig. 3.11), the postfrontal airmass at this time appeared to be moving eastward through Carquinez Strait east of San Francisco and then turning

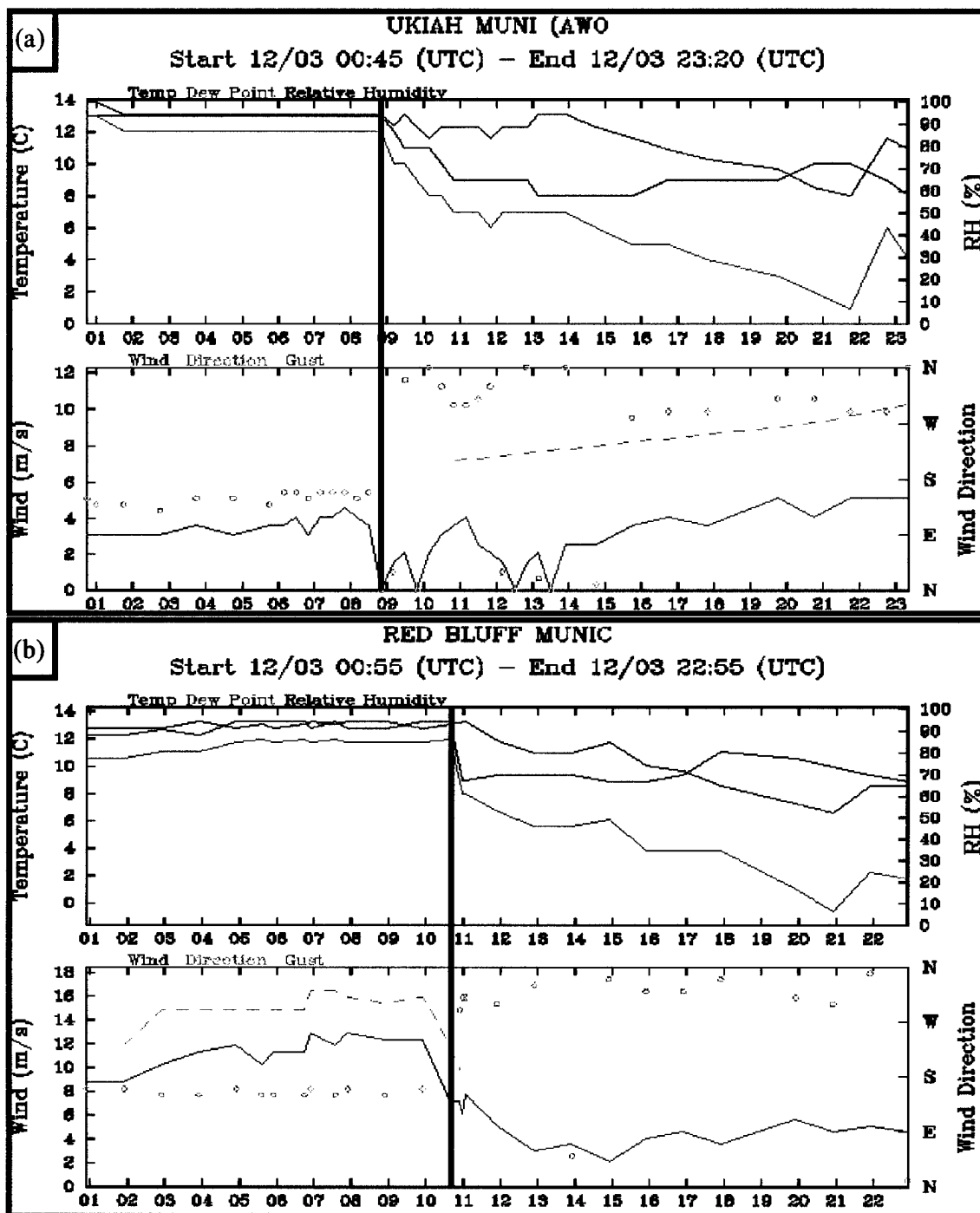


Figure 4.3. Meteograms of temperature (red), dew point (green), relative humidity (blue), wind speed (solid), wind gust (dashed), and wind direction (open circles) at (a) Ukiah, CA (UKI) and (b) Red Bluff, CA (RBL; see Fig. 4.1 for locations) from 0045-2320 UTC 4 December 1998. Solid line denotes frontal passage.

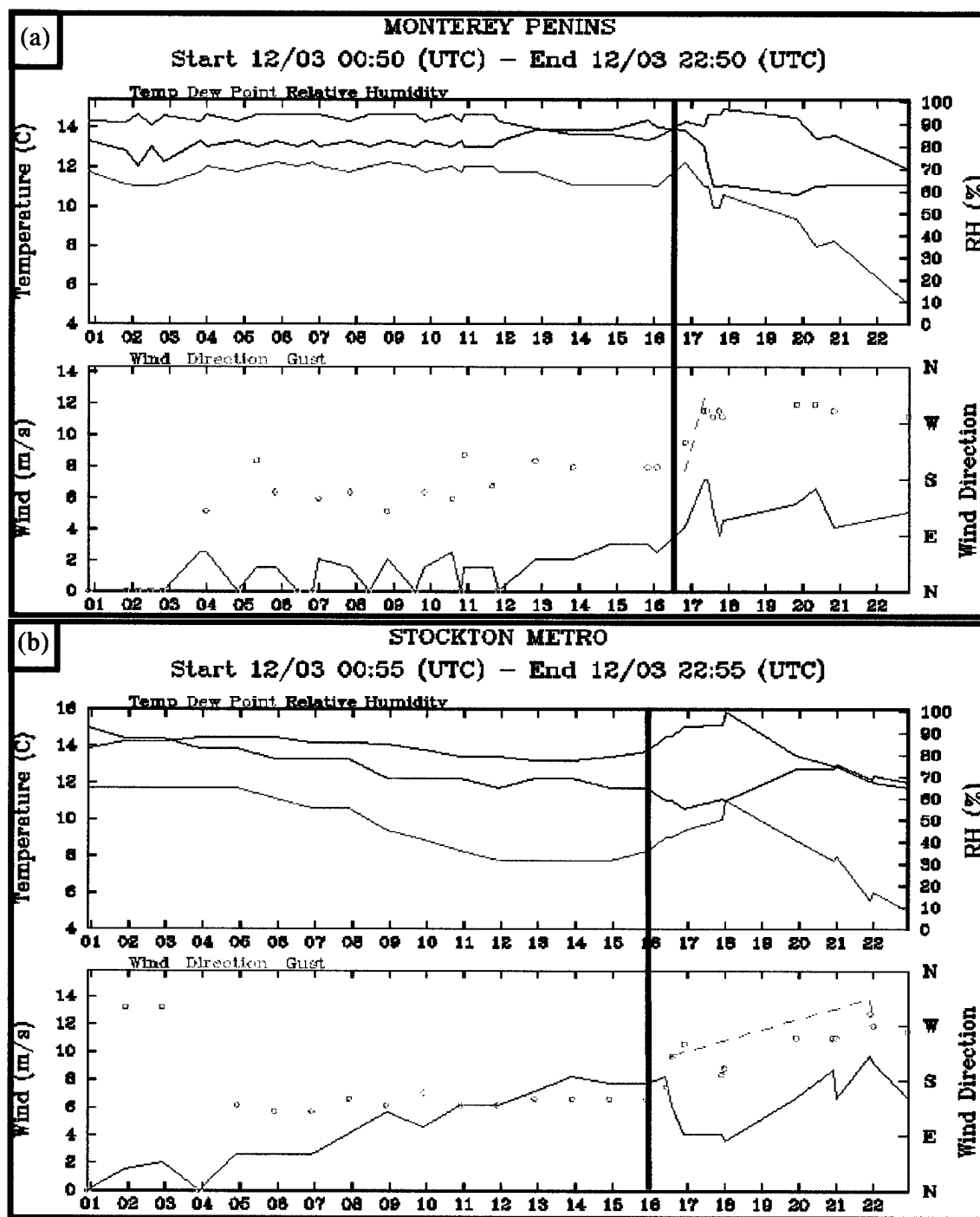


Figure 4.4. Meteograms of temperature (red), dew point (green), relative humidity (blue), wind speed (solid), wind gust (dashed), and wind direction (open circles) at (a) Monterey, CA (MRY) and (b) Stockton, CA (SCK; see Fig. 4.1 for locations) from 0050-2255 UTC 4 December 1998. Solid line denotes frontal passage.

poleward up the Sacramento Valley. This airflow pattern is similar to that observed in the warm season when semipermanent high pressure and a marine boundary layer are present along and off the California Coast (e.g., Seaman et al. 1995).

On the large-scale, the 1800 UTC surface analysis showed significant distortion of the cold front across the Sierra Nevada, which continued to amplify through 0000 UTC 4 December (Figs. 4.2d and 4.5). Along the coast during this period the front appeared to be weakening. Santa Maria (SMX) recorded a diffuse frontal passage, with slight cooling observed ~2000 UTC 3 December, followed by a gradual 90° windshift ~2100 UTC 3 December, and finally a pressure minimum ~2200 UTC (Fig. 4.6). Inland, over the San Joaquin Valley, Fresno (FAT) observed frontal passage around ~2300 UTC (Fig. 4.7). Over the Sierra Nevada crest, the high elevation Lake Tahoe region reported very little in the way of a significant frontal passage. Between 2200 UTC 3 December and 0000 UTC 4 December, a gradual wind shift to westerly occurred, as well as a region-wide 2-3 °C drop in temperature. At Truckee (TRK), the initial temperature drop was slightly delayed (~20 min) from the onset of the gradual wind shift and the first of two, 1-hPa checks in the pressure trace (Fig. 4.8). East of the Sierra Nevada, the front continued to be very well defined with a classic frontal signature (2000 UTC) in the meteogram for Fallon Naval Air Station (NFL; Fig. 4.9).

By 0000 UTC 4 December, the front extended from near Santa Barbara (SBA) northward in an arc stretching along the eastern edge of the San Joaquin Valley. Over Nevada, the front was located from south of Brawley Peaks (BPA) northeastward into the low center over northeastern Nevada. After 0000 UTC, the Pacific Coastal portion of the front weakened rapidly at the surface as it approached the Los Angeles Basin. Los

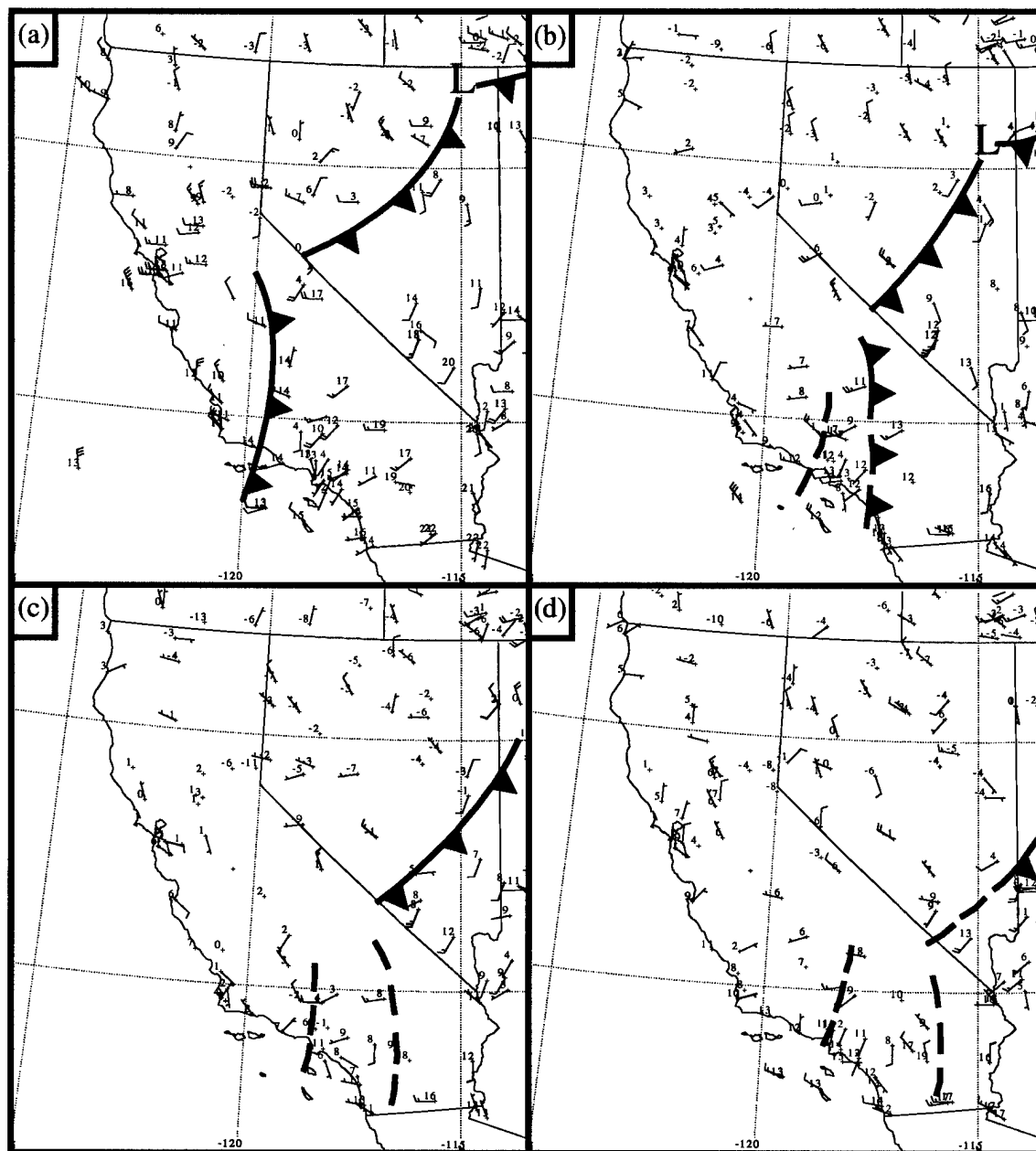


Figure 4.5. Subjective analyses of frontal progression over the western United States for 4 December at (a) 0000 UTC, (b) 0600 UTC, and (c) 1200 UTC and (d) 1800 UTC. Density of station plots reduced for clarity.

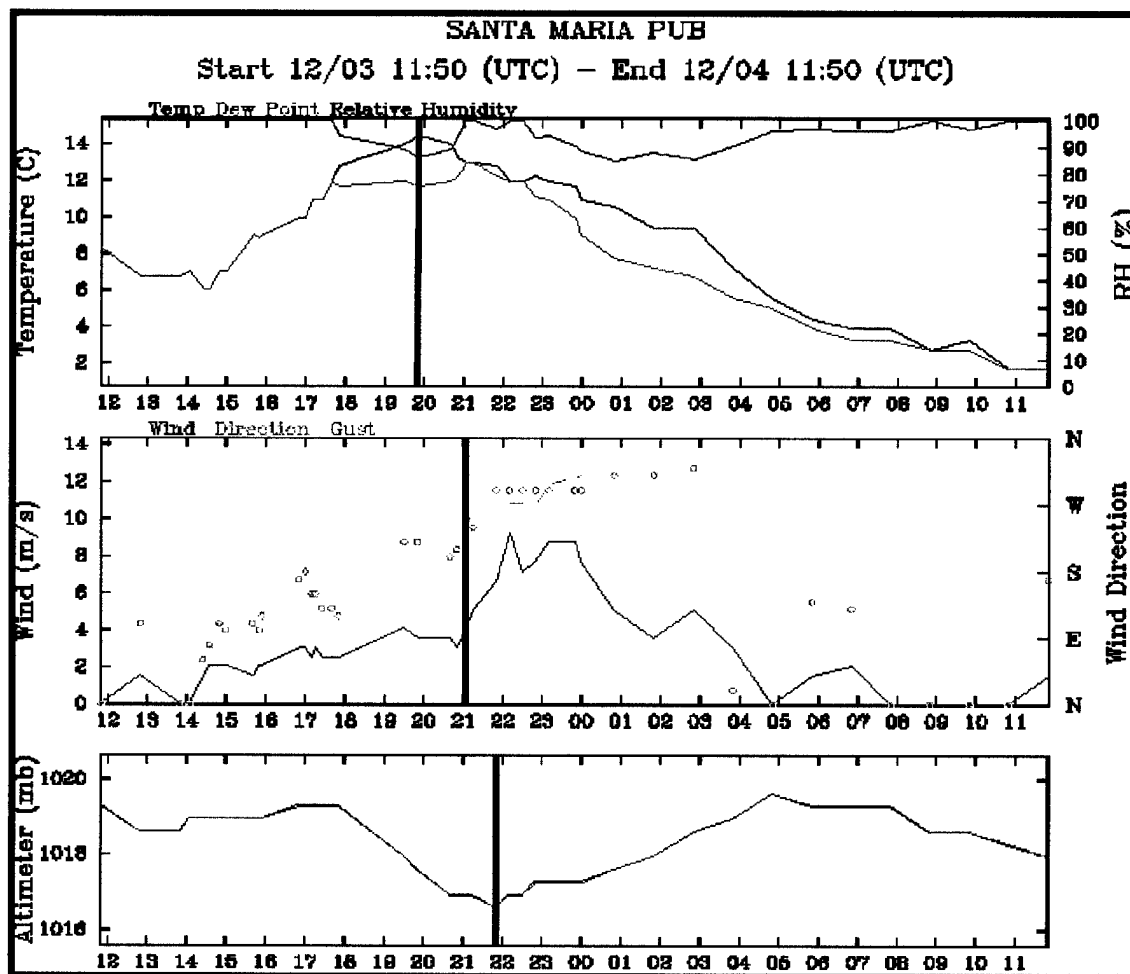


Figure 4.6. Meteograms of temperature (red), dew point (green), relative humidity (blue), wind speed (solid), wind gust (dashed), wind direction (open circles), and altimeter trace at Santa Maria, CA (SMX; see Fig. 4.1 for location) from 1150 UTC 3 December - 1150 UTC 4 December 1998. Solid line denotes apparent frontal passage.

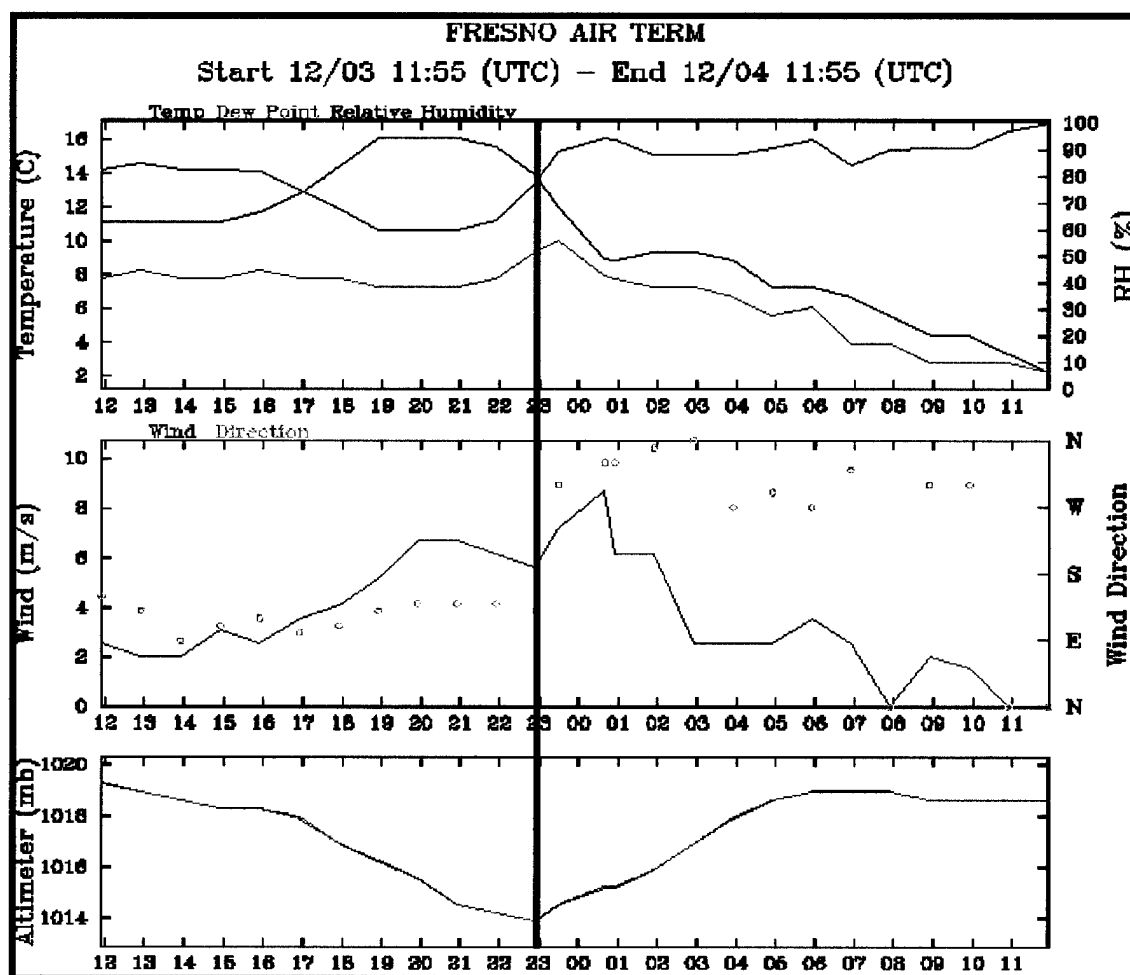


Figure 4.7. Meteograms of temperature (red), dew point (green), relative humidity (blue), wind speed (solid), wind direction (open circles), and altimeter trace at Fresno, CA (FAT; see Fig. 4.1 for location) from 1155 UTC 3 December - 1155 UTC 4 December 1998. Solid line denotes frontal passage.

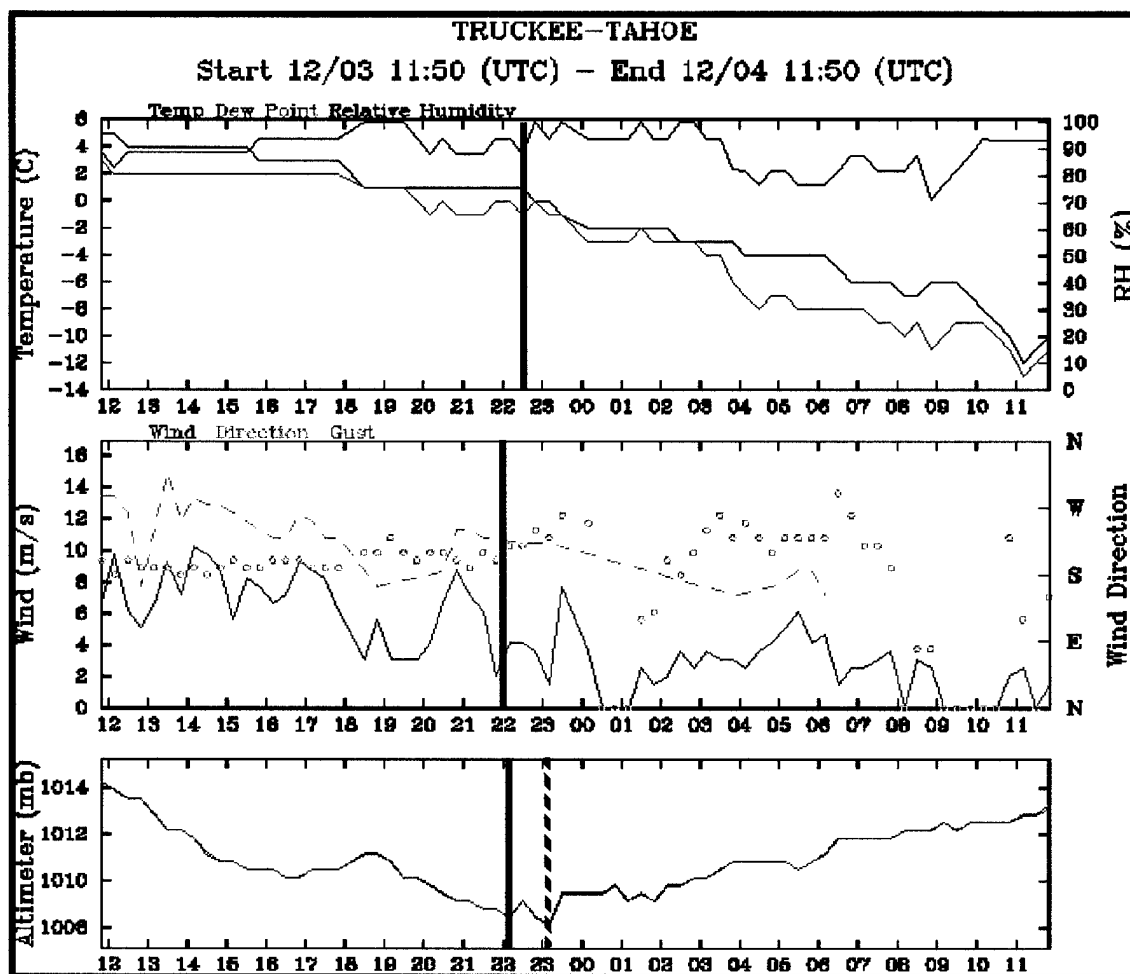


Figure 4.8. Meteograms of temperature (red), dew point (green), relative humidity (blue), wind speed (solid), wind gust (dashed), wind direction (open circles), and altimeter trace at Truckee, CA (TRK; see Fig. 4.1 for location) from 1150 UTC 3 December - 1150 UTC 4 December 1998. Solid line denotes frontal passage; dashed line shows a significant secondary pressure "check."

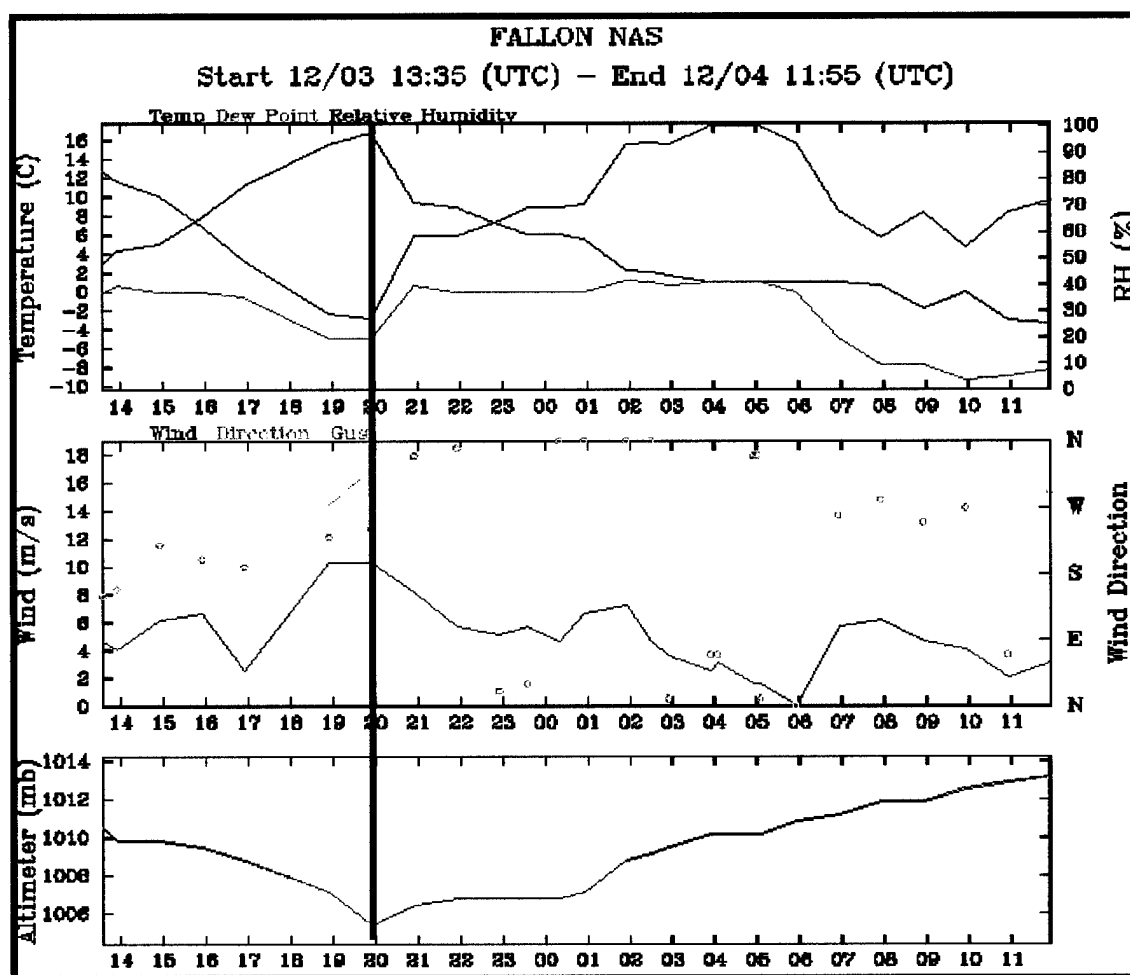


Figure 4.9. Meteograms of temperature (red), dew point (green), relative humidity (blue), wind speed (solid), wind gust (dashed), wind direction (open circles), and altimeter trace at Fallon Naval Air Station, NV (NFL; see Fig. 4.1 for location) from 1335 UTC 3 December - 1155 UTC 4 December 1998. Solid line denotes frontal passage.

Angeles (LAX) recorded a similar, though weaker, frontal passage to SMX, with cooling, followed by a wind shift, and finally a pressure “check” (Fig. 4.10). The initial wind shift, seen on the meteogram at 1900 UTC, was most likely due to a sea breeze and was not related to the front. Although the front was weakening at the surface, at least one southern California station recorded a fairly distinct frontal passage. Sandberg (SDB), located approximately 80 km north-northwest of Los Angeles with an elevation of around 1300 m, reported a 3 °C temperature drop along with a 90° wind shift between 0300-0400 UTC (Fig. 4.11). Although the front weakened as it moved equatorward into southern California, it maintained its strength east of the Sierra Nevada. For example, Austin, NV (U31), recorded a 10 °C temperature drop and a 180° wind shift between 0000-0300 UTC (not shown)¹. Even Brawley Peaks, a fairly isolated high elevation site to the east of the Sierra Nevada, recorded a wind shift and subsequent 2 °C temperature drop with frontal passage between 0100 and 0200 UTC (Fig. 4.12).

The front continued to weaken along the coast, and by 0600 UTC 4 December two separate pressure troughs were evident over southern California (Fig. 4.5b). The first was located west and northwest of the Los Angeles Basin, while the second, which appeared to be the remnant of the decaying cold front, was east of Los Angeles and heading eastward toward the Mojave Desert. The temperature gradient over southern California had nearly dissipated by this time, with pressure and wind the only keys to identifying what remained of the front. However, east of the Sierra, the cold front was still quite evident in the meteograms for stations north of the Tonopah Test Range (Fig. 4.13). Although the

1. During this period, data from Austin, NV were available only at 0000 and 0300 UTC.

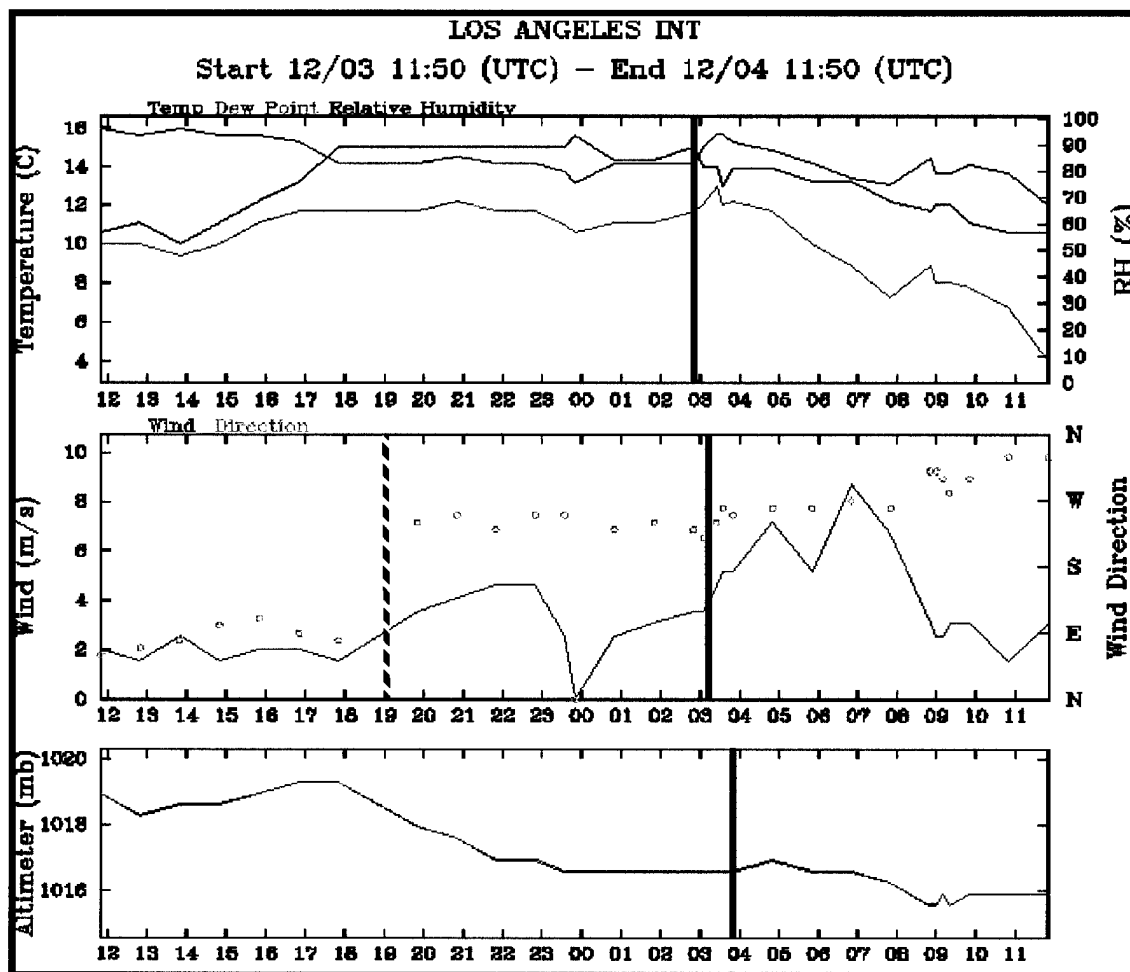


Figure 4.10. Meteograms of temperature (red), dew point (green), relative humidity (blue), wind speed (solid), wind direction (open circles), and altimeter trace at Los Angeles, CA (LAX; see Fig. 4.1 for location) from 1150 UTC 3 December - 1150 UTC 4 December 1998. Solid line denotes frontal passage; dashed line indicates a sea breeze wind shift.

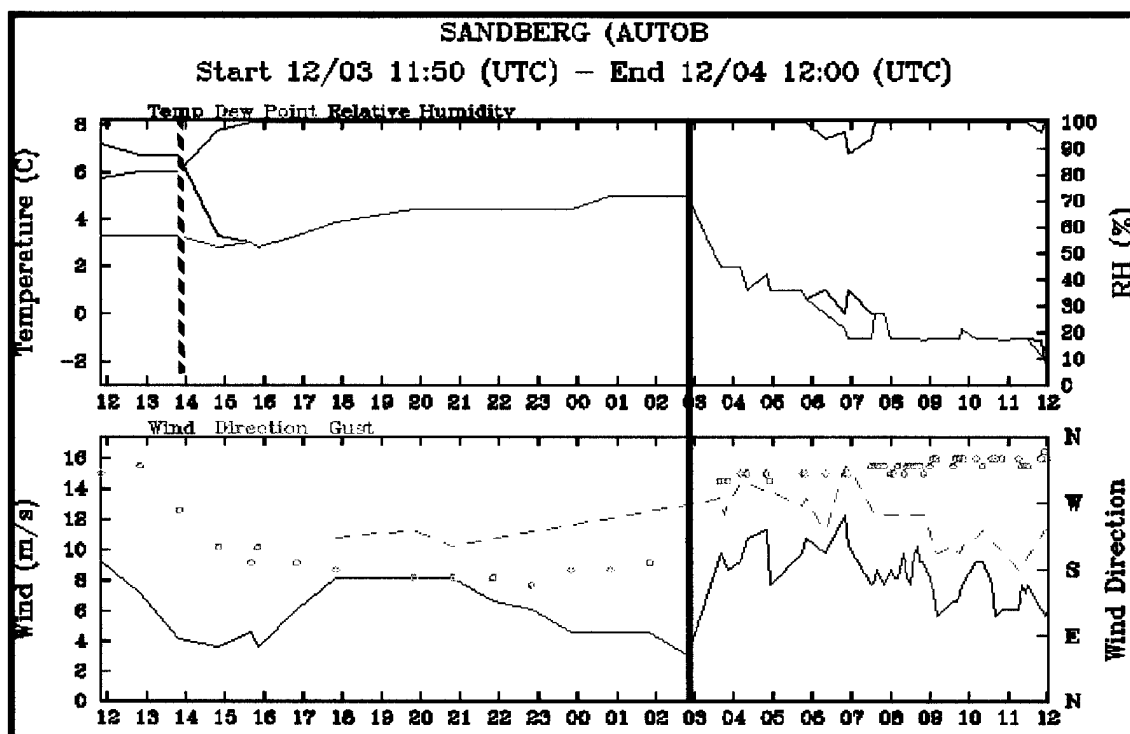


Figure 4.11. Meteograms of temperature (red), dew point (green), relative humidity (blue), wind speed (solid), wind gust (dashed), and wind direction (open circles) at Sandberg, CA (SDB; see Fig. 4.1 for location) from 1150 UTC 3 December - 1200 UTC 4 December 1998. Solid line denotes frontal passage; dashed line indicates prefrontal evaporational cooling.

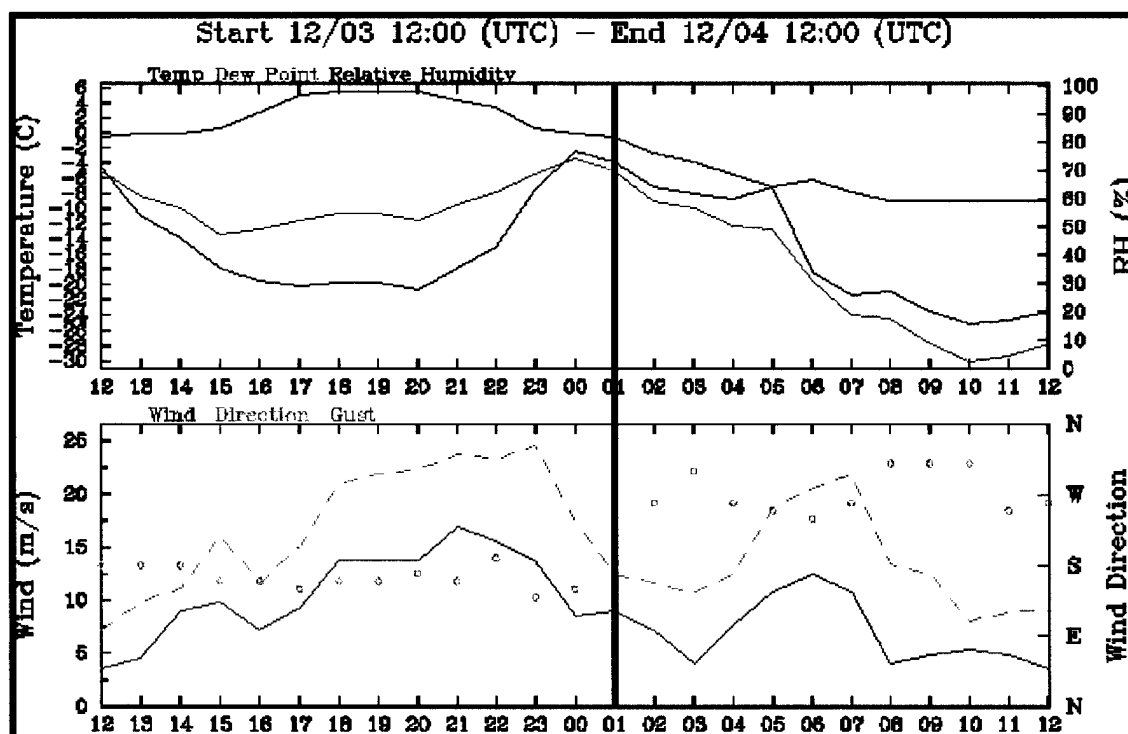


Figure 4.12. Meteograms of temperature (red), dew point (green), relative humidity (blue), wind speed (solid), wind gust (dashed), and wind direction (open circles) at Brawley Peaks, NV (BPA; see Fig. 4.1 for location) from 1200 UTC 3 December - 1200 UTC 4 December 1998. Solid line denotes frontal passage.

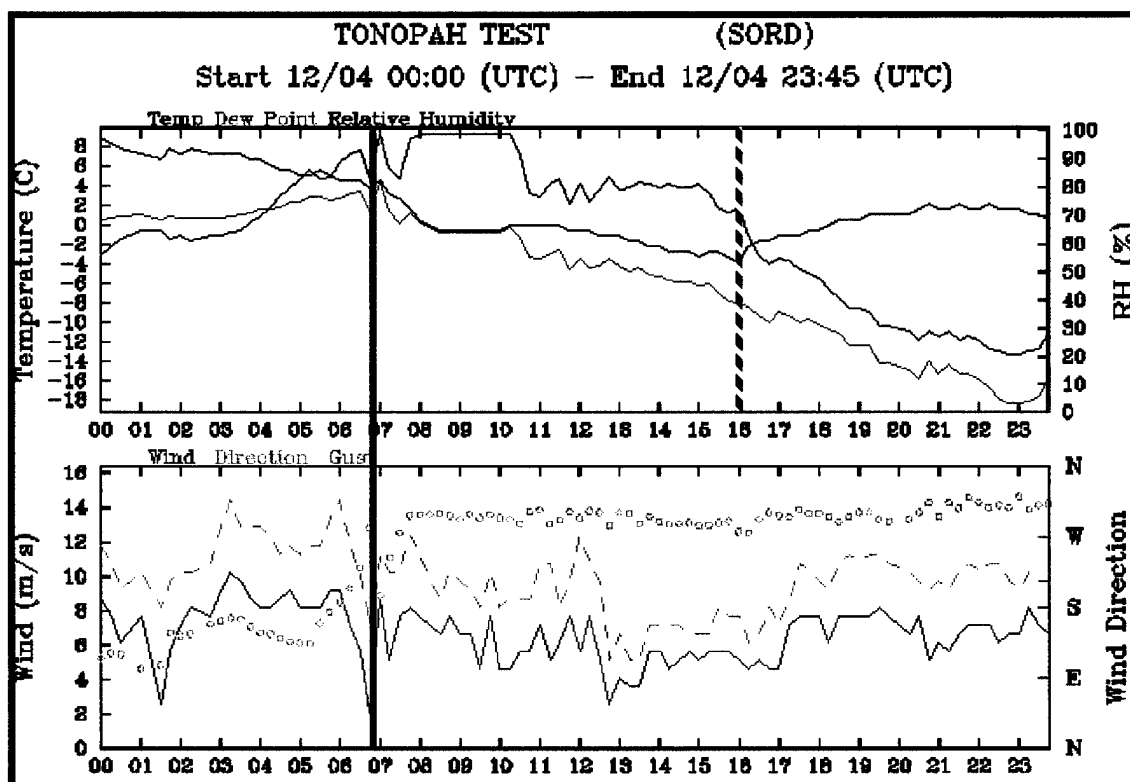


Figure 4.13. Meteograms of temperature (red), dew point (green), relative humidity (blue), wind speed (solid), wind gust (dashed), and wind direction (open circles) at Tonopah Test Range, NV (A35; see Fig. 4.1 for location) from 0000-2345 UTC 4 December 1998. Solid line denotes frontal passage; dashed line denotes commencement of pronounced drying.

temperature gradient had diminished somewhat, a well-pronounced wind shift still accompanied the frontal passage.

By 1200 UTC 4 December, the two pressure troughs remained over southern California with only horizontal pressure and wind fields used to establish their positions (Fig. 4.5c). The western-most trough remained quasi-stationary northwest of the Los Angeles Basin while the eastern trough, extending from the southern tip of the Sierra range southward into the Mojave Desert, continued its slow eastward movement. The cold front over southern Nevada was continuing to decay near the Tonopah Test Range sites. Several stations in the Test Range recorded either a wind shift or reduction in wind speed, or both, but little of any discontinuity in the temperature field. The presence of this change in wind character is evident in a horizontal cross-section of meteograms from the Test Range (A35) southeastward to Music Mountain, AZ (MSC; Figs. 4.13-4.15). Of additional interest is the pronounced drying at the surface for sites shown in Figs. 4.13-4.15. Note that the drying is not coincident with the windshift but rather with initial surface heating, commencing roughly between 1500-1800 UTC. Hence, it appeared that the front was becoming a shearline, with the drying not associated with the shearline but the daytime growth of the boundary layer and associated entrainment of dry air from aloft into the surface layer.

To summarize the frontal evolution over the Sierra Nevada region during this period, isochrones of the cold front are presented in Fig. 4.16. Note the more rapid equatorward progression of the front along the coast of California compared to Nevada, and the apparent retardation of the front over the Sierra Nevada. There are at least two mechanisms that may have contributed to this distortion of the cold front. First,

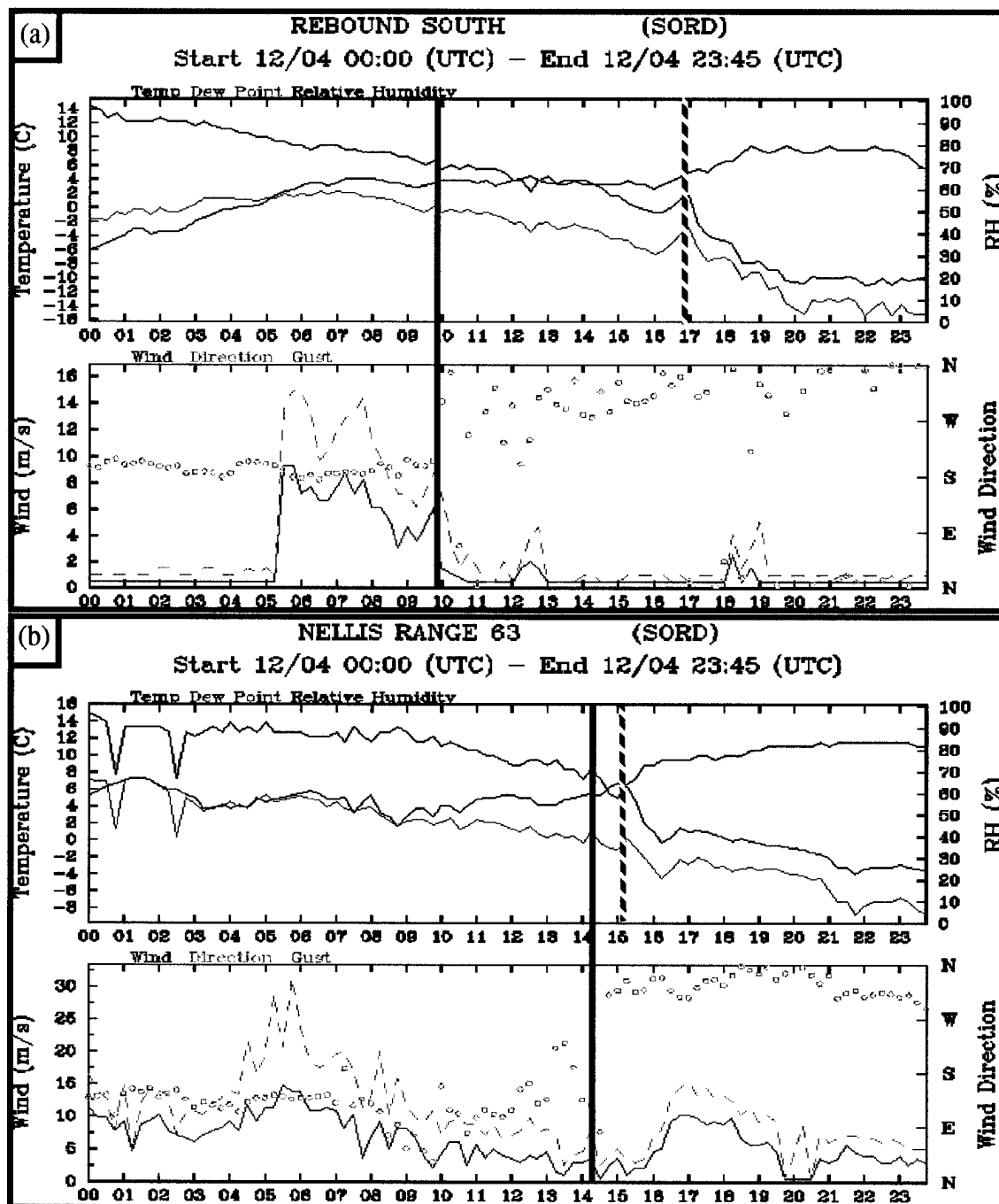


Figure 4.14. Meteorograms of temperature (red), dew point (green), relative humidity (blue), wind speed (solid), wind gust (dashed), and wind direction (open circles) at (a) Rebound South, NV (A45) and (b) Nellis Range Site 63, NV (A36; see Fig. 4.1 for locations) from 0000-2345 UTC 4 December 1998. Solid line denotes frontal passage; dashed line denotes commencement of pronounced drying.

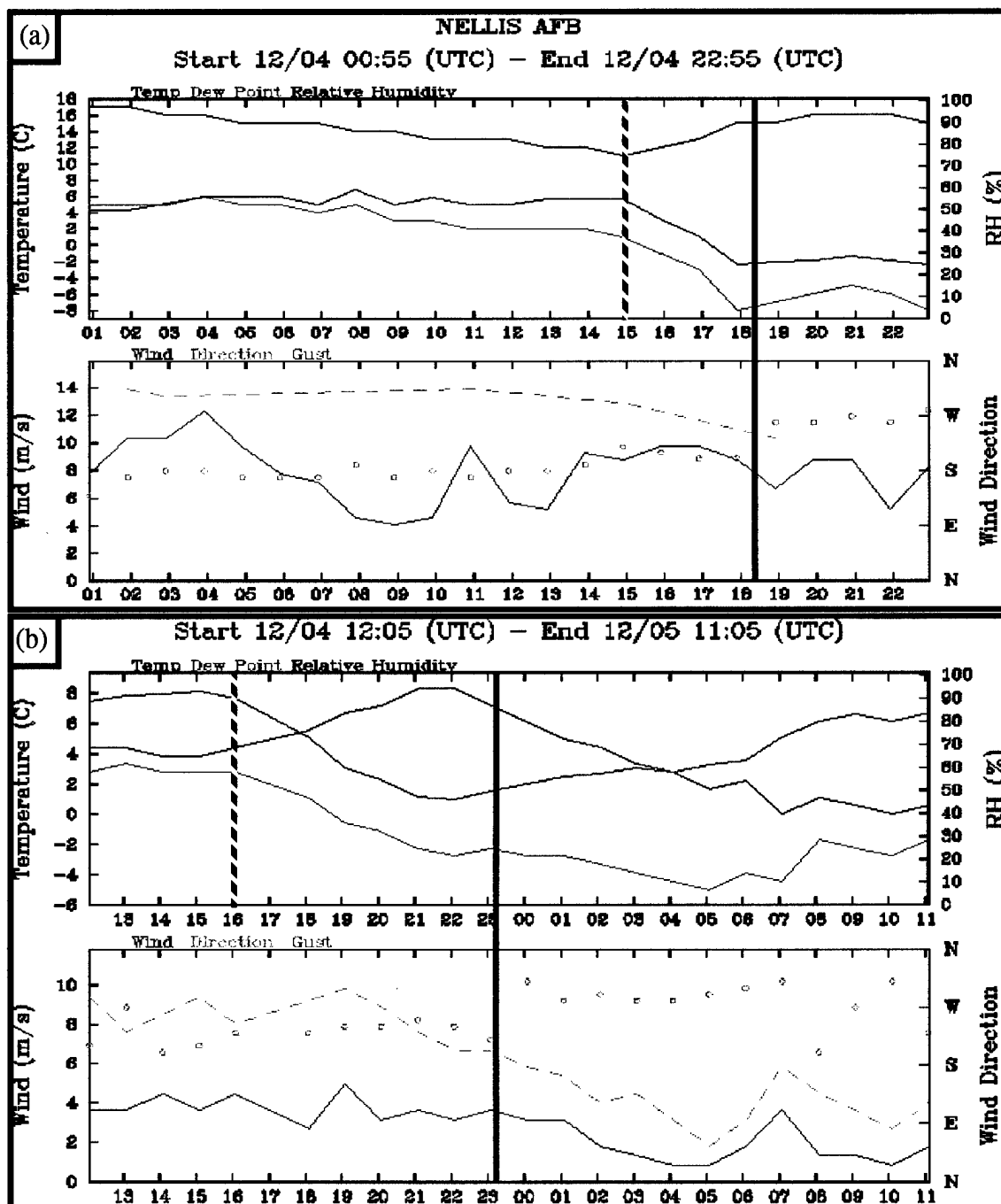


Figure 4.15. Meteograms of temperature (red), dew point (green), relative humidity (blue), wind speed (solid), wind gust (dashed), and wind direction (open circles) at (a) Nellis Air Force Base, NV (LSV) from 0055-2255 UTC 4 December and (b) Music Mountain, AZ (MSC; see Fig. 4.1 for locations) from 1205 UTC 4 December - 1105 UTC 5 December 1998. Solid line denotes frontal passage; dashed line denotes commencement of pronounced drying.

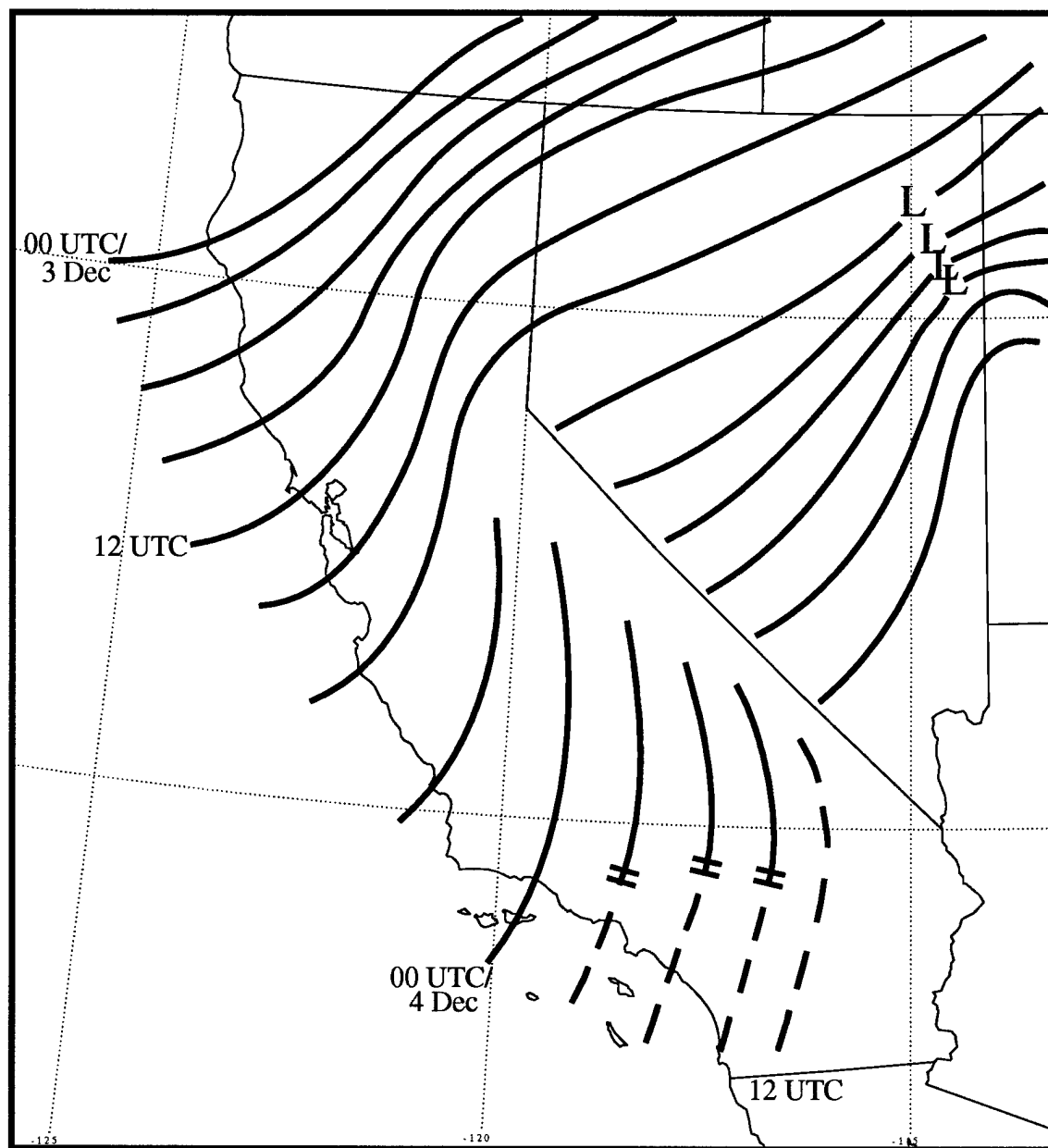


Figure 4.16. Isochrone analysis over the western United States from 0000 UTC 3 December to 1200 UTC 4 December.

topographic blocking and channeling, similar to that documented near other mountain ranges (e.g., Godske et al. 1957; Smith 1985; Hoinka and Heimann 1988), may have produced distortion, with slower equatorward movement of the cold air occurring over and to the lee of the Sierra Nevada and more rapid equatorward movement of cold air occurring on the California Coast. Second, the frontal distortion may also be related to the development of a large scale frontal wave as the upper-level trough and cyclonic potential vorticity anomaly approached California. Similar frontal distortions have been observed by the author during other Great Basin cyclogenesis events, illustrating the need to understand better the interaction between topographic and large-scale processes around the Sierra Nevada.

Frontal Interaction with the Complex Terrain of Northern Utah

Over northern Utah, cyclogenesis and subsequent wave development altered the mesoscale structure of the front as it moved eastward. The topography of this region includes the low elevation basin encompassing the Great Salt Lake Desert and Lake (~1290 m) and several mountain ranges reaching elevations of nearly 3500 m, including the Stansbury, Oquirrh, and Wasatch Mountains (Fig. 4.17). As in the previous section, mesoscale analyses have been performed to examine the interaction of the cyclone and cold front with the topography of northern Utah.

At 0000 UTC 4 December, a closed 1500 m pressure contour was evident across northeastern Nevada and northwestern Utah (Fig. 4.18; for pressure analysis see Fig. 3.13). A low center was placed in the northeastern part of Nevada for two reasons: 1) evidence of a regional prefrontal pressure minimum near Elko, Nevada (EKO; for location

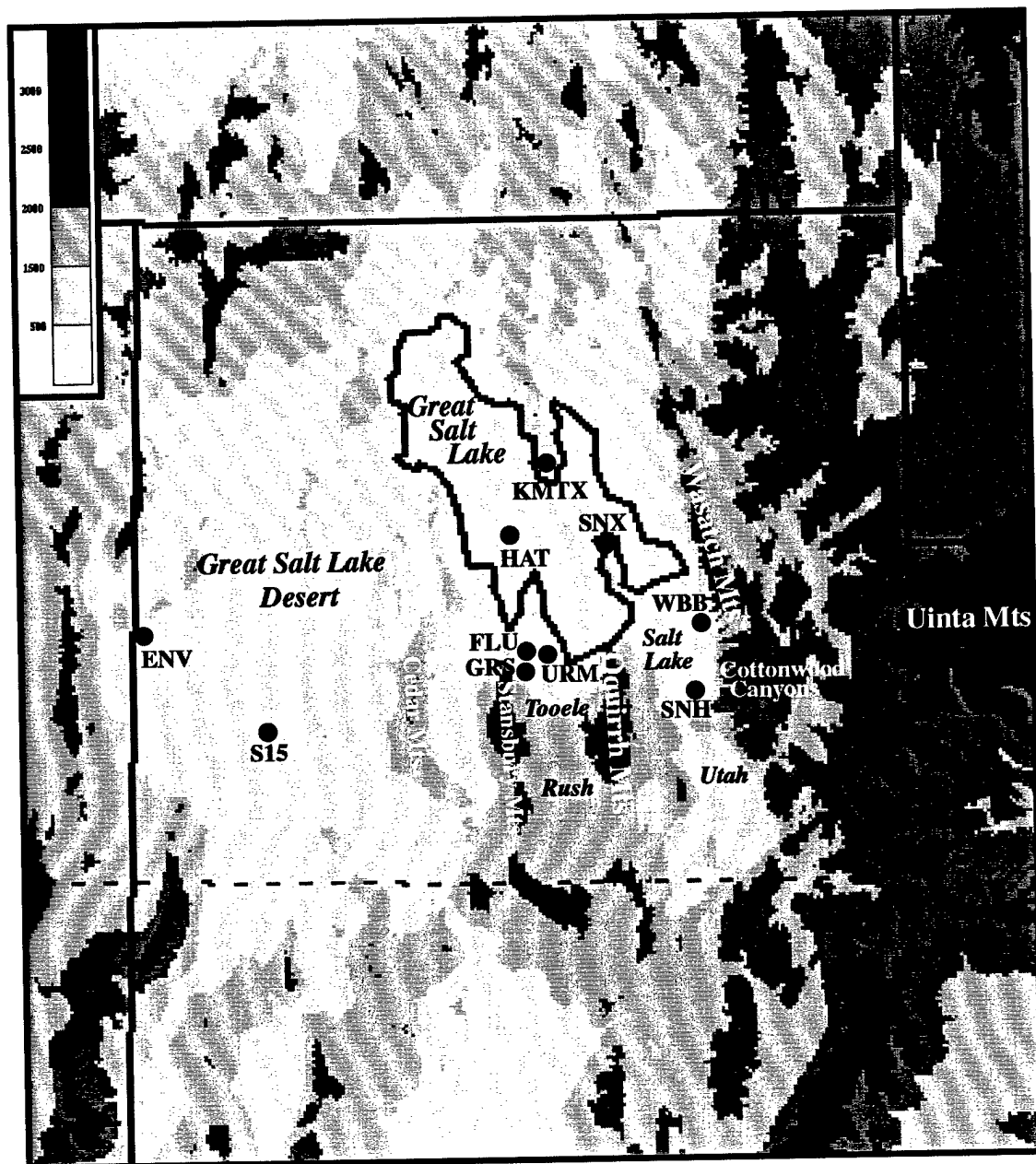


Figure 4.17. Topography and major geographic features of northern Utah. MesoWest stations discussed in text include: Wendover (ENV), Salt Flats (S15), Hat Island (HAT), Antelope Island (SNX), Flux (FLU), Grantsville (GRS), Burmester (URM), University of Utah (WBB), and Sandy (SNH). Also shown is the NEXRAD radar site at Promontory Point (KMTX). Valley names and other specific geographic features are shown in italics. Elevation (m) shaded according to scale at upper left.

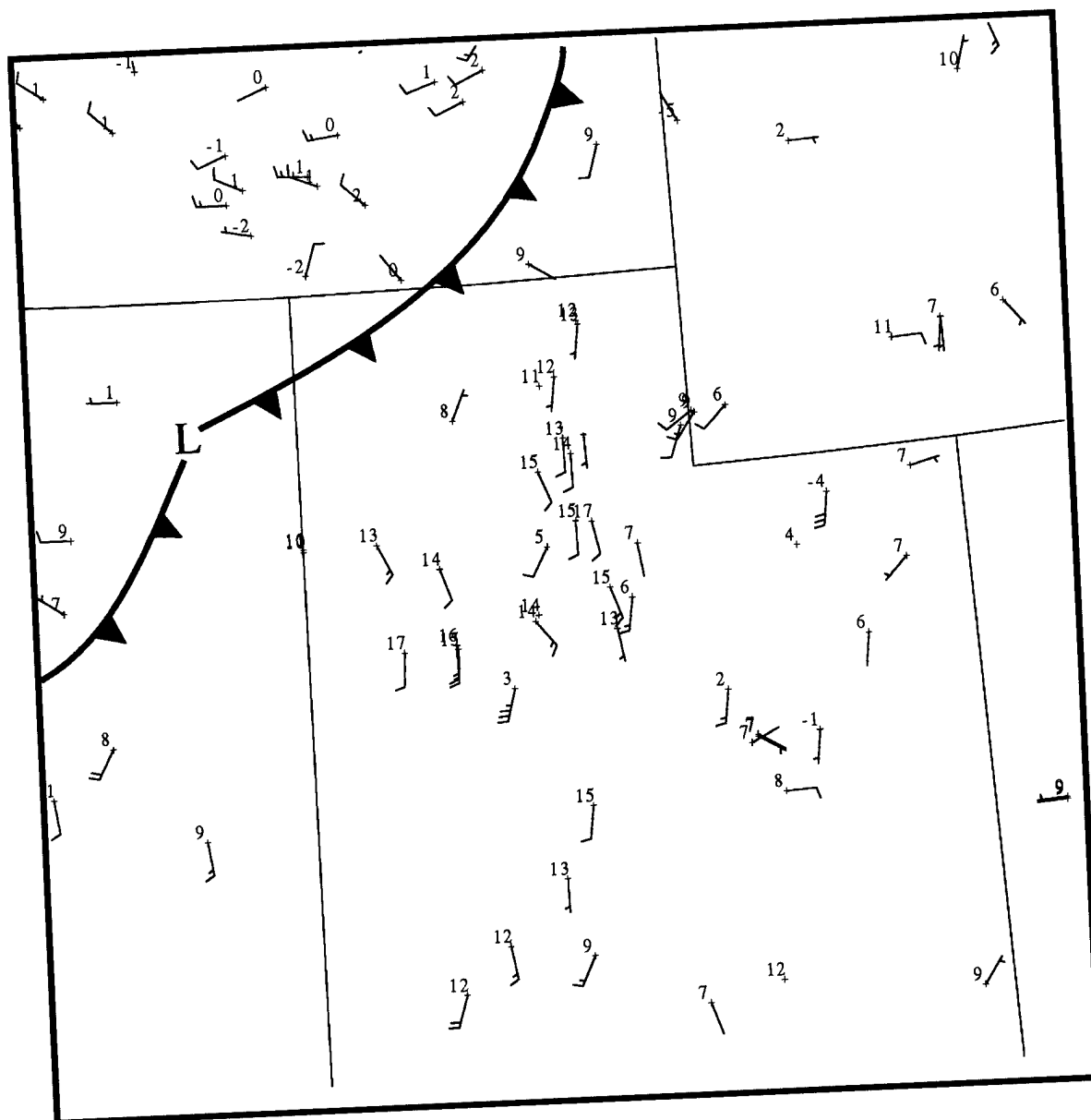


Figure 4.18. Subjective analysis of the main cyclone and attendant frontal structure over northern Utah and the adjacent region for 0000 UTC 4 December.

see Fig. 4.1) at 2100 UTC 3 December (Fig. 3.11)² and 2) an inflection in the baroclinity (not explicitly analyzed). By 0300 UTC 4 December (Fig. 4.19), pressures were continuing to fall over the entire region. Despite the more rapid decrease and overall lower pressure values across northern Utah, the original low over Nevada was still analyzed, primarily because a weak perturbation was still evident in the baroclinity (not explicitly analyzed). Over Utah, a mesoscale circulation center developed along the front over the Great Salt Lake and accelerated the movement of cold air into the deserts and salt flats of western Utah. Enhanced southerly flow to the east of the mesoscale circulation center stalled the front, holding surface temperatures in the 10-15 °C range along the Wasatch Front, a valley region to the west of the Wasatch Mountains. By 0600 UTC, this wave pushed to the eastern shore of the Great Salt Lake, with the cold front trailing south and west toward the original cyclone center over eastern Nevada (Fig. 4.20).

During the existence of this circulation center (0300-0800 UTC 4 December), an intensification of surface wind speeds was evident at many of the observation sites within an 80 km radius (Figs. 4.21-4.23). Salt Flats (S15), located well to the southwest of the developing wave, clearly shows a 8-12 kt increase in wind speed/gust after 0400 UTC and lasting until 0600 UTC (Fig. 4.21a). Hat Island (HAT), located in the western part of the Great Salt Lake and near the frontal wave, recorded an increase in winds from 0430-0730 UTC, despite being in northwesterly surface flow behind the front (Fig. 4.21b). This same time period saw sites in and near the Tooele and Salt Lake Valleys (located to the south and southeast of the wave) show similar increases in wind speed (Figs. 4.22, 4.23).

2. The prefrontal observation was used because of the lack of pressure reporting stations between Elko (EKO) and Wendover (ENV), the nearest station to the east. By 0000 UTC 4 December, pressures had risen at EKO while continuing to fall at ENV, creating a great deal of uncertainty as to where the actual minimum, if any, was located.

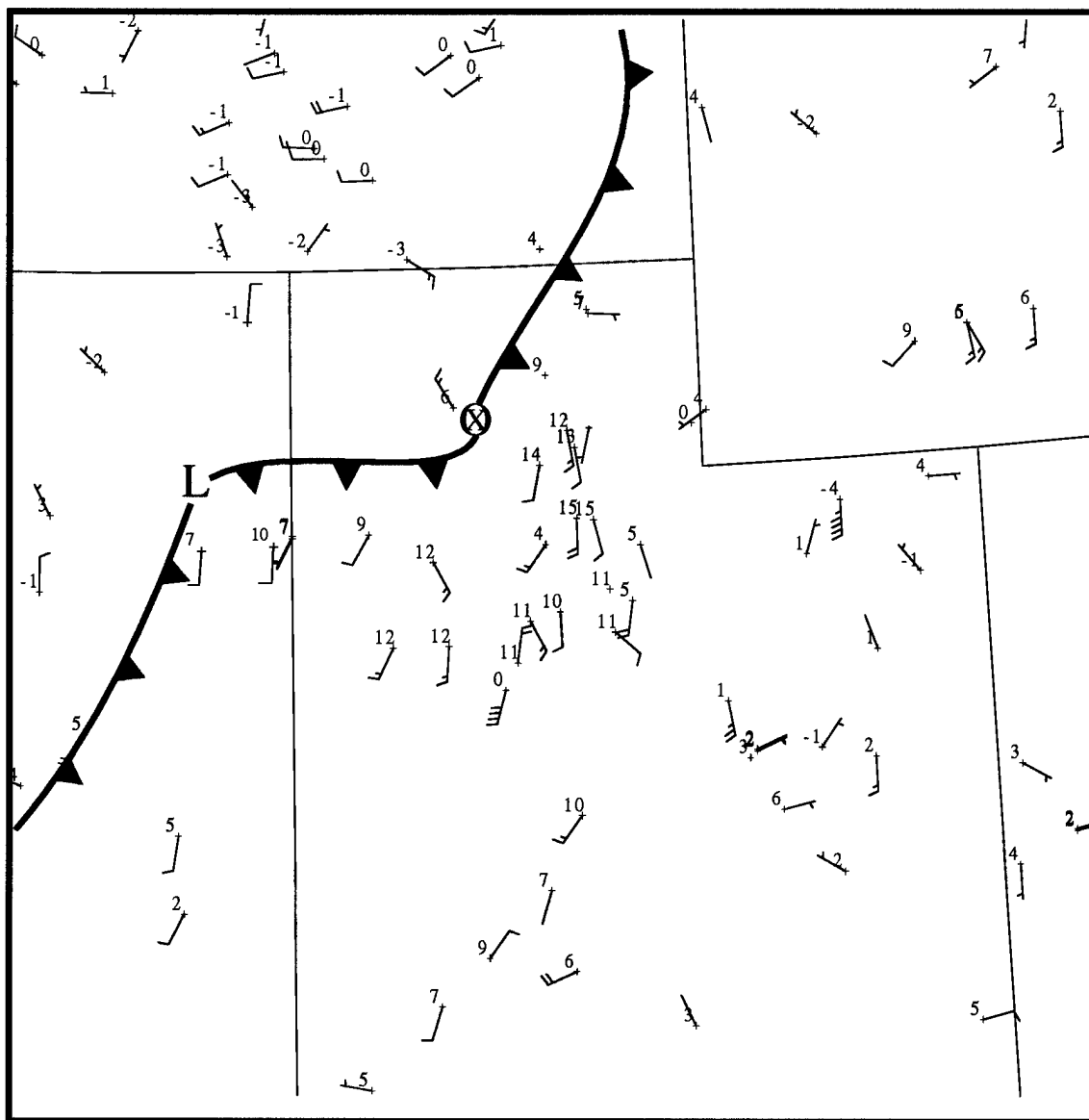


Figure 4.19. Subjective analysis of the main cyclone, attendant frontal structure, and frontal wave (circled x) over northern Utah and the adjacent region for 0300 UTC 4 December.

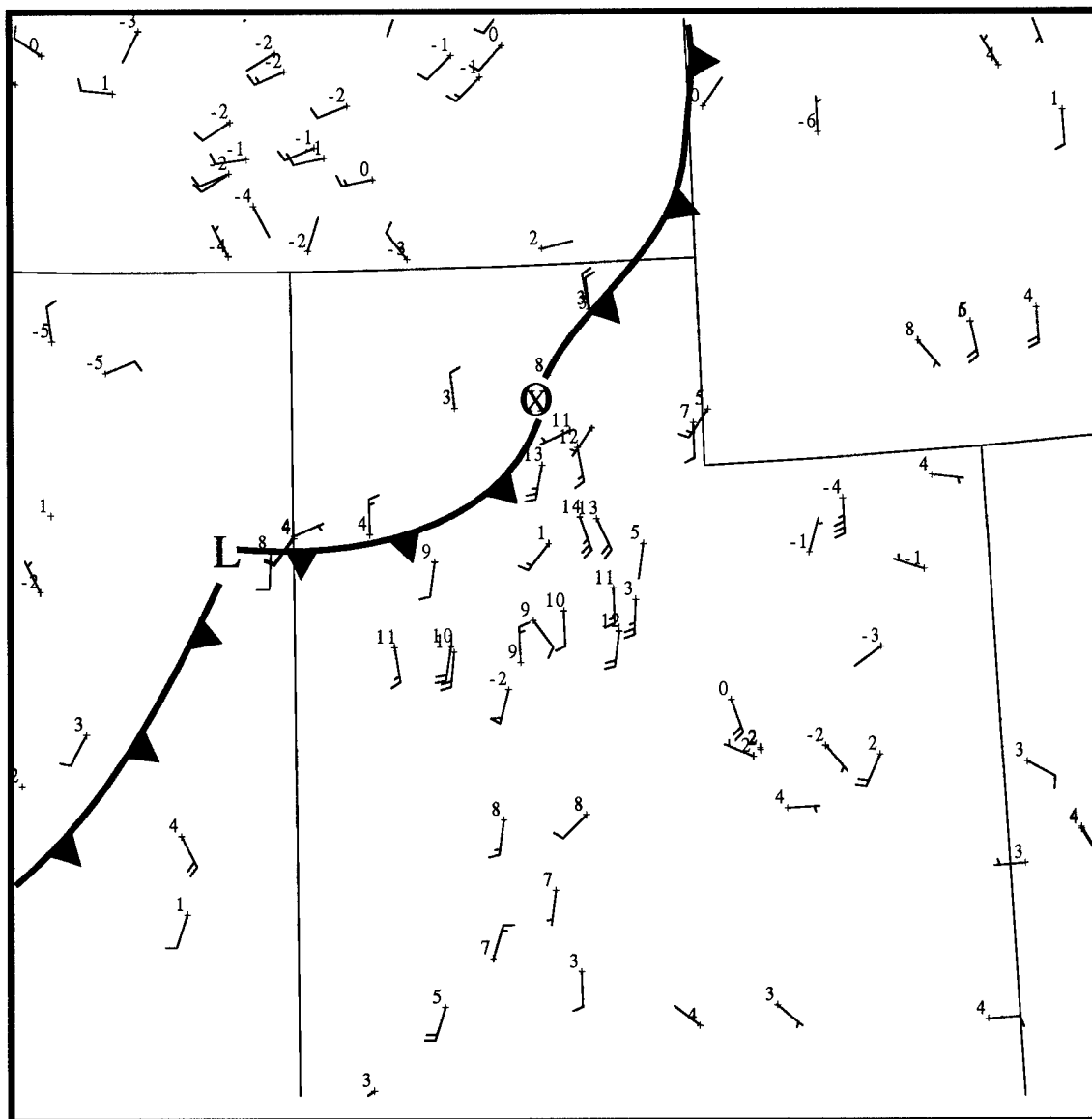


Figure 4.20. Subjective analysis of the main cyclone, attendant frontal structure, and frontal wave (circled x) over northern Utah and the adjacent region for 0600 UTC 4 December.

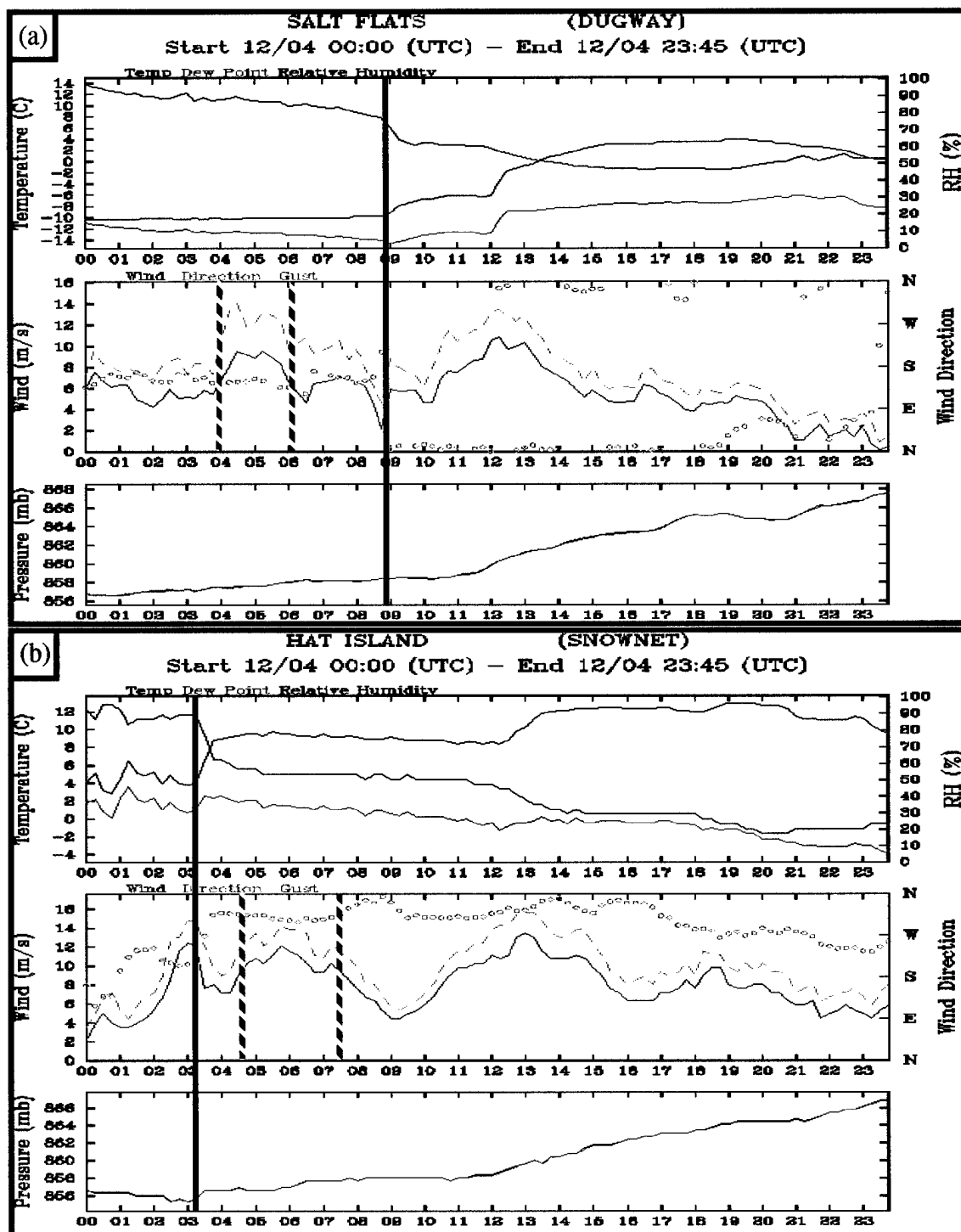


Figure 4.21. Meteorograms of temperature (red), dew point (green), and relative humidity (blue), wind speed (solid), gust (dashed), direction (circles), and altimeter trace at (a) Salt Flats (S15) and (b) Hat Island (HAT; see Fig. 4.17 for locations) from 0000-2345 UTC 4 December 1998. Solid lines denote frontal passage; dashed lines mark possible upper level trough influence.

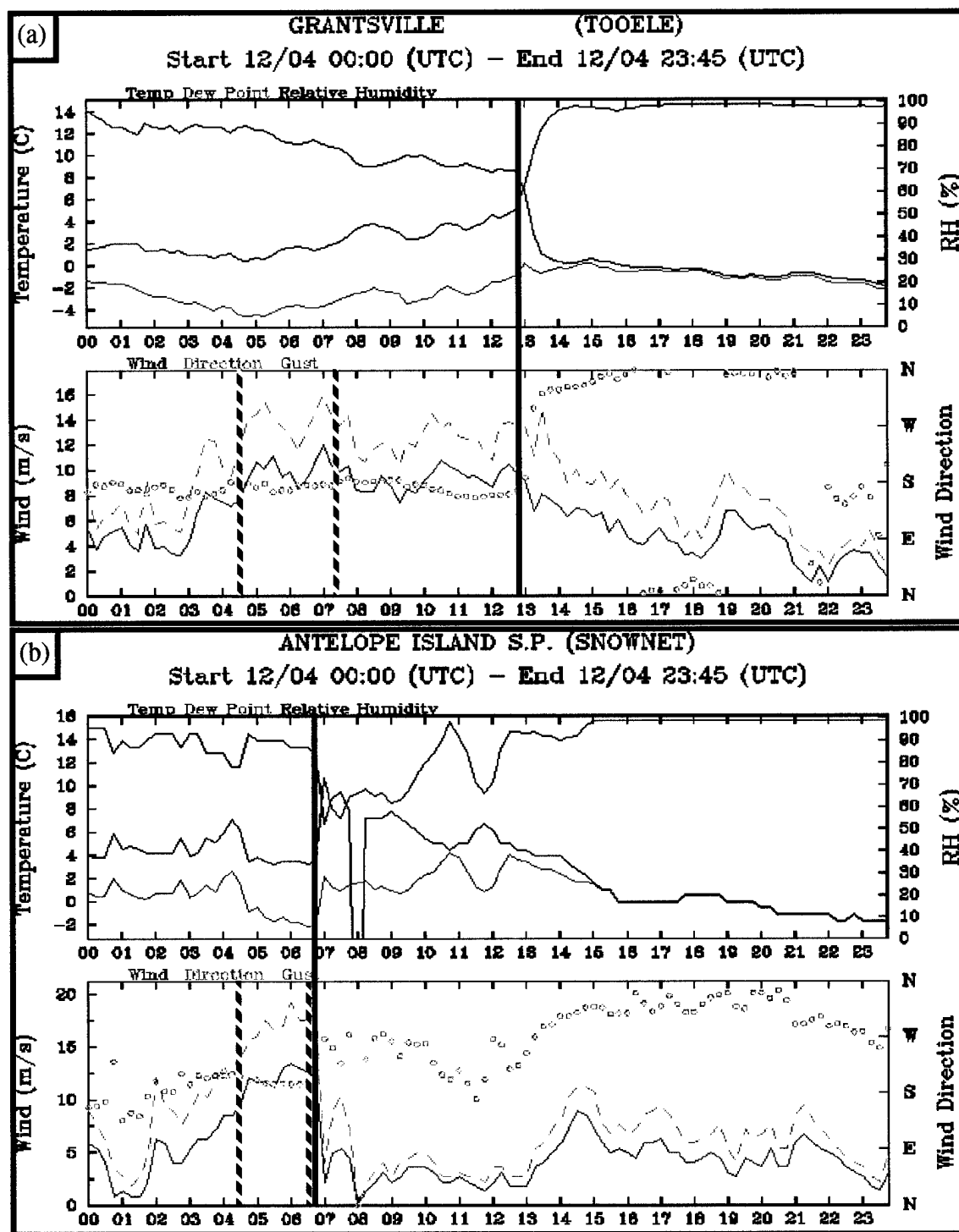


Figure 4.22. Meteograms of temperature (red), dew point (green), and relative humidity (blue), wind speed (solid), gust (dashed), and direction (circles) at (a) Grantsville (GRS) and (b) Antelope Island (SNX; see Fig. 4.17 for locations) from 0000-2345 UTC 4 December 1998. Solid lines denote frontal passage; dashed lines mark possible upper level trough influence. [Note that 0800 UTC temperature at SNX is in error.]

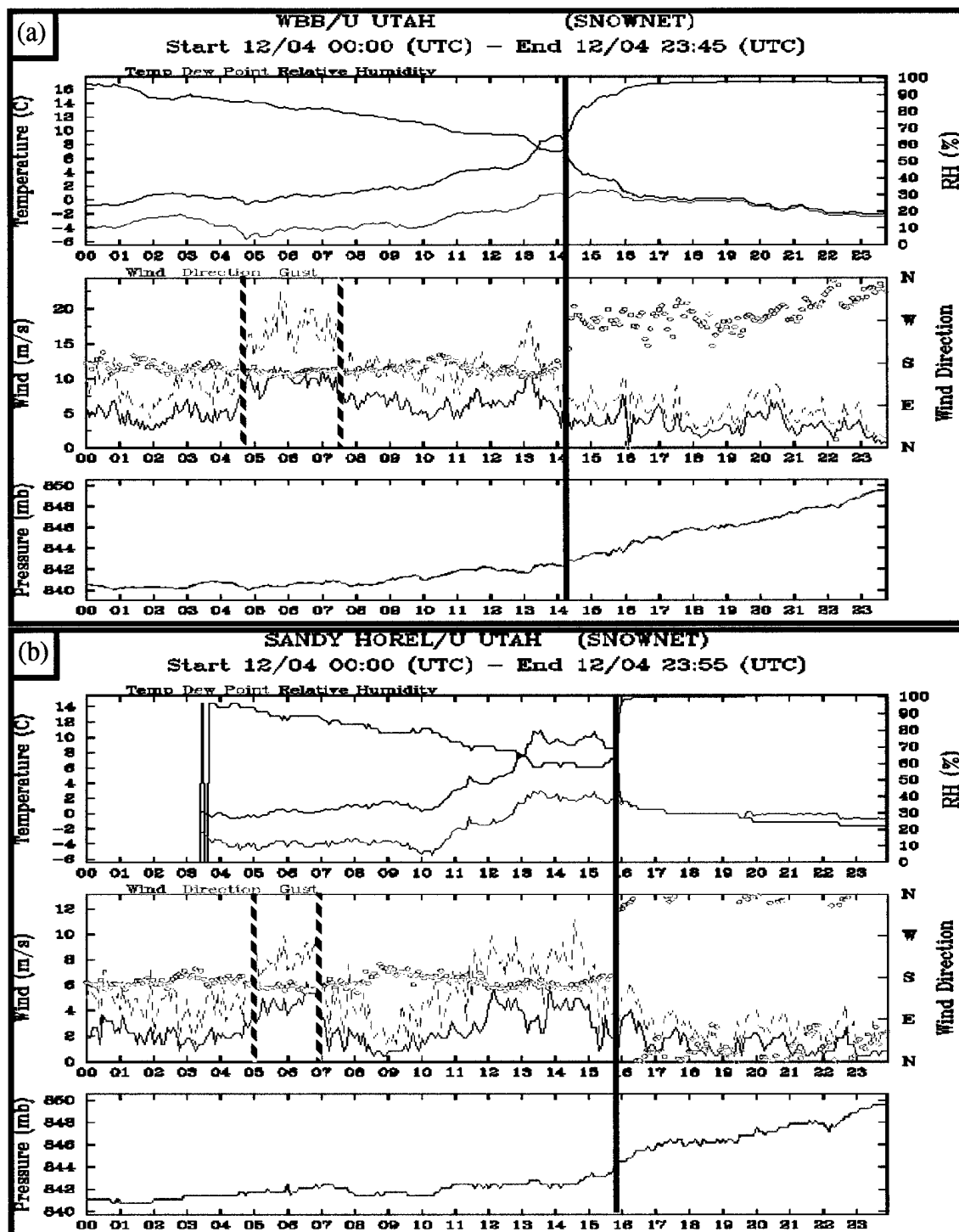


Figure 4.23. Meteorgrams of temperature (red), dew point (green), and relative humidity (blue), wind speed (solid), gust (dashed), direction (circles), and altimeter trace at (a) University of Utah (WBB) and (b) Sandy (SNH; see Fig. 4.17 for locations) from 0000-2355 UTC 4 December 1998. Solid lines denote frontal passage; dashed lines mark possible upper level trough influence.

Interestingly, station pressure traces across the region reveal a fairly flat signal (Figs. 4.21, 4.23). Radar data from the Promontory Point site (KMTX) shows two areas of echoes (25-35 dbz), with the northernmost region prominently oriented along a southwest-northeast axis (Fig. 4.24). This orientation parallels the flow at and above crest level (based on RUC2 700 hPa analysis for 0600 UTC 4 December, not shown) as opposed to the strong southerly surface flow.

By 0900 UTC 4 December, the front was becoming severely distorted over eastern Nevada as the weakening remnants of the original cyclone continued to move very slowly southeastward (Fig. 4.25). Over northern Utah, the mesoscale circulation center over the eastern shore of the Great Salt Lake moved rapidly northeast and eventually dissipated near the Wasatch Mountains while a second circulation developed over western Utah near the Cedar and Stansbury Mountains. This second circulation center can be seen more clearly from the examination of two MesoWest sites to the north and east of its center. These sites, Flux (FLU) and Burmester (URM), initially recorded a cold frontal passage between 0845 and 0945 UTC. FLU, located on the northern edge of the Tooele Valley, reported a 180° wind shift and 5 °C temperature decrease as the front swept through at 0845 UTC (Fig. 4.26a). URM, which is located 10 km east-southeast of FLU, experienced a 90° wind shift and a 2 °C temperature drop at 0945 UTC (Fig. 4.26b). The temperature and wind profile, however, returned to its pre-frontal state at URM by 1015 UTC as the second circulation center approached from the west. The front continued to move north and reached FLU by 1100 UTC, resulting in a brief wind shift and a 3 °C temperature rise. After stalling for a brief period of time, the front then turned southward, passing through FLU at 1200 UTC and URM at 1230 UTC.

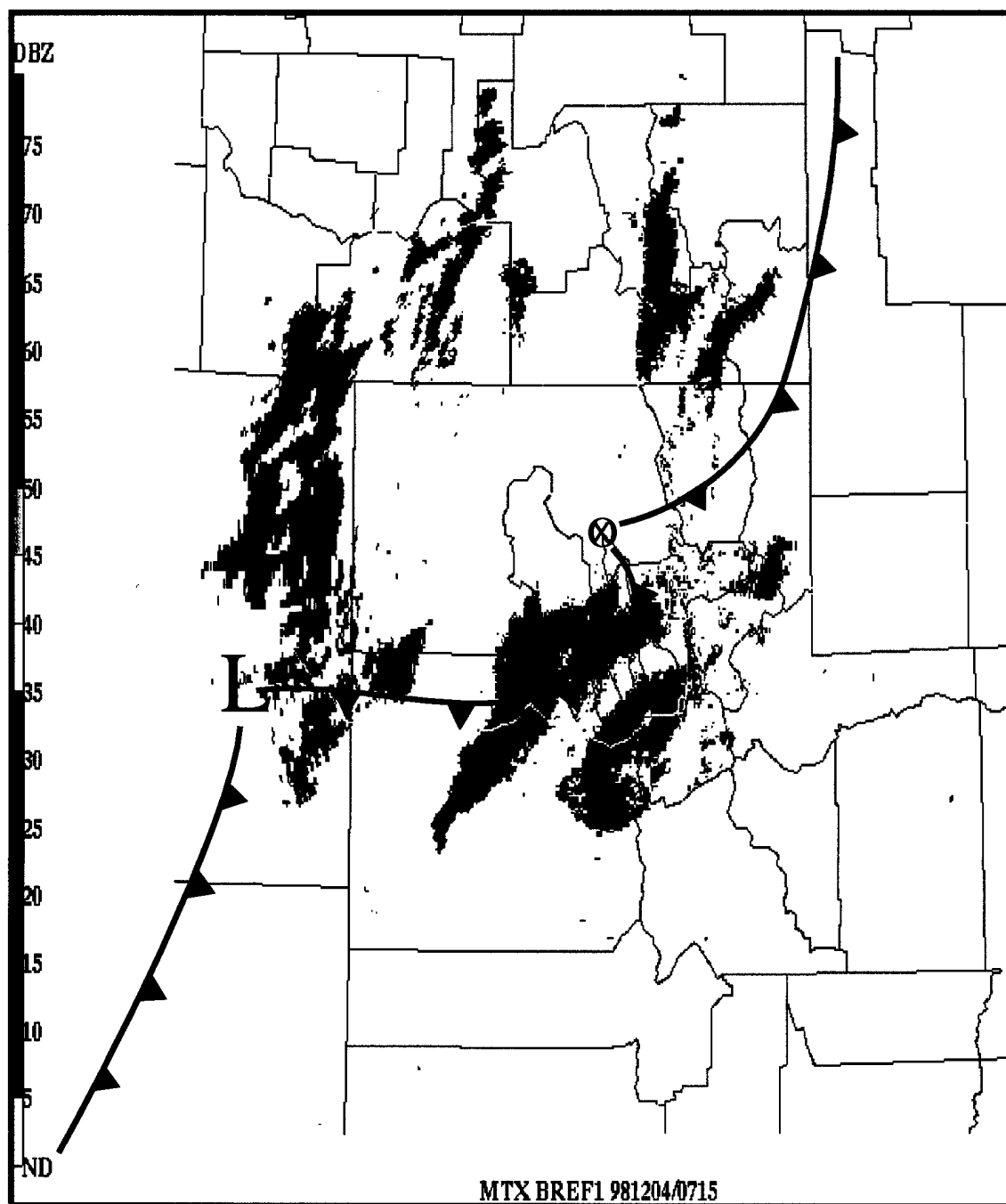


Figure 4.24. Base reflectivity radar imagery from Promontory Point (KMTX) valid 0715 UTC 4 December. Frontal analysis, cyclone (red L) and wave location (red circled x) for 0700 UTC are also shown.

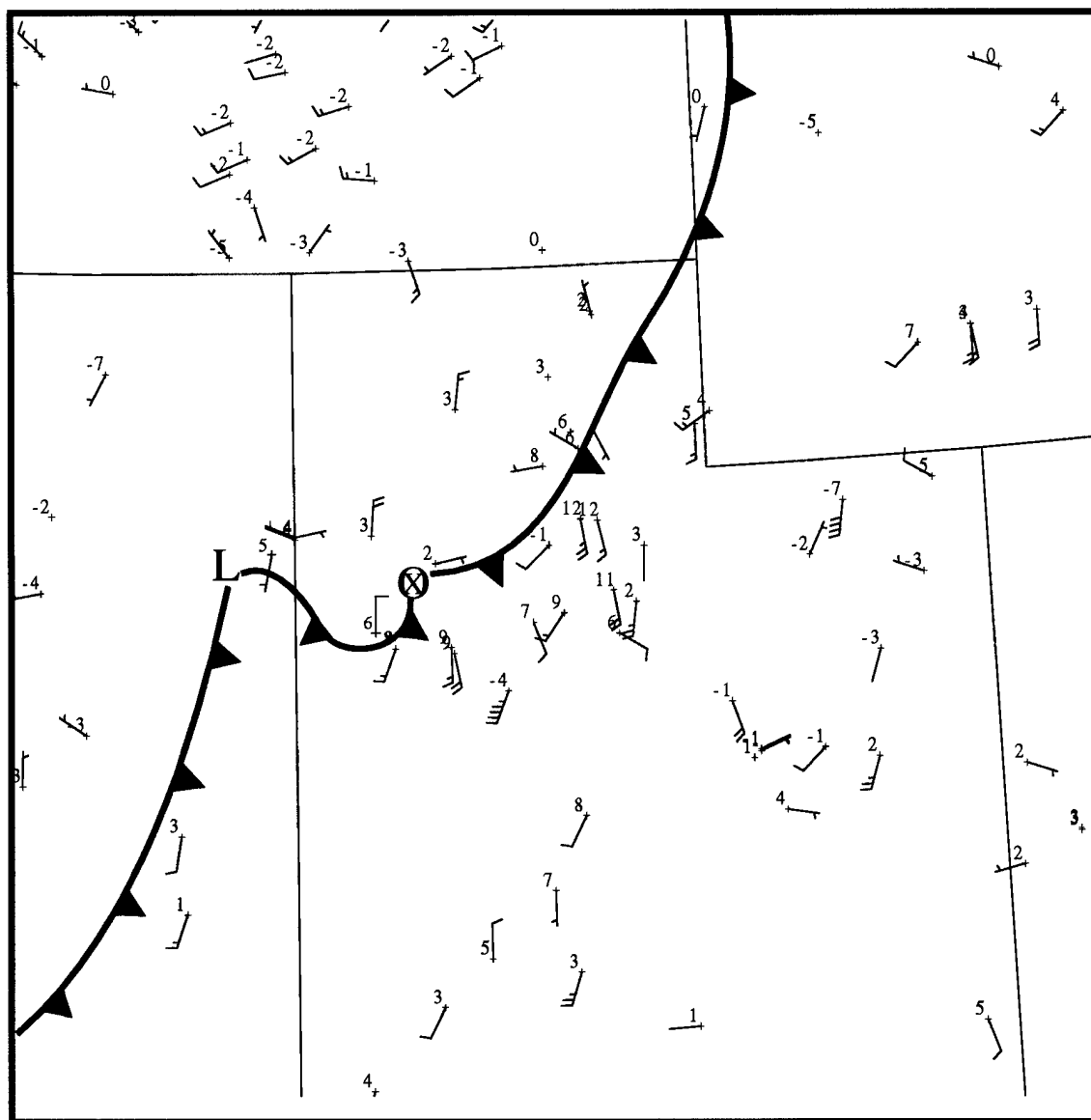


Figure 4.25. Subjective analysis of the frontal structure and frontal wave over northern Utah (circled x) and the adjacent region for 0900 UTC 4 December.

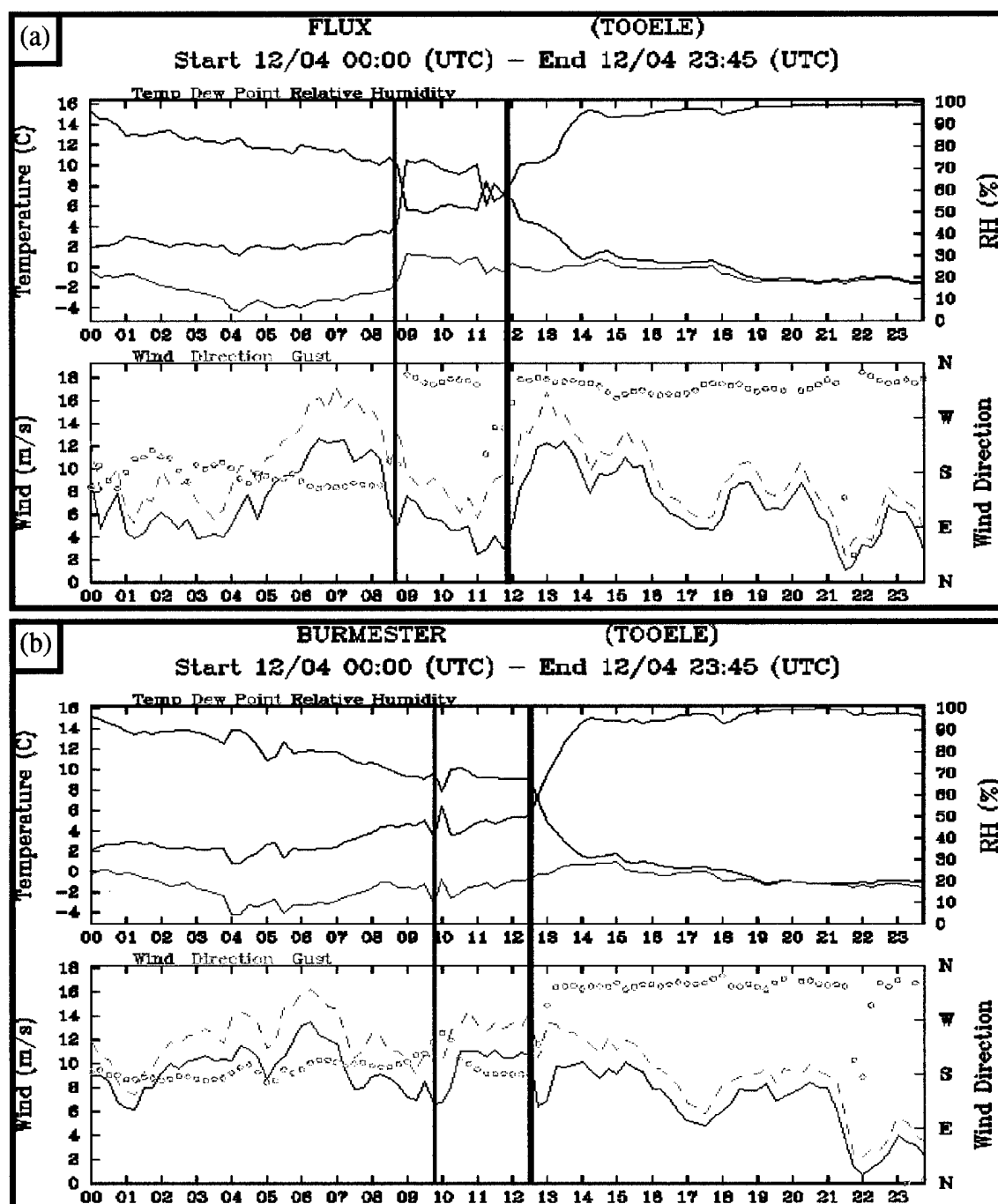


Figure 4.26. Meteorgrams of temperature (red), dew point (green), and relative humidity (blue), wind speed (solid), gust (dashed), direction (circles), and altimeter trace at (a) Flux (FLU) and (b) Burmester (URM; see Fig. 4.17 for locations) from 0000-2345 UTC 4 December 1998. Solid lines denote initial frontal passage (thin) and secondary frontal passage (thick).

By 1200 UTC 4 December, the front over eastern Nevada was moving more rapidly southeastward and signs of the persistent pressure minimum had mostly disappeared (Fig. 4.27; for pressure analysis, see Fig. 3.17). The second mesoscale circulation slowly moved eastward and became the main feature along the front. As was the case with the first circulation center, the hint of a surface wind increase is apparent following the development of this second circulation (1100-1500 UTC), most notably in Figs. 4.21, 4.23, and 4.26a. By 1500 UTC, the wave was located over the Rush Valley as the trailing cold front continued to move rapidly eastward (Fig. 4.28). A pronounced acceleration of the front was also apparent across the Rush Valley as cold air moved cyclonically around the southern extent of the Oquirrh mountains. This allowed cold air to enter the Utah Valley from both the north as well as from the west. Precipitation was becoming more widespread in the postfrontal environment with two distinct characteristics in the echo regime (Fig. 4.29). In the deeper cold air behind the front, a wide cold-frontal precipitation band was evident, while nearer the frontal boundary the precipitation had a more cellular structure. Additionally, precipitation was beginning to focus along the topography, especially over the Wasatch mountains north of the cold front.

Little evidence of a closed pressure minimum existed along the front by 1800 UTC as the wave continued to move eastward, then northeastward toward the Wasatch Mountains (Fig. 4.30; pressure analysis not shown). Radar imagery from this time indicated that widespread precipitation continued in the postfrontal environment with evidence of two separate wide bands (Fig. 4.31, marked 1 and 2, respectively). These bands merged around 1850 UTC and briefly intensified the radar echoes over the southern Great Salt Lake (Fig. 4.32). By 2100 UTC, only a small perturbation existed along the

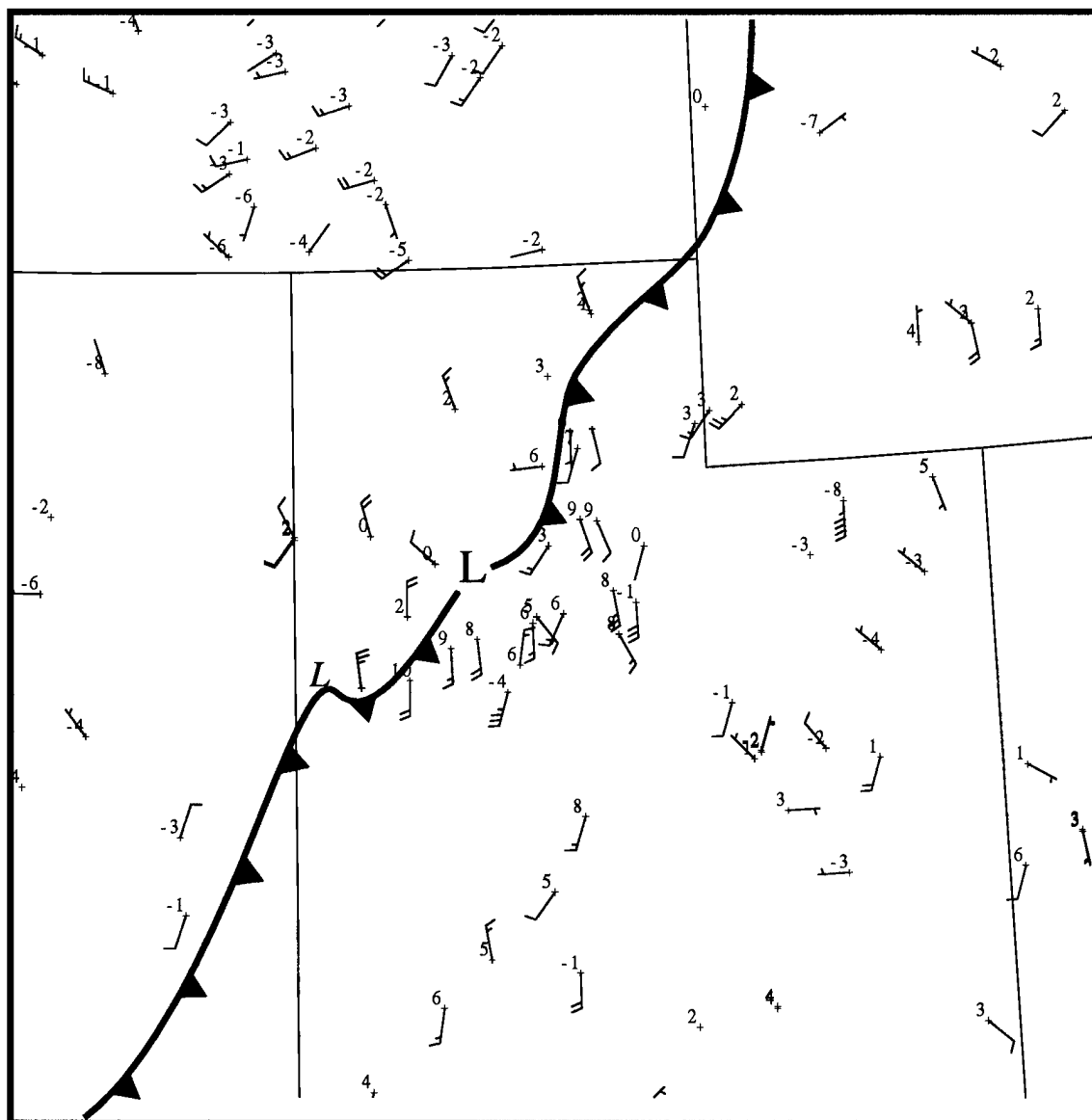


Figure 4.27. Subjective analysis of the new cyclone (large L), decaying parent cyclone (small, italicized L), and attendant frontal structure over northern Utah and the adjacent region for 1200 UTC 4 December.

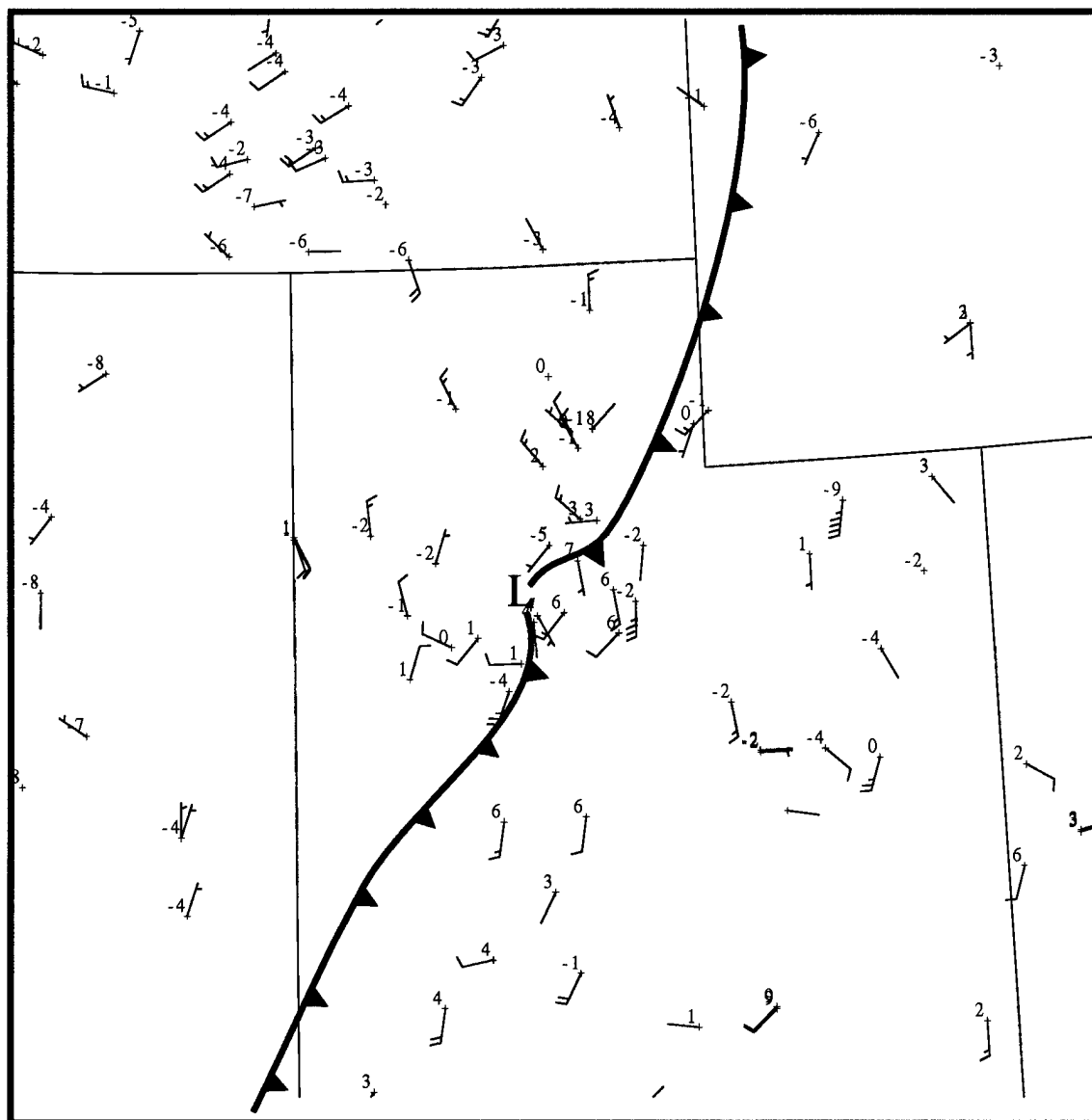


Figure 4.28. Subjective analysis of the cyclone and attendant frontal structure over Utah and the adjacent region for 1500 UTC 4 December.

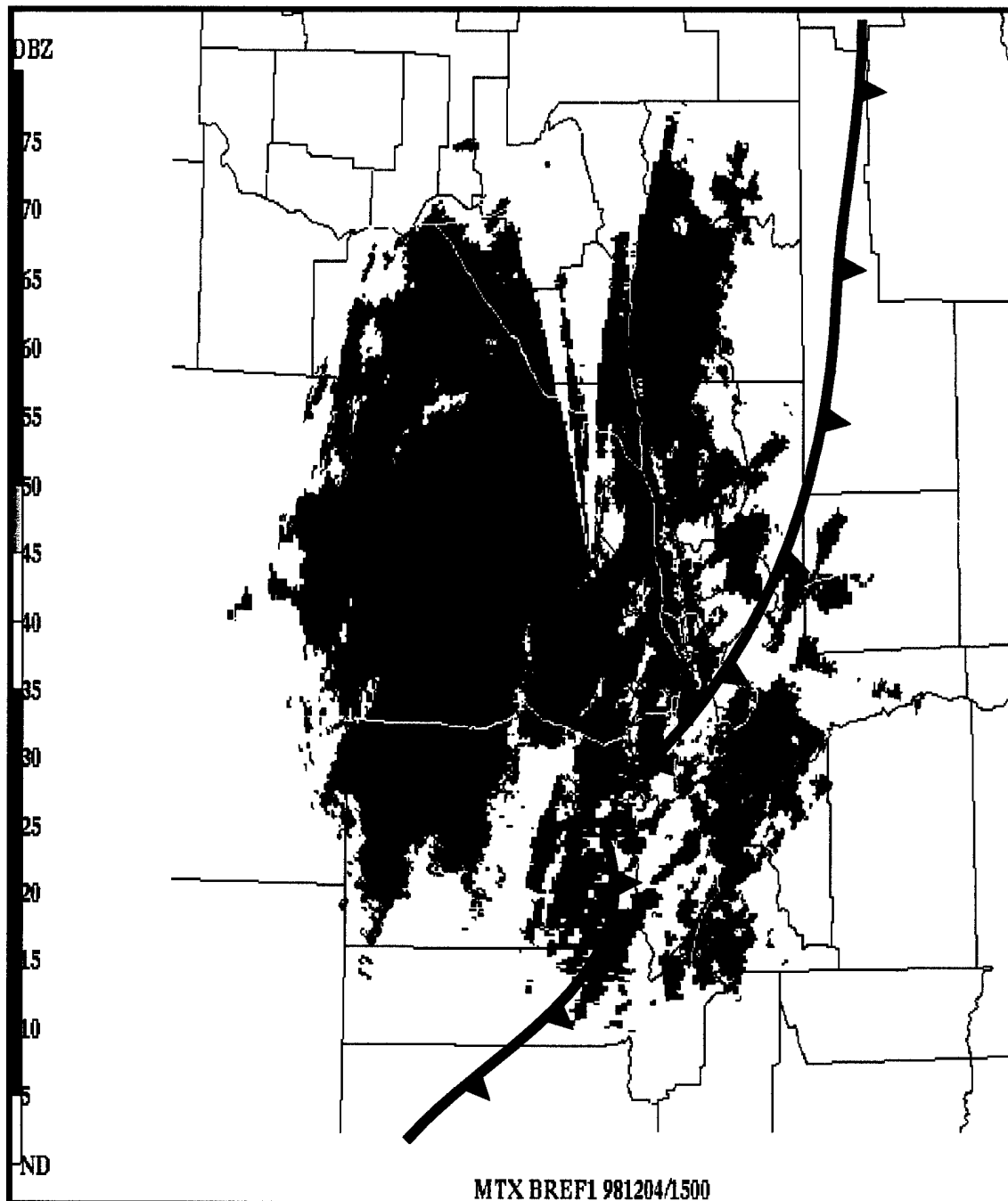


Figure 4.29. Base reflectivity radar imagery from Promontory Point (KMTX) valid 1500 UTC 4 December. Frontal analysis with cyclone position (red "L") for 1500 UTC are also shown.

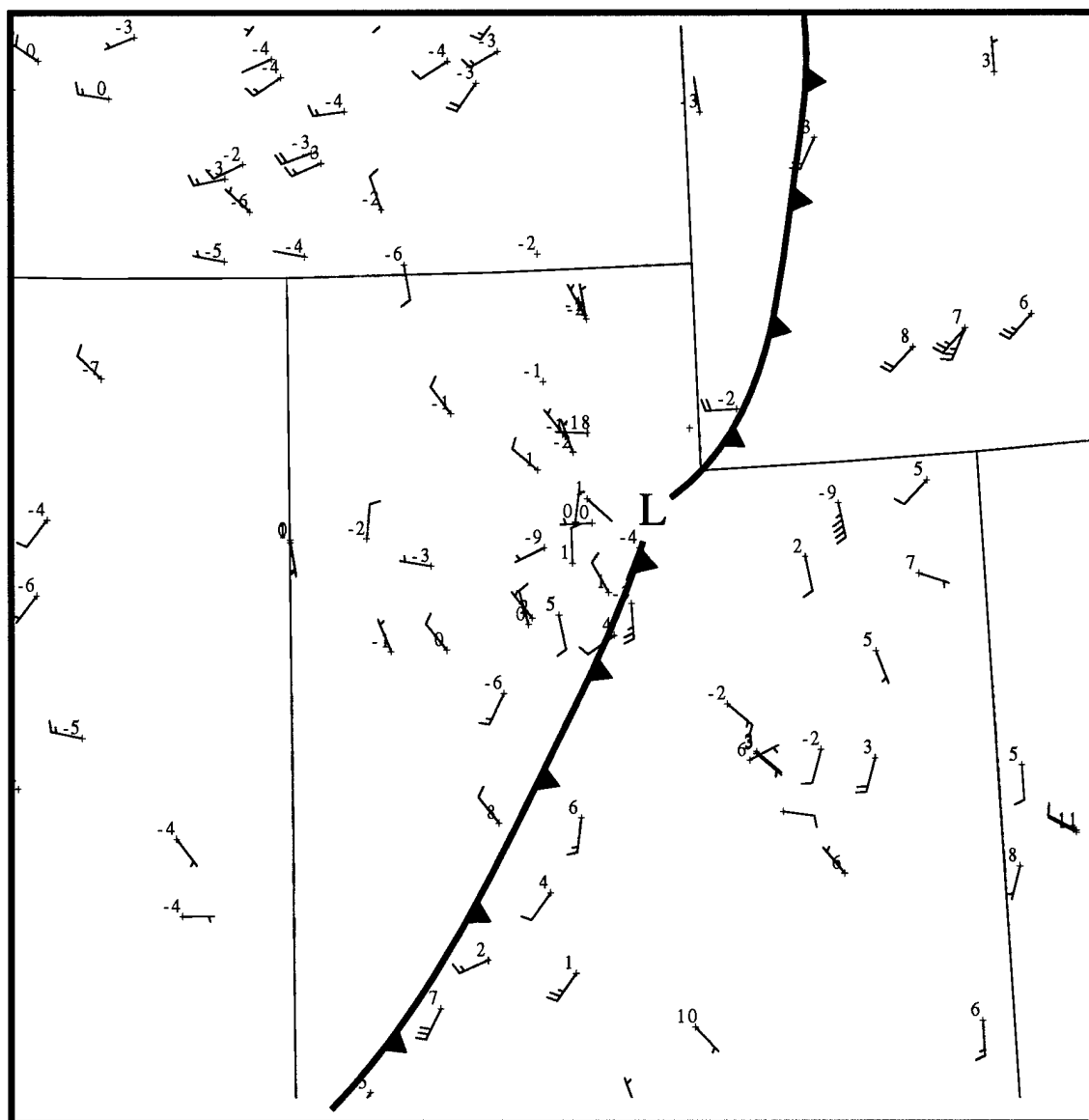


Figure 4.30. Subjective analysis of the cyclone and attendant frontal structure over Utah and the adjacent region for 1800 UTC 4 December.

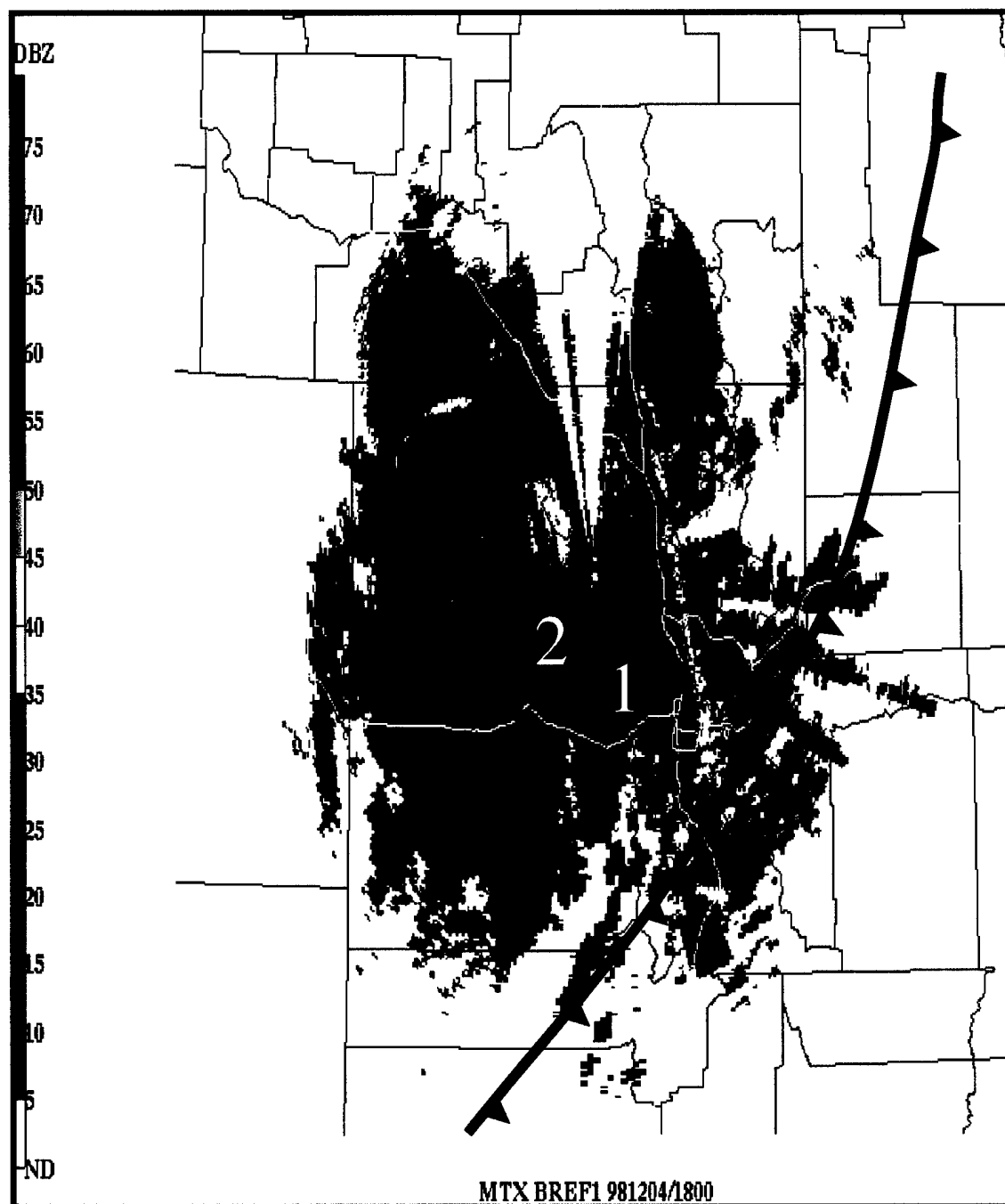


Figure 4.31. Base reflectivity radar imagery from Promontory Point (KMTX) valid 1800 UTC 4 December. Frontal analysis with cyclone position (red L) for 1800 UTC are also shown. Separate cold-frontal precipitation bands are labeled 1 and 2.

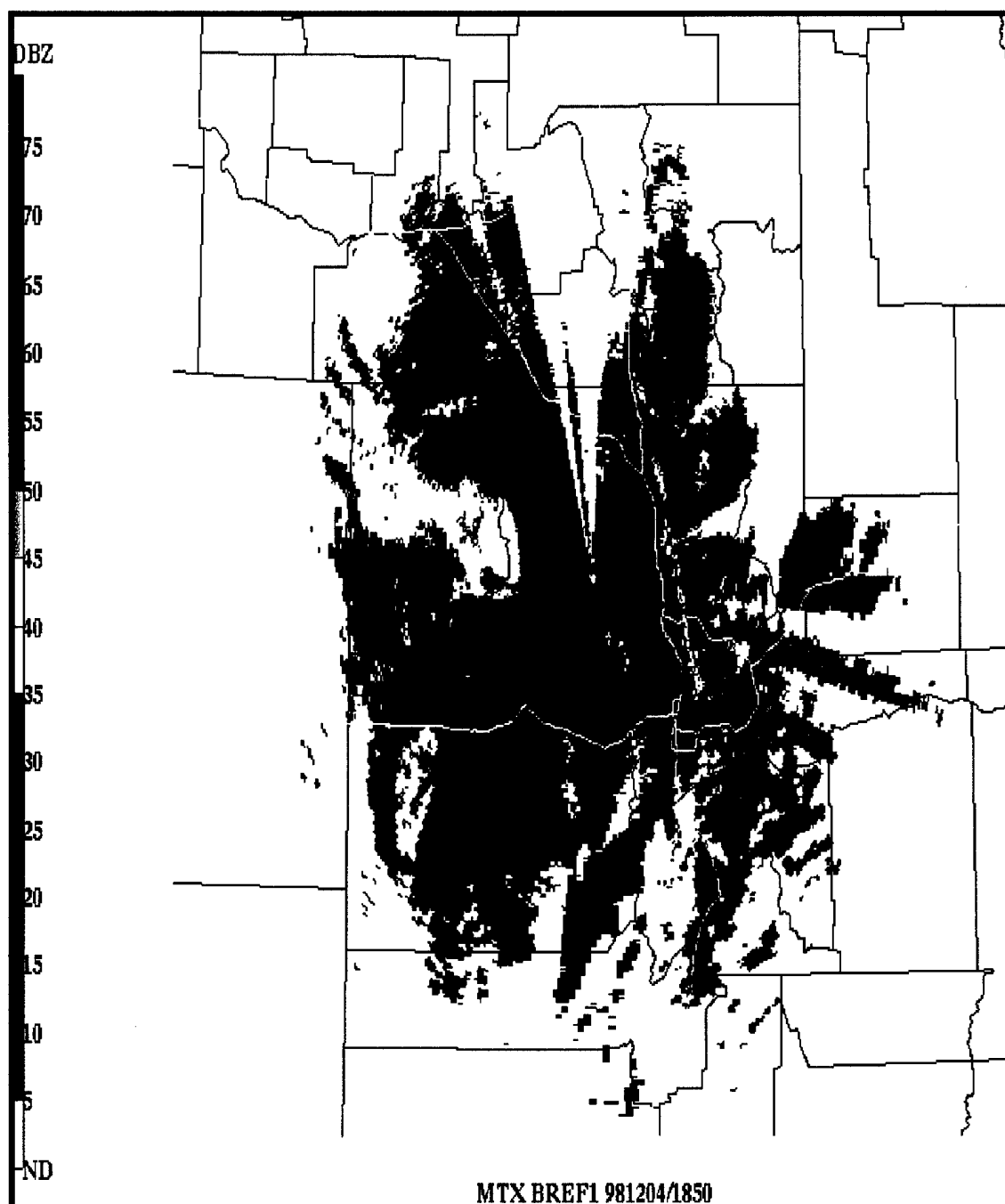


Figure 4.32. Base reflectivity radar imagery from Promontory Point (KMTX) valid 1850 UTC 4 December.

front near the Uinta mountains (Fig. 4.33) as a new low strengthened over central Wyoming (not shown). Radar composites showed slightly less areal coverage of precipitation at this time (not shown), though this may have been partially an artifact of mountain obstruction across the region. Snow was still falling at an impressive rate ($5\text{--}10\text{ cm h}^{-1}$) in portions of the Wasatch mountains, especially around the Cottonwood Canyons southeast of Salt Lake City.

Thus it appears that multiple mesoscale circulation centers developed along the cold front over northern Utah. Similar features have been observed near the inner-core of extratropical cyclones over oceanic regions by Neiman et al. (1993). The present work, however, appears to be the first documentation of such features over the complex terrain of the western United States. Such features were also observed over northern Utah during the Intermountain Precipitation EXperiment (IPEX) field program that was held in February 2000 (Schulz et al. 2000). Additional research is needed to examine the physical processes responsible for the generation of such features in regions of complex orography.

Southern Idaho Orographic Effects and Development of Snake River Convergence Zone

The most prominent terrain feature of southern Idaho is the Snake River Plain (SRP), which is approximately 100 km in width and runs east from the Oregon border toward Wyoming and eventually north toward Montana (Fig. 4.34). Nearly 700 km in length, the SRP is bounded by the central Idaho Mountains to the north, and several high mountain ranges to the south. The central Idaho Mountains consist of individual ranges such as the Sawtooth and Bitterroots, and rise sharply to elevations of nearly 3800 m. The ranges to the south, while not as continuous, run mostly in a north-south orientation and

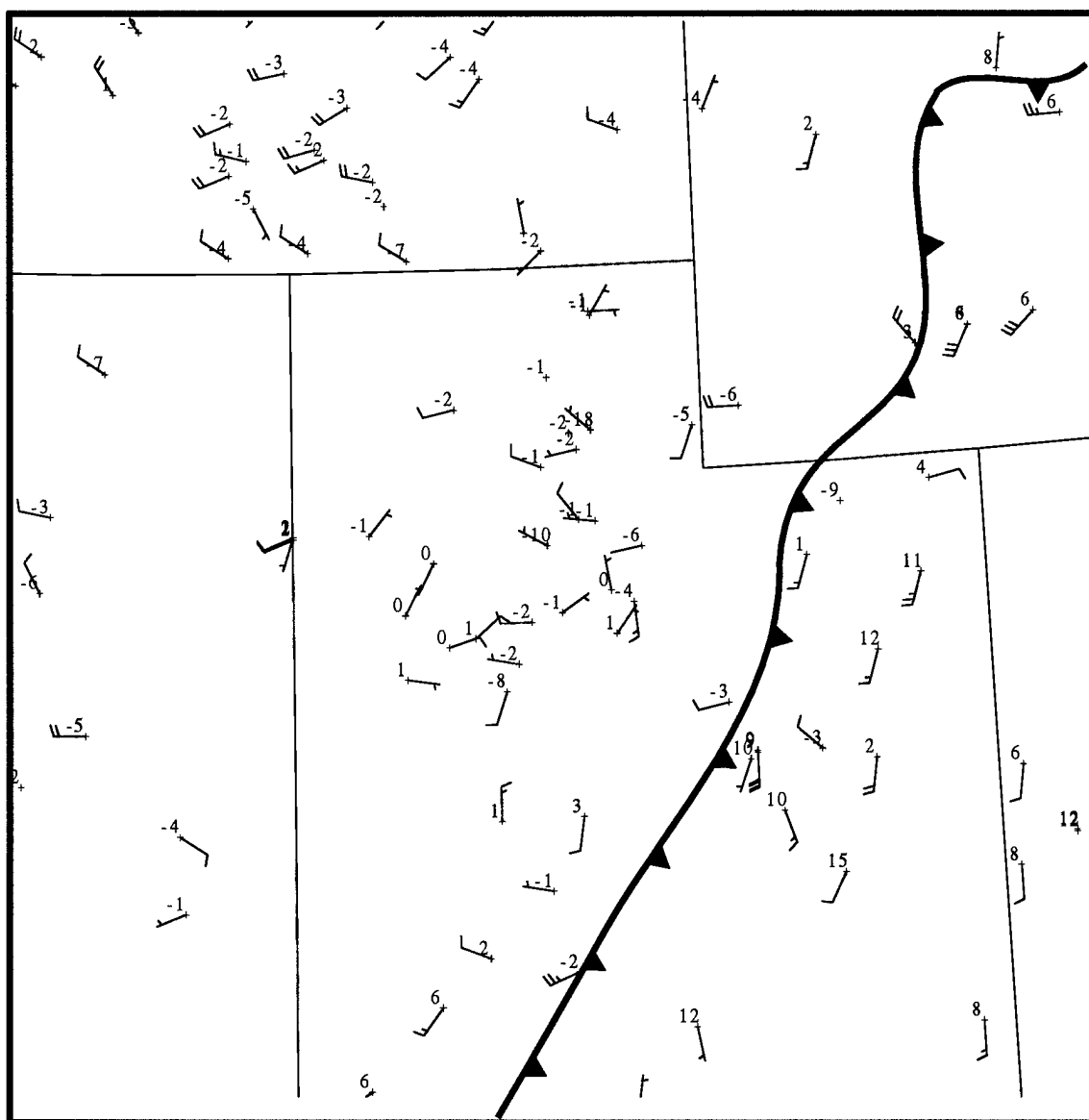


Figure 4.33. Subjective analysis of the frontal structure over Utah and the adjacent region for 2100 UTC 4 December.

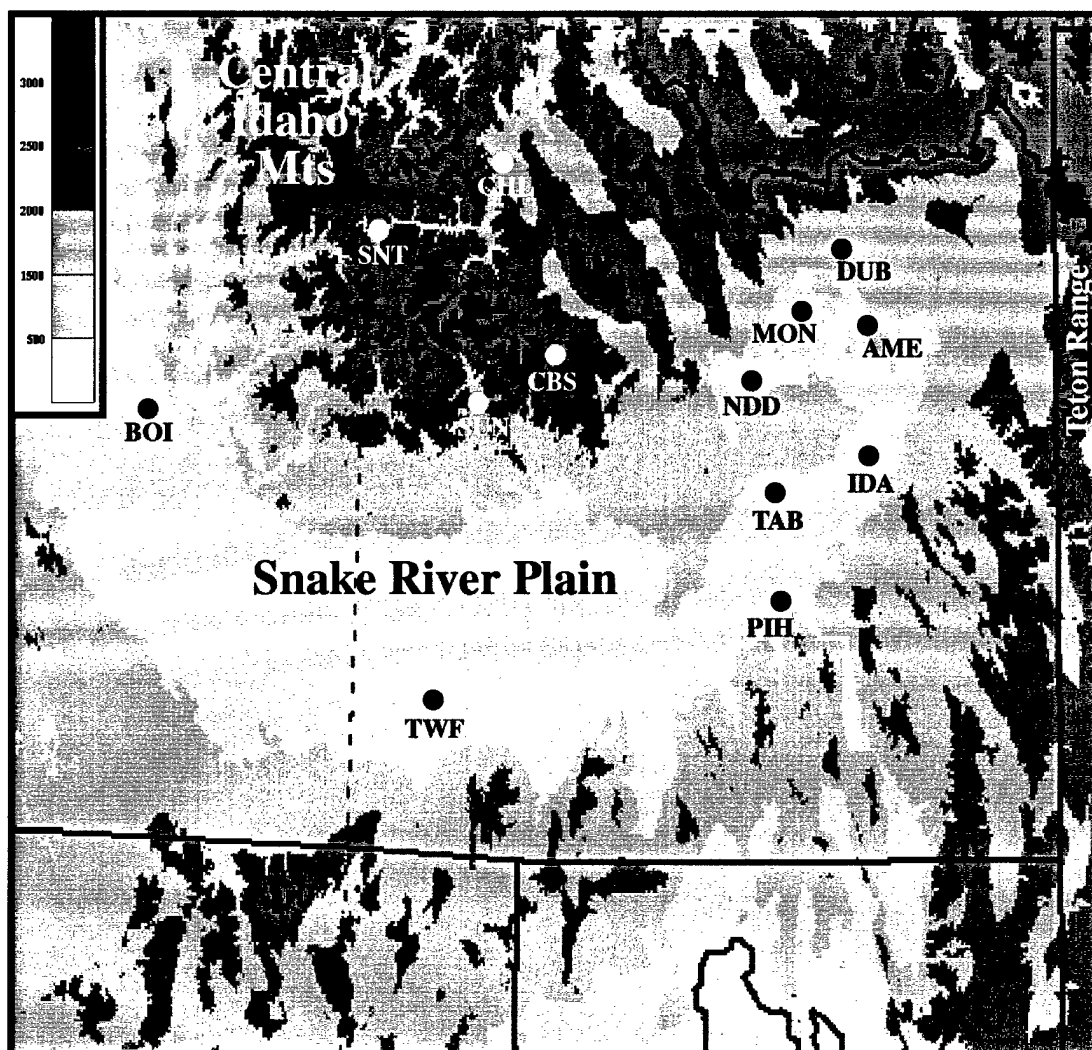


Figure 4.34. Topography and major geographic features of southern Idaho. MesoWest stations discussed in text include: Boise (BOI), Stanley (SNT), Challis (CHL), Hailey (SUN), Copper Basin (CBS), Twin Falls (TWF), Pocatello (PIH), Taber (TAB), Idaho Falls (IDA), Sand Dunes (NDD), Montevue (MON), Camus (AME), and DuBois (DUB). Elevation (m) shaded according to scale at upper left.

slope more gradually toward several individual peaks with elevations from 2700–3000 m. Towards its eastern terminus, the SRP is bordered by the Teton Range. This configuration of topography typically creates several interesting mesoscale effects, including frontal distortions and low-level convergence zones (e.g., Wendell 1972; Andretta and Hazen 1998). Many of these features were evident during the 3–5 December cyclone event.

At 0000 UTC 3 December, a cold front was draped southwest to northeast across the northwestern United States (see Fig. 3.4). Six hours later, the front extended across the western SRP, central Idaho Mountains, and southwestern Montana, where a weak 1500-m pressure minimum was developing along the front (Fig. 4.35, pressure analysis not shown). By 1200 UTC, the front was moving rapidly up the SRP, but was becoming increasingly difficult to identify in the central Idaho mountains (Fig. 4.36). After Stanley (SNT; Fig. 4.37a) and Challis (CHL; not shown) recorded fairly sharp frontal passages (1300–1500 UTC), the front became almost impossible to identify over the central Idaho Mountains. Conversely, the front was easily tracked throughout the SRP, from Twin Falls (TWF, 1400 UTC; not shown), to Pocatello (PIH, 1800 UTC; Fig. 4.37b), to Idaho Falls (IDA, 2100 UTC; not shown). Further north, the section of the front over southwestern Montana was making very slow southward progress but was identifiable at several valley locations (Fig. 4.38; meteograms not shown). Also during this period, the pressure minimum initially located over southwest Montana moved southeastward and became positioned in northeastern Idaho by 0000 UTC 4 December (Fig. 4.39; for pressure analysis, see Fig. 3.13)

As cold air moved equatorward from Montana and up the SRP, 1500-m pressures rose quickly in these regions. Meanwhile, the pressure minimum over northeastern Idaho

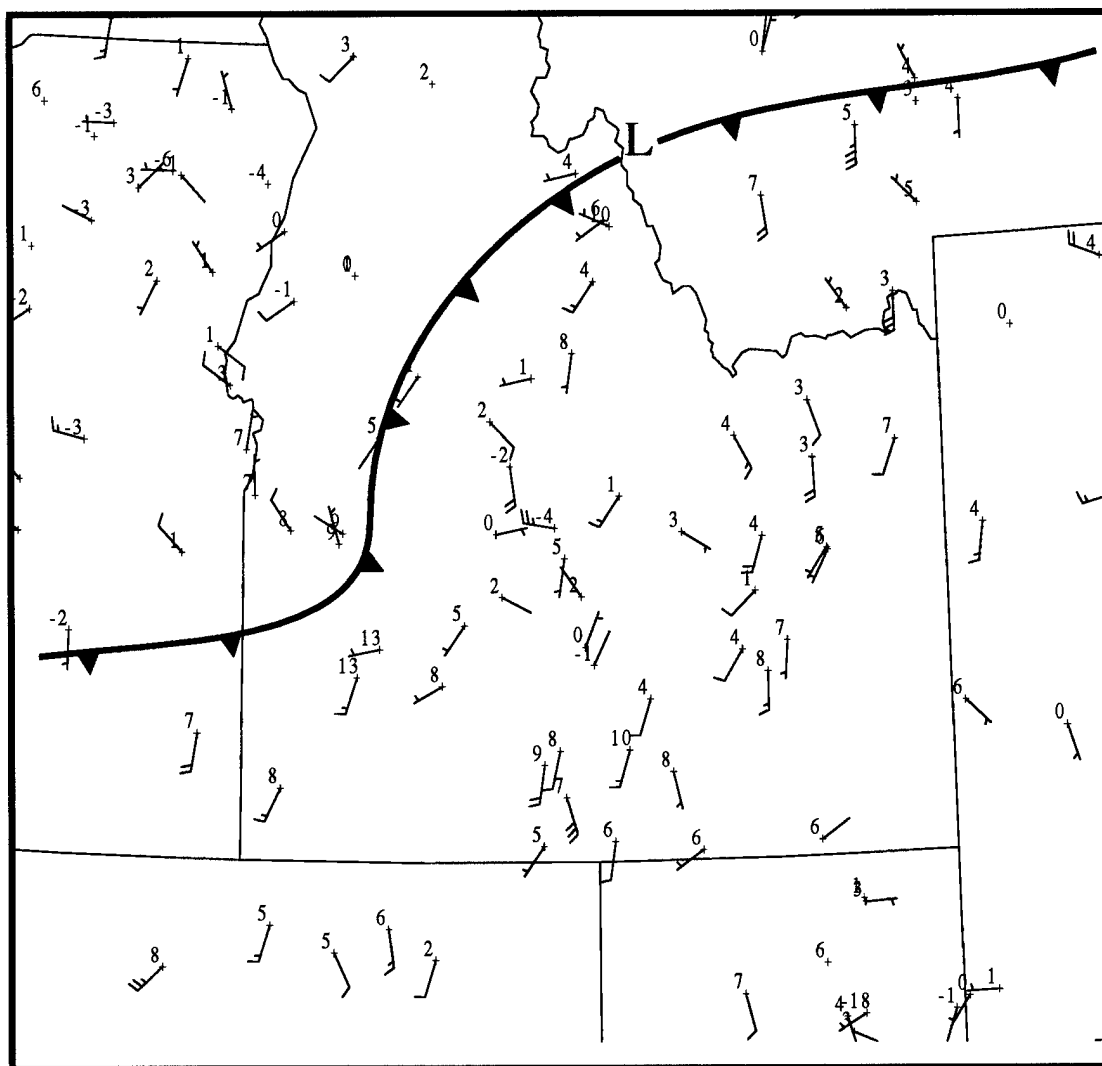


Figure 4.35. Subjective analysis of frontal position over Idaho and the surrounding region for 0600 UTC 3 December.

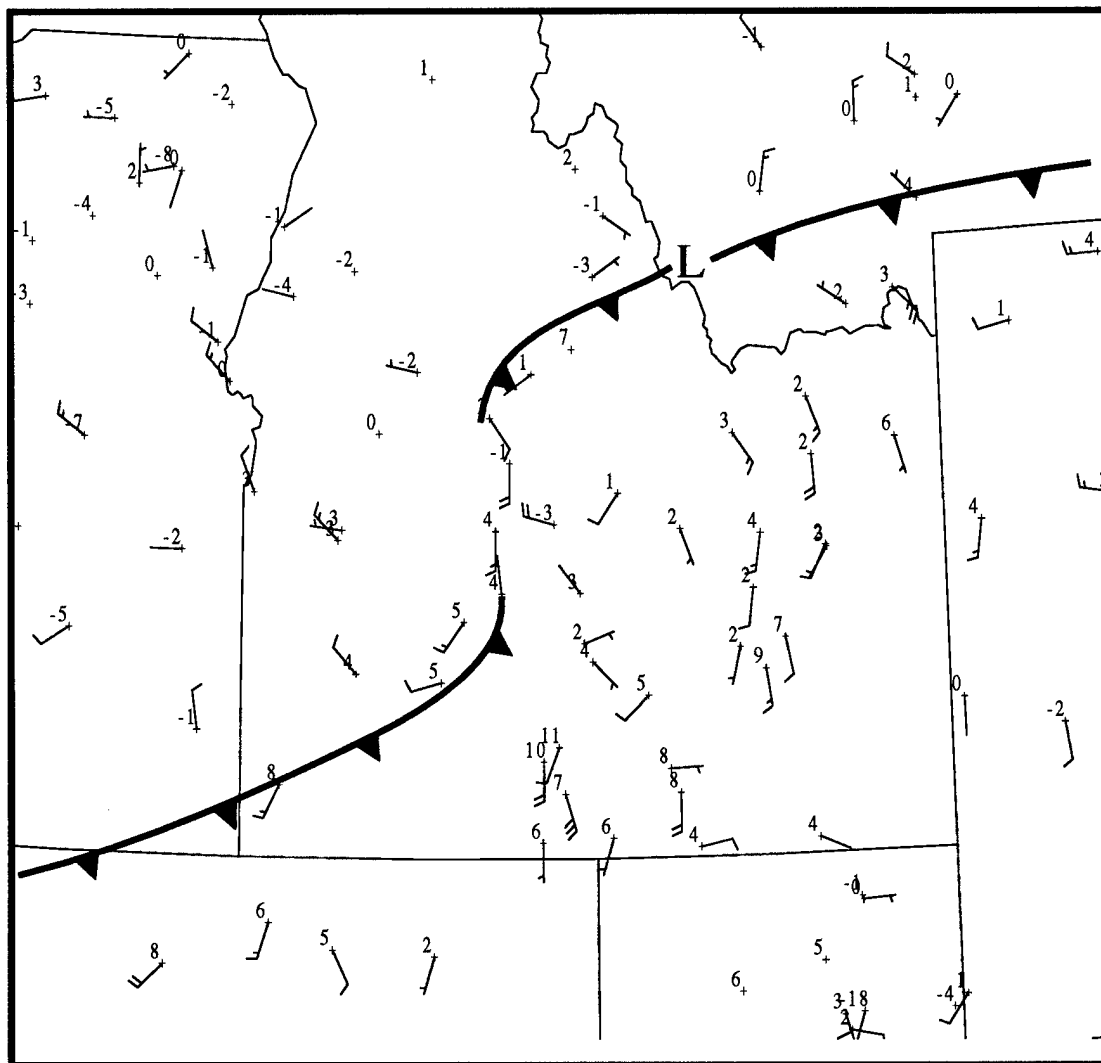


Figure 4.36. Subjective analysis of frontal position over Idaho and the surrounding region for 1200 UTC 3 December.

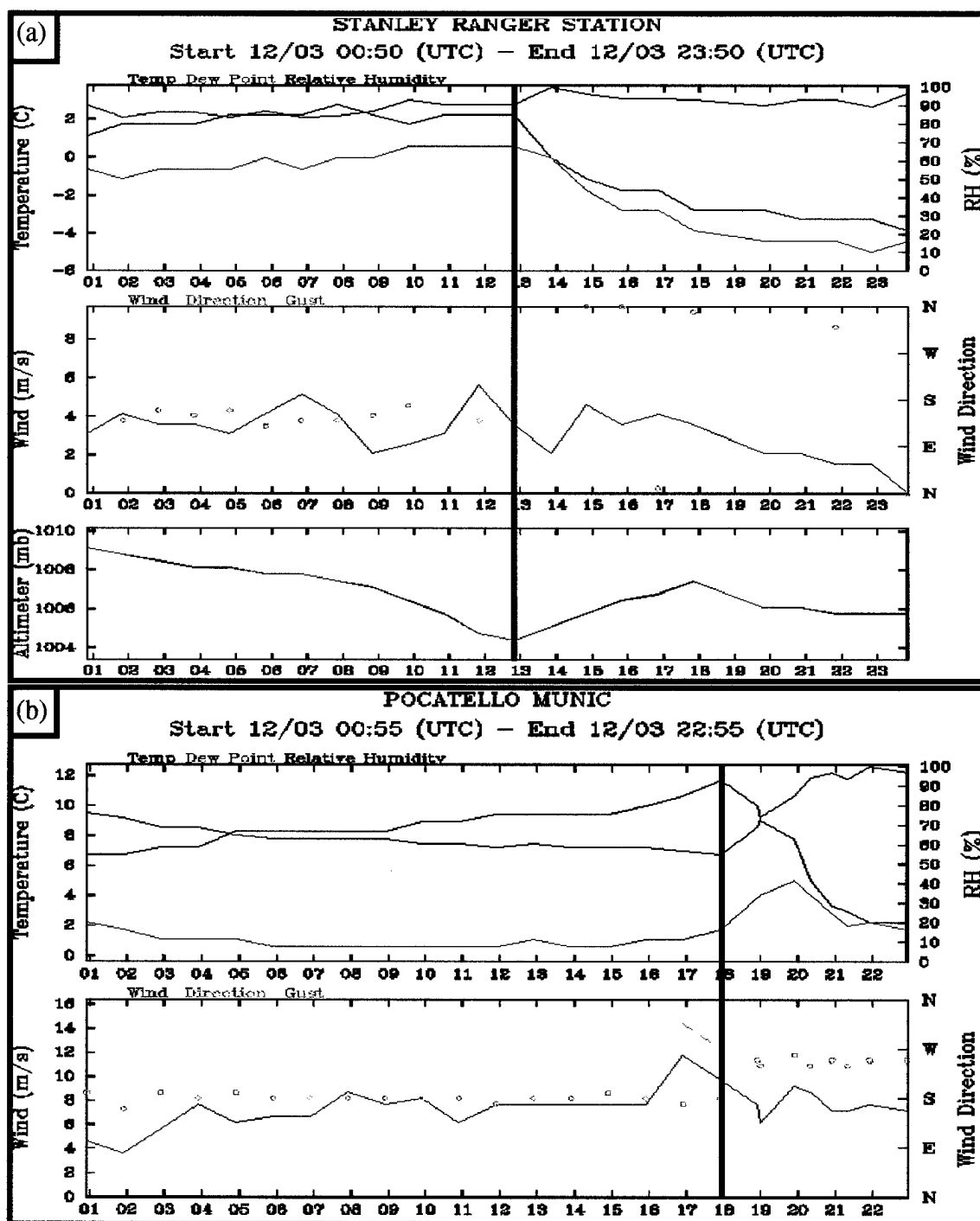


Figure 4.37. Meteograms of temperature (red), dew point (green), and relative humidity (blue), wind speed (solid), gust (dashed), direction (circles), and altimeter trace (top panel only) at (a) Stanley (SNT) and (b) Pocatello (PIH; see Fig. 4.34 for locations) from 0050-2350 UTC 3 December 1998. Solid lines denote frontal passage.

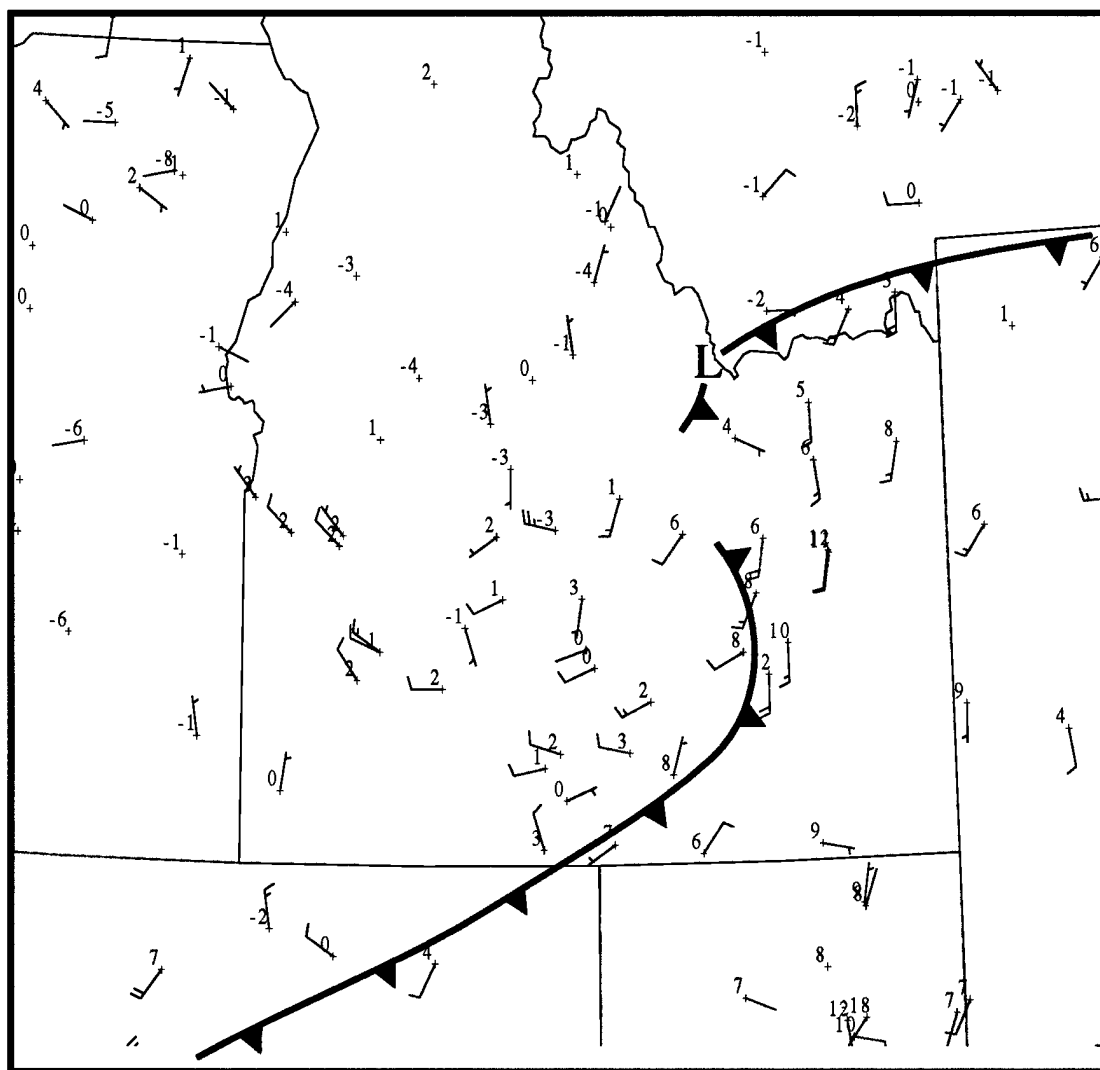


Figure 4.38. Subjective analysis of frontal position over Idaho and the surrounding region for 1800 UTC 3 December.

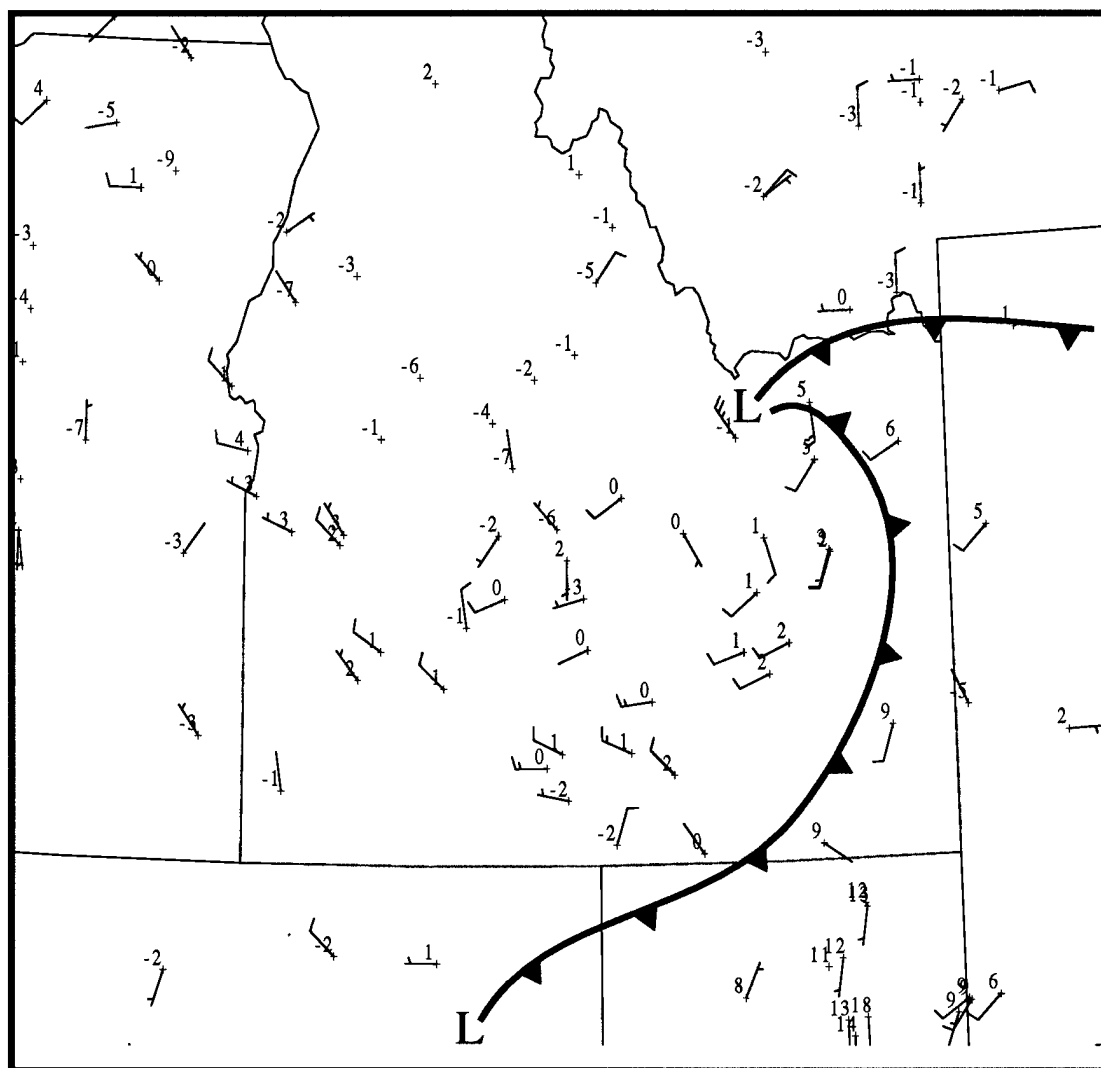


Figure 4.39. Subjective analysis of frontal position over Idaho and the surrounding region for 0000 UTC 4 December.

remained quasi-stationary with a trough axis trailing westward into the central Idaho mountains (Fig. 3.13) where the 1500-m pressure was 3-8 hPa lower than over the surrounding region. Typically, in the case of strong flow over a barrier, one expects pressure troughing to develop to the lee of the barrier. However, in this event, the troughing extended from the upper SRP westward across the barrier. Pressure reduction likely did not contribute significantly to the observed pressure minimum since all regional observations are within 450 m of the 1500-m height level. Instead the pressure trough appeared to be a hydrostatic reflection of the movement of the front up the SRP such that the central Idaho Mountains were surrounded by a colder, more dense airmass. This lag can be demonstrated by comparing the Copper Basin (CBS) site to other regional observations. The average station in the SRP, some 1000 m lower than CBS, had temperatures nearly 10 °C warmer at 1500 UTC 3 December but were nearly identical by 0000 UTC 4 December. The 0000 UTC 4 December sounding at Boise, ID (BOI), showed a free air temperature of -7 °C at the equivalent elevation of CBS while the actual air temperature at CBS was 0 °C. By 1200 UTC, the temperatures were -7 °C at CBS with -11 °C free air over BOI. These observations point to the existence of a thermally induced pressure trough that was also evident on the RUC2 700 hPa analysis (Fig. 3.16c).

As the front cleared the upper SRP, southwesterly surface flow prevailed in its wake by 0300 UTC 4 December. However, northwesterly flow prevailed in and near the canyons on the western side of the SRP, creating a convergence axis that was draped from a mesoscale circulation center in the northwest corner of the SRP, southwestward along the foot of the mountains (Fig. 4.40). As the flow continued from the canyons on the western side of the upper SRP, this convergence axis moved slowly southeast toward

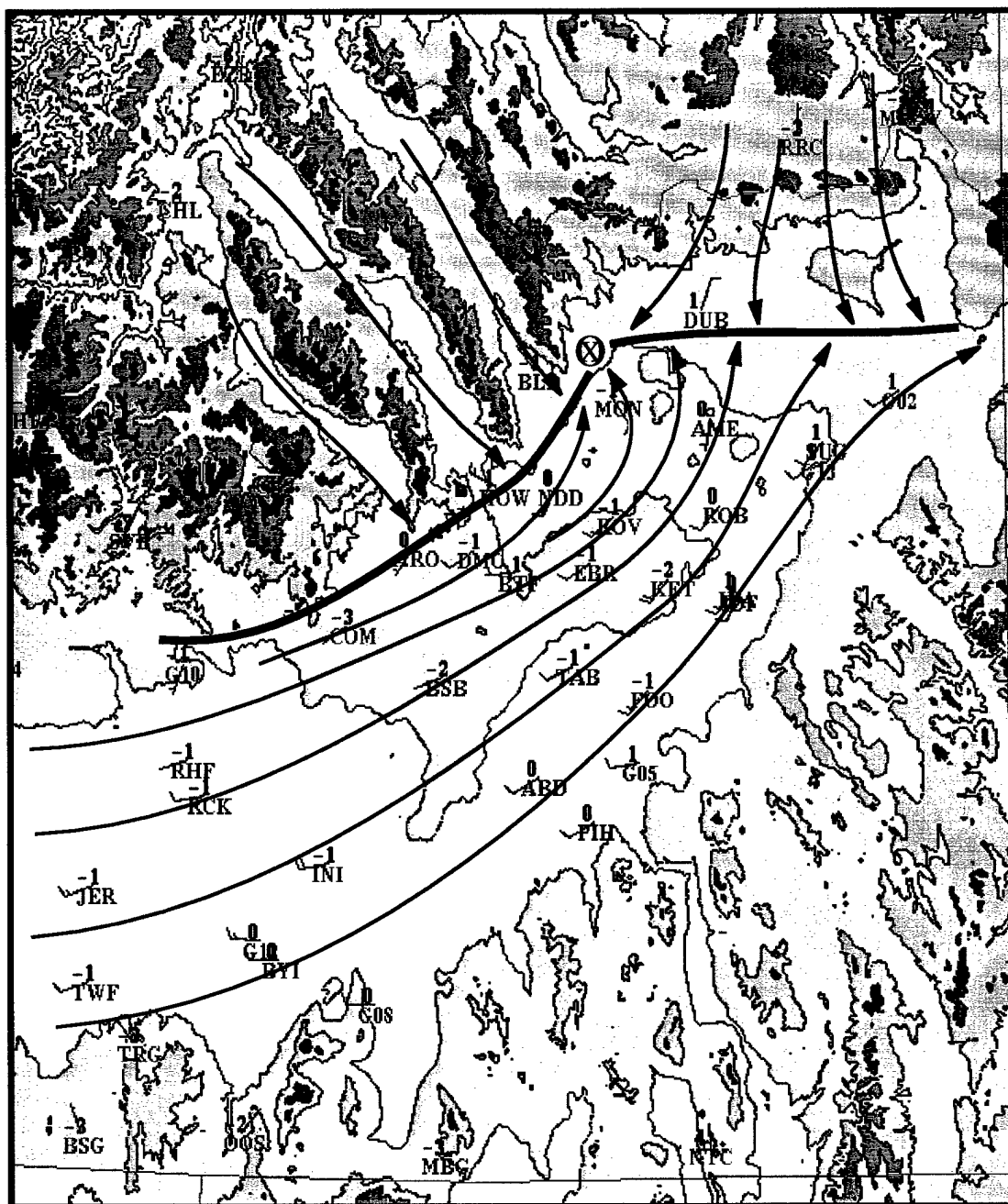


Figure 4.40. Streamline analysis for 0300 UTC 4 December. Mesoscale circulation center is shown as red circled "x" with convergence axis as thick solid line.

Kettle Butte (KET) and Taber (TAB) by 0600 UTC (Fig. 4.41). The cyclonic signature in the wind field suggested an eastward movement of the mesoscale circulation center along the convergence zone axis. By 1200 UTC, the axis reached its furthest southeastward extent, lying just south of KET. Meanwhile, the mesoscale circulation center moved toward the Wyoming border (Fig. 4.42). As the convergence axis reached this southeastward extent, the pressure difference was less than .5 hPa between IDA and the stations in the central mountains [i.e., Hailey (SUN) and SNT]. Once the axis moved northwest, IDA's pressure increased to a value 2 hPa higher than SUN and SNT (not shown).

Between 1200 and 1800 UTC 4 December, a strengthening isallobaric gradient (not shown) and strong southwest winds pushed up-valley and the convergence axis began to retreat westward toward the mountains. By 1800 UTC, a substantial retreat of the convergence axis had occurred (Fig. 4.43) as northerly flow was limited to canyon mouths and a handful of stations north of KET. Sand Dunes (NDD), approximately 60 km west-northwest of IDA, recorded a distinct wind shift, typical of other regional stations, as the convergence axis passed around 1630 UTC (Fig. 4.44). South to southwest winds were prevalent across the upper SRP by 0000 UTC 5 December as the convergence axis made a complete retreat to the western side of the valley (Fig. 4.45). During this period (1200-2200 UTC 4 December), snow was widespread across the region, as shown by the radar image from Pocatello, ID (Fig. 4.46). It also appears that precipitation rates were enhanced near the convergence axis especially to the south and east of KET and ARO.

By 0300 UTC 5 December, another mesoscale circulation center formed over the northwest corner of the upper SRP (Fig. 4.47). Based on a subjective analysis of the wind



Figure 4.41. Streamline analysis for 0600 UTC 4 December. Mesoscale circulation center is shown as red circled "x" with convergence axis as thick solid line.

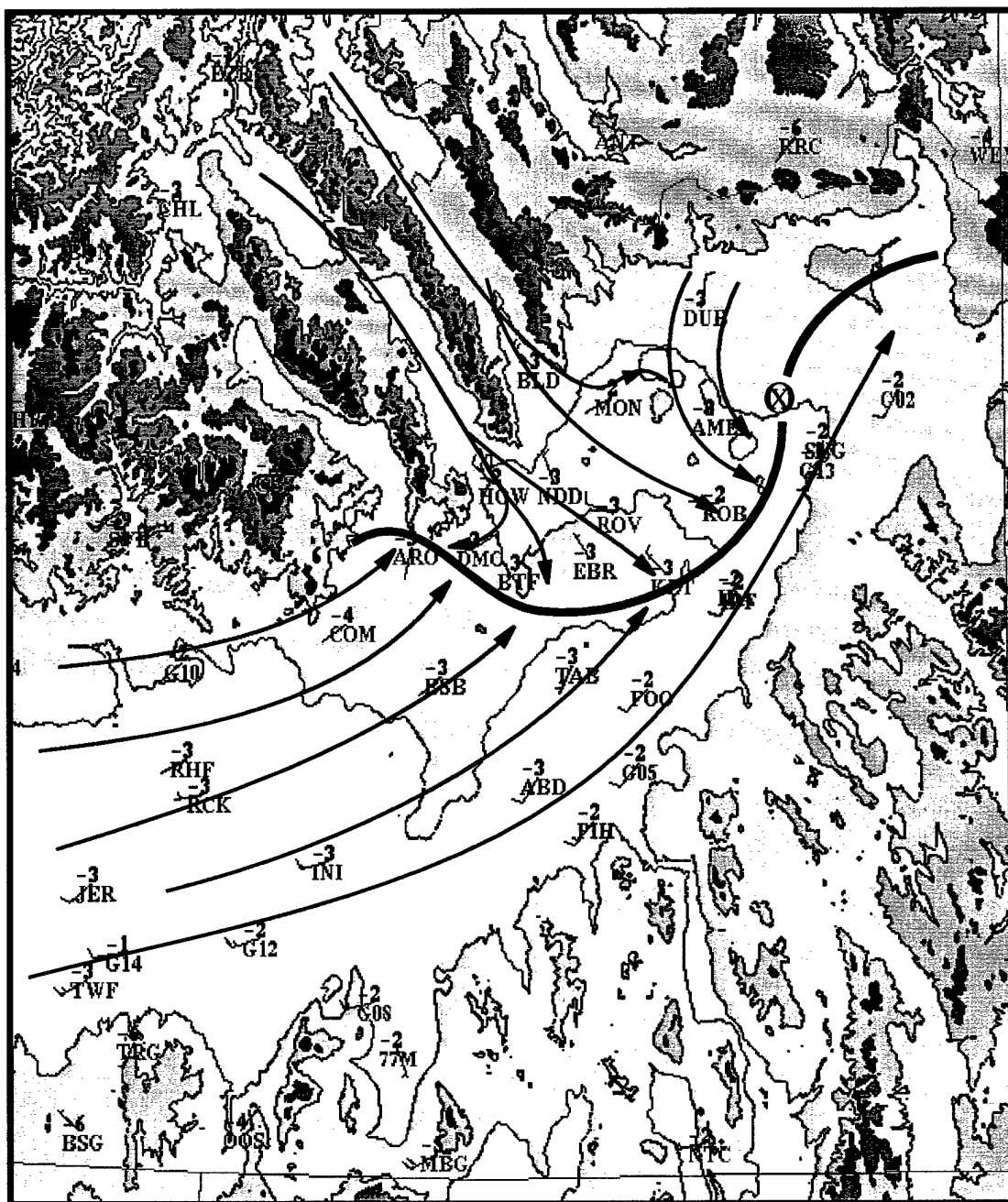


Figure 4.42. Streamline analysis for 1200 UTC 4 December. Mesoscale circulation center is shown as red circled "x" with convergence axis as thick solid line.



Figure 4.43. Streamline analysis for 1800 UTC 4 December. Mesoscale circulation center is shown as red circled “x” with convergence axis as thick solid line.

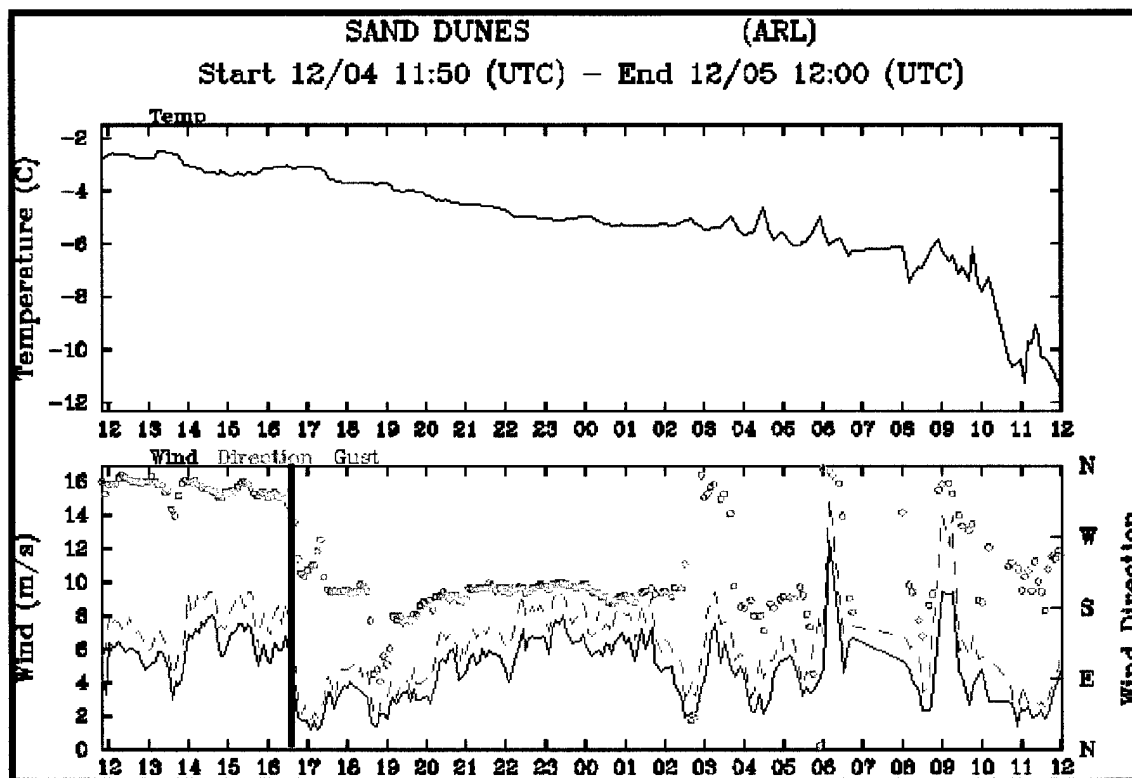


Figure 4.44. Meteograms of temperature (red), wind speed (solid), wind gust (dashed), and wind direction (open circles) at Sand Dunes (NDD; see Fig. 4.34 for locations) from 1150 UTC 4 December to 1200 UTC 5 December 1998. Solid line denotes wind shift associated with convergence axis passage.

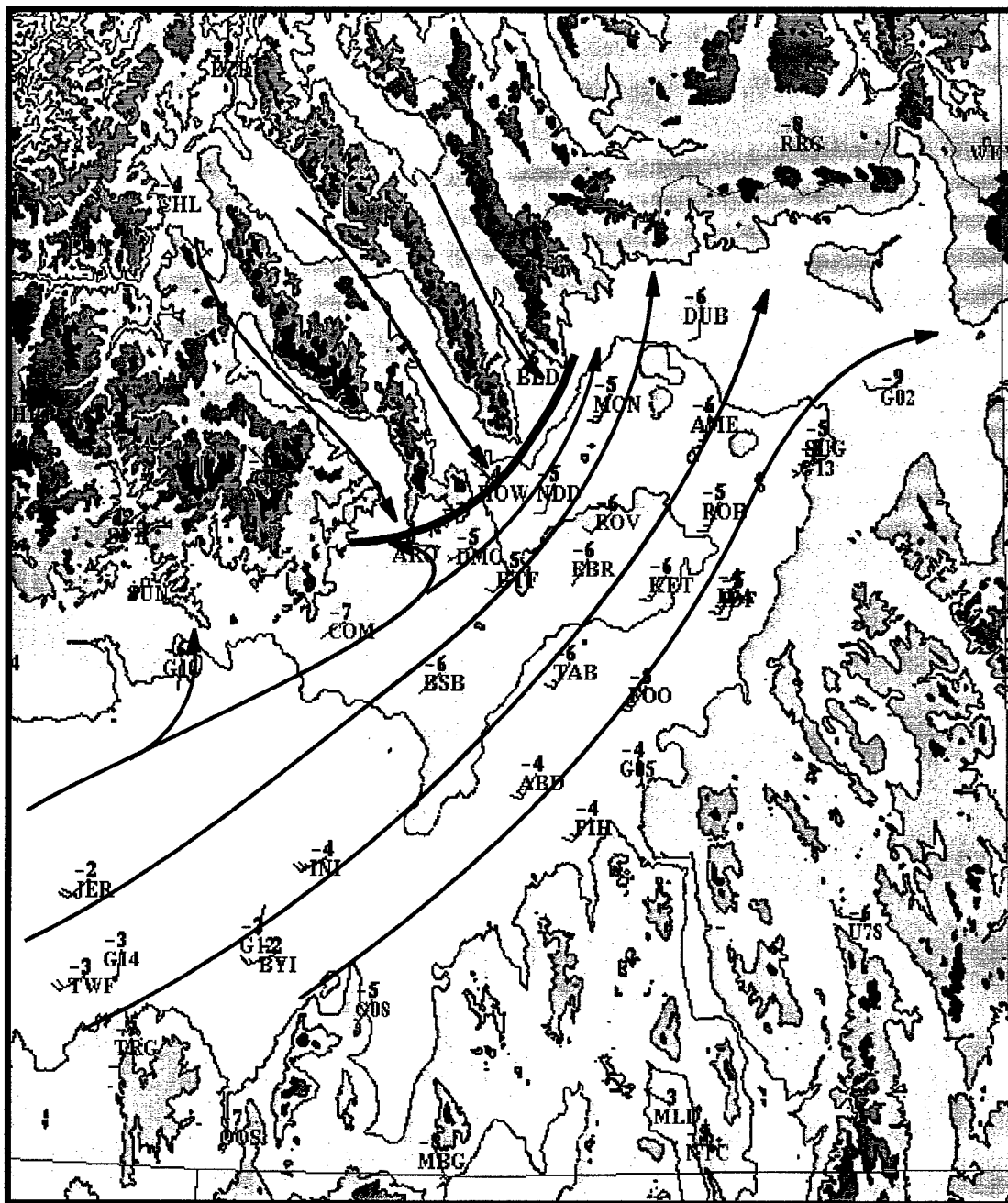


Figure 4.45. Streamline analysis for 0000 UTC 5 December. Convergence axis shown as thick solid line.

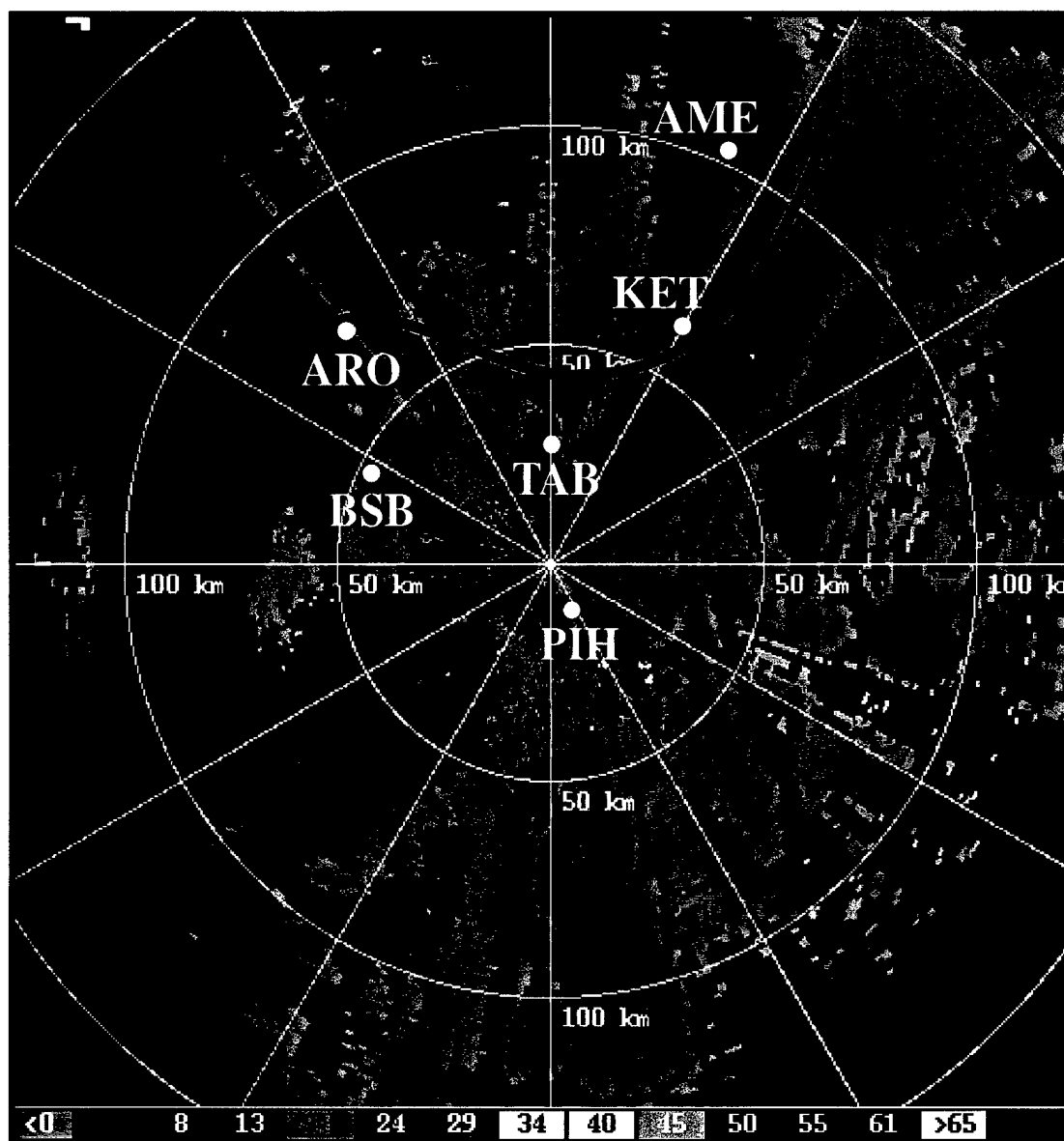


Figure 4.46. Radar imagery from Pocatello, ID, for 1248 UTC 4 December 1998. Mesoscale circulation and convergence axis at 1200 UTC 4 December 1998 are overlaid as circled red "x" and thick solid line, respectively. Stations listed include: Arco (ARO), Big South Butte (BSB), Taber (TAB), Pocatello (PIH), Kettle Butte (KET), and Camus (AME). Range rings every 50 km with radials every 30°.



Figure 4.47. Streamline analysis for 0300 UTC 5 December. Mesoscale circulation center is shown as red circled "x", with convergence axis as thick solid line.

field, the center was placed between three stations: Montevue (MON; Fig. 4.48a), Camus (AME; Fig. 4.48b), and Dubois (DUB; not shown), with the convergence axis trailing to the south-southwest. As the mesoscale circulation center moved east, all three sites recorded a distinct wind shift to the north-northwest as well as a drastic decrease in speed. By 0600 UTC, a second mesoscale circulation center formed in the northwest corner of the upper SRP (Fig. 4.49). The second mesoscale circulation center tracked south of MON (Fig. 4.50) as the winds at MON showed a gradual backing tendency between 0800 UTC and 1200 UTC (Fig. 4.48a). AME had a distinct wind shift (Fig. 4.48b) as the mesoscale circulation center moved north of the site and the trailing convergence axis passed through around 1200 UTC (Fig. 4.51). DUB remained on the northern side of the vortex passage and had lighter winds, resulting in a less pronounced wind shift between 1000-1100 UTC (not shown). Subsequent wind shifts are seen across the region on 5 December, though to a much lesser degree than those seen at AME. Between 1200 and 1800 UTC, AME recorded a continual backing wind ($\tau=3\text{h}$ for complete 360° cycle) as though weak mesoscale circulation centers were repeatedly crossing the site (Fig. 4.48b).

The upper SRP convergence zone has been documented as a significant mesoscale feature (Andretta and Hazen 1998). Though precipitation in this event was not due solely to the existence of the convergence zone, it appears that amounts were enhanced along it. Topographically channeled flow up the SRP and the presence of several mesoscale circulation centers, as also documented across northern Utah, appear to play an integral part in the development and subsequent movement of the convergence axis within the USRP. Further research is required to determine the necessary environment for development of these mesoscale circulation centers and the potential existence of

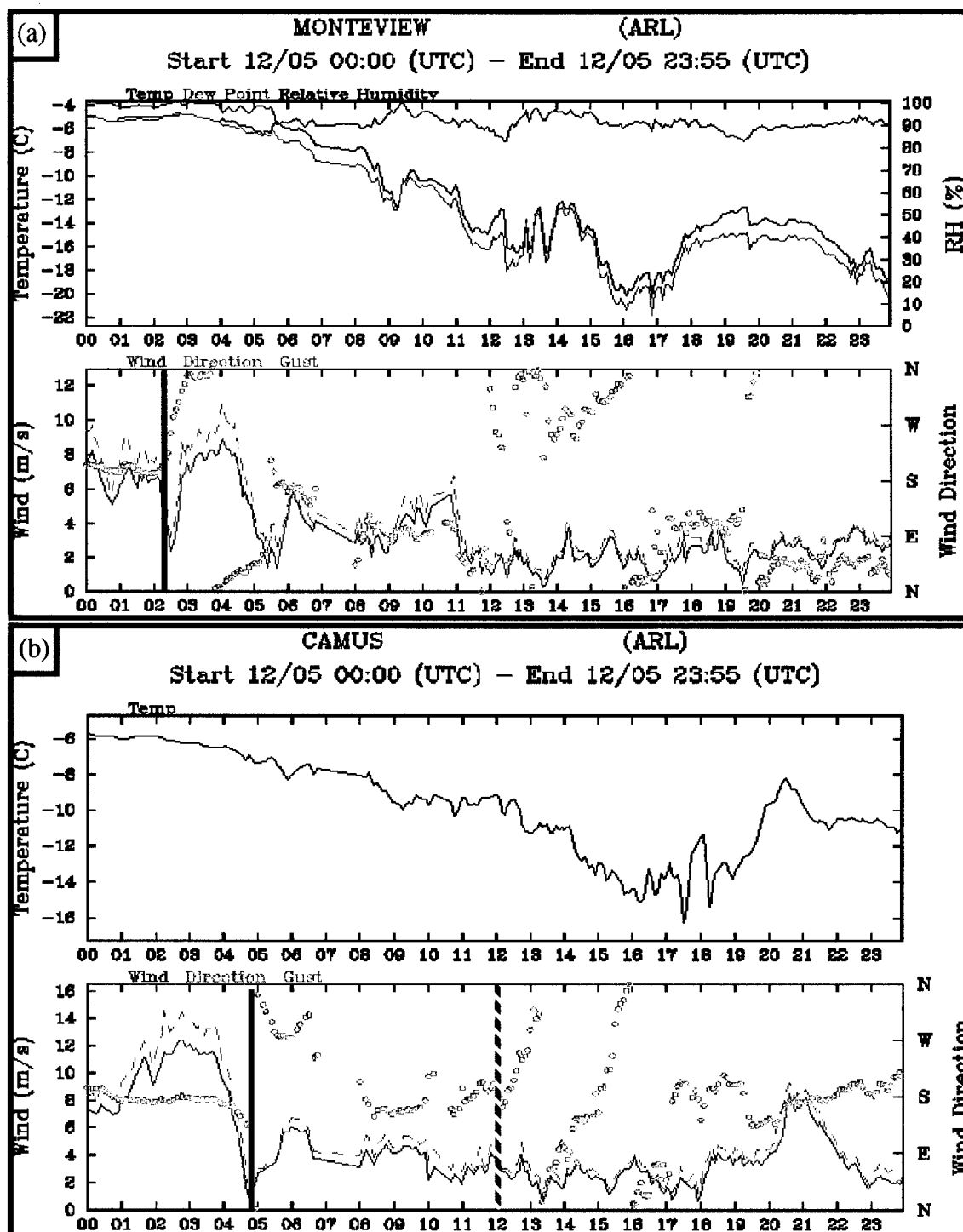


Figure 4.48. Meteograms of temperature (red), dew point (green), relative humidity (blue), wind speed (solid), wind gust (dashed), and wind direction (open circles) at (a) Montevieu (MON) and (b) Camus (AME; see Fig. 4.34 for locations) from 0000-2355 UTC 5 December 1998. Solid lines denote windshift along convergence axis; dashed line in (b) denotes commencement of veering winds.



Figure 4.49. Streamline analysis for 0600 UTC 5 December. Mesoscale circulation centers are shown as red circled "x" with convergence axis as thick solid line.



Figure 4.50. Streamline analysis for 0900 UTC 5 December. Mesoscale circulation center is shown as red circled "x" with convergence axis as thick solid line.

additional mesoscale circulation centers that enhance precipitation along the convergence axis.

CHAPTER 5

SUMMARY AND CONCLUSIONS

This thesis has documented the evolution of an extratropical cyclone that developed over the Great Basin from 3–5 December 1998. By utilizing high-density MesoWest observations, in combination with traditional meteorological observations, the mesoscale structure of the cyclone was examined. The primary goals of this research were to document the interaction of a cyclone and its attendant fronts with the complex topography of the Great Basin, and to begin to understand how such topography affects regional weather systems.

Prior to cyclogenesis, a surface-based cold front extended across northern California east-northeastward into Montana while an upper-level trough approached from the west. A pronounced distortion of the front developed over California and Nevada as it moved equatorward during this period. Specifically, the equatorward movement of the front along the California coast was substantially faster than that observed over and to the east of the Sierra Nevada. As a result, a pronounced frontal wave developed that was centered over the Sierra Nevada Crest, and may have been the result of at least two effects. First, the frontal distortion may have been related to topographic effects as observed during the interaction of low-level fronts with the European Alps and other mountain ranges (e.g., Godske et al. 1957; Steinacker 1981; Smith 1986). Second, the frontal wave may also have been induced by the approach of the upper-level trough and cyclonic

potential vorticity anomaly, as commonly occurs over oceanic regions (e.g., Bader et al. 1995). Erosion of the frontal baroclinity, and transition of the front into a shearline as it continued to move equatorward, were also documented over southern California and Nevada.

As the upper-level trough moved inland, cyclogenesis occurred along the cold front over eastern Nevada at 0000 UTC 4 December 1998. As the inner core of the cyclone moved across northeastern Nevada and northern Utah, two mesoscale circulation centers developed along the cold front as it moved across the Great Salt Lake basin. Similar features have been documented near the inner core of oceanic cyclones (e.g., Neiman et al. 1993), and observed over northern Utah during the Intermountain Precipitation EXperiment (IPEX) field program held during February 2000 (Schulz et al. 2000). The circulation centers contributed to an erratic movement of the front through northern Utah. South of the Great Salt Lake, the evolution of the front was also influenced by the local basin and range topography, specifically, blocking by the Stansbury and Oquirrh mountains. In this particular example, the Rush and Utah Valleys recorded frontal passages from the north and west as the flow was channeled around the topography.

Frontal distortion was also documented over sections of Idaho as the front passed through the Snake River Plain and the adjacent central Idaho mountains. In particular, topographic channeling resulted in an acceleration of the front up the Snake River Plain, while the central Idaho Mountains appeared to retard the frontal motion, although the front was difficult to trace through the latter region. As cold air channeled through the Snake River Plain, and filled other lower-elevation regions in Montana and northern Idaho, a persistent 1500-m pressure minimum developed over the central Idaho Mountains. This

pressure minimum appeared to be a hydrostatic reflection of the cold airmass surrounding, but unable to penetrate into, the central Idaho Mountains. The pressure minimum did not appear to be related to pressure reduction since observations from valley locations within the mountains were significantly warmer and featured lower 1500-m pressures than those from similar elevation stations in surrounding lowland regions.

In the postfrontal environment, a Snake River Plain convergence zone developed over southeastern Idaho (e.g., Andretta and Hazen 1998). Slightly enhanced precipitation totals were observed near the convergence zone axis, which appeared to be modulated diurnally by outflow from major canyons in the Central Idaho Mountains. In addition, several mesoscale circulation centers developed and migrated along the convergence zone axis, modifying its location and orientation over the upper Snake River Plain.

This research has identified several mesoscale characteristics and features of cyclone evolution over the Great Basin. Additional work is needed to better understand how the interaction of the large-scale flow with the Sierra Nevada produced the frontal wave observed during this event, and the dynamics of the mesoscale circulation centers that were observed along the cold front over northern Utah and in the post-frontal environment over the Snake River Plain. Such features have been observed by the author in other cyclogenesis events and were found during IPEX to modulate orographic precipitation. Further knowledge of the evolution and dynamics of such events will be useful for operational weather forecasters.

This research has also demonstrated the value of high spatial and temporal resolution observations provided by MesoWest. As illustrated by the analyses presented in this thesis, such high resolution data is needed to even begin to resolve mesoscale aspects

of cyclone and frontal evolution over the Great Basin. In addition, the large number of MesoWest observations greatly improves frontal analysis in complex terrain by allowing the meteorologist to identify when near-surface processes are obscuring large-scale air mass changes associated with frontal passages.

REFERENCES

- Andretta, T. A., and D. S. Hazen, 1998: Doppler radar analysis of a Snake River Plain convergence event. *Wea. Forecasting*, **13**, 482-491.
- Bader, M. J., G. S. Forbes, J. R. Grant, R. B. E. Lilley, and A. J. Waters, 1995: *Images in Weather Forecasting*, Cambridge Press, 499 pp.
- Baer, V. E., 1991: The transition from the present radar dissemination system to the NEXRAD Information Dissemination Service (NIDS). *Bull. Amer. Meteor. Soc.*, **72**, 29-33.
- Bannon, P. R., 1983: Quasi-geostrophic frontogenesis over topography. *J. Atmos. Sci.*, **40**, 2266-2277.
- , 1984: A semigeostrophic model of frontogenesis over topography. *Beitr. Phys. Atmos.*, **57**, 393-408.
- , 1992: A model of Rocky Mountain lee cyclogenesis. *J. Atmos. Sci.*, **49**, 1510-1522.
- Bell, G. D., and L. F. Bosart, 1994: Midtropospheric closed cyclone formation over the southwestern United States, the eastern United States, and the Alps. *Mon. Wea. Rev.*, **122**, 791-813.
- Benjamin, S. G., and P. A. Miller, 1990: An alternative sea level pressure reduction and a statistical comparison of geostrophic wind estimates with observed surface winds. *Mon. Wea. Rev.*, **118**, 2099-2116.
- , K. A. Brewster, R. Brümmer, B. F. Jewett, T. W. Schlatter, T. L. Smith, and P. A. Stamus, 1991: An isentropic three-hourly data assimilation system using ACARS aircraft observations. *Mon. Wea. Rev.*, **119**, 888-906.
- , K. J. Brundage, and L. L. Marone, 1994: The Rapid Update Cycle. Part I: Analysis/model description. Technical Procedures Bulletin No. 416 NOAA/NWS, 16 pp.
- Bjerknes J., and H. Solberg, 1922: Life cycles of cyclones and the polar front theory of atmospheric circulation. *Geofys. Publ.*, **2**, 1-60.

- Bluestein, H. B., 1986: Fronts and jet streaks: A theoretical perspective. *Mesoscale Meteorology and Forecasting*. (P. S. Ray, Ed.), Amer. Meteor. Soc., 173-215.
- Buzzi, A., and S. Tibaldi, 1978: Cyclogenesis in the lee of the Alps: A case study. *Quart. J. Roy. Meteor. Soc.*, **104**, 271-287.
- Carruthers, D. J., and J. C. R. Hunt, 1990: Fluid mechanics of airflow over hills: turbulence, fluxes, and waves in the boundary layer. *Atmospheric Processes Over Complex Terrain*. (W. Blumen, Ed.), Amer. Meteor. Soc., 83-107.
- Conger, M. C., 1994: Forecasting a Great Basin cyclogenetic event using the Nested Grid Model: A case study evaluation of model performance. *Nat. Wea. Digest*, **18**, 4, 2-15.
- Crum, T. D., R. L. Alberty, and D. W. Burgess, 1993: Recording, archiving, and using WSR-88D data. *Bull. Amer. Meteor. Soc.*, **74**, 645-653.
- Davis, C. A., 1997: The modification of baroclinic waves by the Rocky Mountains. *J. Atmos. Sci.*, **54**, 848-868.
- , and M. T. Stoelinga, 1999: Interpretation of the effect of mountains on synoptic-scale baroclinic waves. *J. Atmos. Sci.*, **56**, 3303-3320.
- Durrán, D. R. 1986: Mountain waves and downslope winds. *Atmospheric Processes Over Complex Terrain*. (W. Blumen, Ed.), Amer. Meteor. Soc., 59-81.
- Egger, J., 1972: Numerical experiments on the cyclogenesis in the Gulf of Genoa. *Beitr. Phys. Atmos.*, **45**, 320-346.
- Eisenson, R. N., 1984: Lee cyclogenesis in the Great Basin. M.S. Thesis, Dept. of Meteorology, University of Utah, 89 pp. [Available from Dept. of Meteorology, University of Utah, 145 South 1460 East, Room 819, Salt Lake City, UT 84112-0110.]
- Horel, J. D., and C. V. Gibson, 1993: Analysis and simulation of a winter storm over Utah. *Wea. Forecasting*, **9**, 479-494.
- Godske, G. L., T. Bergeron, J. Bjerknes, and R. C. Bundgaard, 1957: *Dynamic Meteorology and Weather Forecasting*, Amer. Met. Soc., Boston, 800 pp.
- Hobbs, P. V., J. D. Locatelli, and J. E. Martin, 1996: A new conceptual model for cyclones generated in the lee of the Rocky Mountains. *Bull. Amer. Meteor. Soc.*, **77**, 1169-1178.
- Hoinka K. P., and D. Heimann, 1988: Orographic channeling of a cold front by the Pyrenees. *Mon. Wea. Rev.*, **116**, 1817-1823.

- Keyser, D., 1986: Atmospheric fronts: An observational perspective. *Mesoscale Meteorology and Forecasting*. (P. S. Ray, Ed.), Amer. Meteor. Soc., 216-258.
- Klein, W. H., 1957: Principal tracks and mean frequencies of cyclones and anticyclones in the Northern Hemisphere. Res. Pap. No. 40, U. S. Weather Bureau. U. S. Government Printing Office, Washington, D.C., 60 pp.
- Mass, C. F., 1991: Synoptic frontal analysis: Time for a reassessment. *Bull. Amer. Meteor. Soc.*, **72**, 348-363.
- _____, W. J. Steenburgh, and D. M. Schultz, 1991: Diurnal surface-pressure variations over the continental United States and the influence of sea level reduction. *Mon. Wea. Rev.*, **119**, 2814-2830.
- Mattocks, C., and R. Bleck, 1986: Jet streak dynamics and geostrophic adjustment processes during the initial stages of lee cyclogenesis. *Mon. Wea. Rev.*, **114**, 2033-2056.
- McClain, E. P., 1960: Some effects of the western Cordillera of North America on cyclone activity. *J. Meteor.*, **17**, 104-115.
- McGinley, J. A., 1982: A diagnosis of Alpine lee cyclogenesis. *Mon. Wea. Rev.*, **110**, 1271-1287.
- Neiman, P. J., and M. A. Shapiro, 1993: The life cycle of an extratropical marine cyclone. Part I: General characteristics and dynamics. *Mon. Wea. Rev.*, **118**, 2579-2598.
- _____, F. M. Ralph, M. A. Shapiro, B. F. Smull, and D. Johnson, 1998: An observational study of fronts and frontal mergers over the Continental United States. *Mon. Wea. Rev.*, **126**, 2521-2554.
- Newton, C. W., 1956: Mechanisms of circulation change during a lee cyclogenesis. *J. Meteor.*, **13**, 528-539.
- Palmen, E., and C. W. Newton, 1969: *Atmospheric Circulation Systems*. Academic Press, 603 pp.
- Pauley, P. M., 1998: An example of uncertainty in sea level pressure reduction. *Wea Forecasting*, **13**, 833-850.
- Petterssen, S., 1940: *Weather Analysis and Forecasting*. 1st ed., McGraw-Hill, 503 pp.
- _____, 1956: *Weather Analysis and Forecasting, Vol. 1, Motion and Motion Systems*. 2nd ed., McGraw-Hill, 286 pp.

- Roark, D. O., 1976: An objective analysis of mountain effects on North American cyclones. M.S. Thesis, Dept. of Meteorology, University of Utah, 79 pp. [Available from Dept. of Meteorology, University of Utah, 145 South 1460 East, Room 819, Salt Lake City, UT 84112-0110.]
- Sanders, F., 1999: A proposed method of surface map analysis. *Mon. Wea. Rev.*, **127**, 945-955.
- _____, and C. A. Doswell III, 1995: A case for detailed surface analysis. *Bull. Amer. Meteor. Soc.*, **76**, 505-521.
- Sangster, W. E., 1960: A method of representing the horizontal pressure gradient force without reduction of station pressure to sea level. *J. Meteor.*, **17**, 166-176.
- Schulz, D. M., W. J. Steenburgh, J. Trapp, D. Kingsmill, and L. B. Dunn, 2000: Preliminary results from the Intermountain Precipitation Experiment. *Preprints, Ninth Conference on Mountain Meteorology*, Aspen, CO, Amer. Meteor. Soc.
- Seaman, N. L., D. R. Stauffer, and A. M. Lario-Gibbs, 1995: A multi-scale four-dimensional assimilation system applied in the San Joaquin Valley during SARMAP. Part I. Modeling design and basic performance characteristics. *J. Appl. Meteor.*, **34**, 1739-1761.
- Smith, R. B., 1986: Mesoscale mountain meteorology in the Alps. Scientific Results of the Alpine Experiment, Vol. II. GARP Publ. Ser., No. 27, WMO/TD No. 108, 407-423.
- Splitt, M. E., and J. D. Horel, 1998: Use of multivariate linear regression for meteorological data analysis and quality assessment in complex terrain. *Preprints, 10th Symposium on Meteorological Observations and Instrumentation*, Phoenix AZ, Amer. Meteor. Soc., 359-362.
- Steinacker, R., 1981: Analysis of the temperature and wind field in the Alpine region. *Geophys. Astrophys. Fluid Dyn.*, **17**, 51-62.
- Tafferner, A., and J. Egger, 1992: Modification of fronts by the Alps: Simulations and numerical experimentation. *Meteor. Atmos. Phys.*, **48**, 193-203.
- Tibaldi, S., A. Buzzi, and A. Speranza, 1990: Orographic cyclogenesis. Extratropical Cyclones: The Erik Palmén Memorial Volume, C. Newton and E. O. Holopainen, Eds., American Meteorological Society, 107-127.
- Uccellini, L. W., S. F. Corfidi, N. W. Junker, P. J. Kocin, and D. A. Olson, 1992: Report on the surface analysis workshop at the National Meteorological Center 25-28 March 1991. *Bull. Amer. Meteor. Soc.*, **73**, 459-471.

- Wendell, L. L., 1972: Mesoscale wind fields and transport estimates determined from a network of wind towers. *Mon. Wea. Rev.*, **100**, 565-578.
- Whiteman, C. D., 1990: Observations of thermally developed wind systems in mountainous terrain. *Atmospheric Processes Over Complex Terrain*. (W. Blumen, Ed.), Amer. Meteor. Soc., 5-42.
- Whittaker, L. M., and L. H. Horn, 1984: Northern Hemisphere extratropical cyclone activity for four mid-season months. *J. Climatol.*, **4**, 297-310.
- Williams, R. T., M. S. Peng, and D. A. Zankofski, 1992: Effects of topography on fronts. *J. Atmos. Sci.*, **49**, 287-305.
- Williams, P., Jr., 1962: Forecasting the formation of cut-off lows over the western plateau. U. S. Weather Bureau, Washington, D. C., unpublished. [Available from Professor W. James Steenburgh, Dept. of Meteorology, University of Utah, 145 South 1460 East, Room 819, Salt Lake City, UT 84112-0110.]
- Zehnder, J., and P. Bannon, 1988: Frontogenesis over a mountain ridge. *J. Atmos. Sci.*, **45**, 628-645.
- Zishka, K. M., and P. J. Smith, 1980: The climatology of cyclones and anticyclones and surrounding ocean environs for January and July, 1950-77. *Mon. Wea. Rev.*, **108**, 387-401.